# MULTIPHOTON TRANSITIONS IN SOLIDS

THESE No 924 ( 1991 )

PRESENTEE AU DEPARTEMENT DE PHYSIQUE

ECOLE POLYTECHNIQUE FEDERALE DE LAUSANNE

POUR L'OBTENTION DU GRADE DE DOCTEUR ES SCIENCES

PAR

ALFREDO PASQUARELLO

physicien diplômé de l'Université de Pisa et de l'Ecole Normale Supérieure de Pisa
de nationalité italienne

acceptée sur proposition du jury :

Prof. A. Quattropani , rapporteur
Prof. A. Baldereschi, corapporteur
Prof. F. Bassani, corapporteur
Prof. A. Mysyrowicz, corapporteur

Lausanne, EPFL
1991

## Résumé

Dans cette thèse, nous approfondissons certains aspects théoriques des transitions à plusieurs photons dans les solides. La probabilité de transition est donnée par une formule dérivée à partir de la théorie des perturbations dépendant du temps. Quand deux photons ou plus sont absorbés simultanément, des difficultés, absentes lors de transitions à un photon, apparaissent. Premièrement, le calcul de la probabilité de transition implique dans ce cas une sommation sur les états intermédiaires du système. Une connaissance de tous ces états est en général difficile, et l'approximation consistant à en négliger une partie est souvent nécessaire. A ce stade se pose le problème de maintenir l'invariance de jauge des résultats, car on sait que si l'on considère un ensemble incomplet d'états, on aboutit à des résultats différents pour jauges différentes. Une fois les problèmes de couplage avec la radiation réglés, il reste à effectuer pratiquement la sommation sur les états retenus essentiels. Deuxièmement, quand le nombre de photons absorbés augmente, la probabilité de transition dépendra de plusieurs vecteurs de polarisation. Pour déterminer cette dépendance, il est nécessaire d'effectuer une analyse de symétrie. Dans cette thèse, nous nous intéressons à ces deux aspects, et nous fournissons à des expériences récentes le soutien théorique nécessaire.

La première application étudiée nous a emmené à calculer la probabilité de transition à deux photons dans les puits quantiques de GaAs-$Ga_{1-x}Al_xAs$. L'objet de cette étude est de comprendre les spectres d'excitation expérimentaux, qui montrent en particulier une forte dépendance de la polarisation. Pour des polarisations parallèles à l'axe de croissance, on a un spectre avec des marches marquées par de forts pics excitoniques, tandis que dans le cas de polarisations parallèles aux couches, le spectre est presque linéaire avec des effects ex-

citoniques négligeables. Nous avons commencé par étudier l'absorption entre sous-bandes pour un puits quantique avec des barrières de hauteur infinie concentrant notre attention sur le couplage avec la radiation. Du fait que notre modèle n'inclut que les états de la bande de conduction et de celle de valence, il est nécessaire, afin d'obtenir des résultats invariants de jauge, d'effectuer le couplage au courant du puits quantique. Nous avons pu expliquer ainsi les marches et la dépendance linéaire des spectres. Ensuite, nous avons considéré les effets dus aux barrières de hauteur finie. Nous avons décrit les états de continuum du puits quantique dans un formalisme qui dérive de la théorie des distributions, et effectué explicitement la sommation sur tous les états intermédiaires du modèle. Enfin, nous avons inclus les effets excitoniques. La description des états excitoniques intermédiaires étant complexe, nous avons appliqué une nouvelle méthode variationelle, qui ne nécessite pas une connaissance explicite des états intermédiaires pour obtenir les probabilités de transition. Une comparaison des spectres théoriques et expérimentaux montre un très bon accord entr'eux.

Récemment, il a été possible d'obtenir expérimentalement des spectres d'excitation à trois photons dans les halogénures alcalins. Le problème se posait de comprendre les règles de sélections et la dépendance des polarisations des photons pour les transitions permises. Nous avons d'abord examiné le problème général des règles de sélection de transitions à $n$ photons. Ensuite, nous avons donné une interprétation théorique aux spectres d'excitation des halogénures alcalins. Nous avons trouvé que, en sus des règles de sélections habituelles de dipôle et de polarisation, il peut y avoir une autre règle de sélection dans le cas où quelques uns des photons ont la même fréquence. Nous avons effectué une analyse de symétrie qui tient compte des propriétés de permutation des polarisations et des fréquences et déterminé ainsi ces nouvelles règles de sélection.

L'étude montre aussi qu'il n'est pas toujours possible de factoriser la probabilité de transition en une partie géométrique, qui ne dépend que des polarisations, et en une dynamique, qui contient la dépendence des fréquences. En conséquence, la dépendence des polarisations n'est pas déterminée uniquement par la symétrie de l'état initial et final. Finalement, nous avons consideré en détail le cas de symétrie $O_h$ (symétrie des crystaux des halogénures alcalins) et ajouté l'effet d'un champ magnétique. La théorie permet de donner une interprétation aux spectres expérimentaux et suggère l'existence de nouvelles raies.

# Contents

# Chapter 1

# Introduction

## 1.1 General aspects of multiphoton transitions

The experimental availability of intense monochromatic sources has allowed to detect electronic transitions in which two or more photons are absorbed simultaneously. In such processes the transition energy is equal to the sum of the energies of the absorbed photons. Although the probability rate of multiphoton transitions is several orders of magnitude lower than that of typical one-photon processes, multiphoton spectroscopy has become in the last decades a powerful tool to investigate electronic properties in solids. The main reason for this development is that spectroscopic techniques which differ because of the number of photons participating in the interaction process generally provide alternative and complementary information.

Historically, two-photon effects were first studied theoretically in 1931 by Maria Göppert-Mayer [1], but only 30 years later with the development of lasers it became possible to detect two-photon transitions in the optical energy region [2]. At present, non-linear spectroscopy is still attracting considerable interest.

In fact, two-photon spectroscopy, which has become nowadays a well established technique, is currently used in addition to one-photon spectroscopy in order to extract information on electronic properties. Moreover, the development of new non-linear techniques which involve three photons has occured, allowing to determine physical parameters which are unreachable either with one- or two-photon spectroscopy [3]. In the following we compare multiphoton to one-photon spectroscopy in order to point out the main differences and stress some peculiar aspects of multiphoton transitions.

It is important to notice that selection rules for multiphoton transitions differ in general from those for one-photon transitions. The selection rules are different according to the number of participating photons. For instance, in the case of inversion symmetry, one-photon spectroscopy allows one to detect only states of odd parity. On the other hand, in two-photon transitions, which are second-order processes, these states are forbidden and only even states can be excited. A famous example is the measurement by two-photon spectroscopy of the $1s$–$2s$ energy separation in the hydrogen atom. In general, the symmetry of the final states can be found by considering the angular momentum carried by the photon and the order of the process. For instance in atoms, only states of angular momentum $l = 1$ are allowed in one-photon transitions. In two-photon transitions allowed states have $l = 0, 2$, in three-photon transitions $l = 1, 3$, and so on. In two-photon transitions atomic states of $l = 1$ are not allowed because of the parity selection rule. In molecules or solids, when an inversion centre is lacking, it is possible to excite states which have a crystal symmetry which corresponds to the spherical $l = 1$ symmetry. Analogously, in three-photon spectroscopy, for states with symmetry corresponding to $l = 0, 2$. It is therefore evident that with the increase of the number of involved photons generally more

transitions become allowed. For example, in solids of $O_h$ symmetry, more states can be excited in three-photon spectroscopy than in one-photon spectroscopy, although the parity selection rule is the same [3].

In contrast to one-photon spectroscopy, an additional degree of freedom in multiphoton spectroscopy consists in the possibility of changing independently the polarization vectors of the absorbed photons. This aspect is essential for the determination of the symmetry of the excited states, particularly when the number of absorbed photons is large and states of many different symmetries can be excited [4, 5, 6, 7]. By choosing the polarization vectors carefully it is often possible to excite selectively states of definite symmetry. However, in multiphoton transitions, a drawback occurs when the number of absorbed photons becomes large. In fact, in one-photon transitions it is generally possible, as long as the symmetry group is not too small, to separate the transition rate into a geometrical and a dynamical factor. The geometrical factor depends only on the polarization vectors, whereas the dynamical factor contains the transition matrix element. In this way, transitions to states of equal symmetry have the same polarization dependence. In the case of groups of high symmetry, this property also holds for two-photon transitions. However, when smaller symmetry groups or higher order transitions are considered, it is often no longer possible to separate geometrical and dynamical factors. In this case, the polarization dependence of transitions to states of a given symmetry contains parameters which depend on the final state itself.

An advantage of multiphoton with respect to one-photon spectroscopy is the possibility of varying the relative direction of the wavevectors. The total wavevector can therefore be changed without changing the transition energy. Two-photon spectroscopy has been used successfully in order to study the $k$-

dispersion of excitonic polaritons and even to excite the longitudinal excitons [8]. In crystals with inversion symmetry, two-photon transitions to polariton states are forbidden because of the parity selection rule. In fact, the first experiment in which the excitonic polariton was observed was performed on CuCl, which lacks inversion symmetry and in which the polariton states can be excited in one- as well as in two-photon spectroscopy [8]. Very recently, with the use of three-photon spectroscopy, it has also been possible to excite polariton states in crystals which have an inversion centre [3, 9]. We note that the possibility of varying the direction of the wavevectors allows in atomic physics to reduce very effectively the Doppler broadening with the use of counter-propagating beams [10].

Another important aspect of multiphoton transitions is the possibility of varying the ratio of the frequencies of the absorbed photons keeping their sum fixed and equal to the transition energy. Although only virtual excitation of intermediate states occurs in a multiphoton process, the transition rate can be enhanced by several orders of magnitude when an intermediate state happens to be resonant [10]. In this way it is possible to perform intermediate-state spectroscopy.

The possibility of varying the number of radiation beams is another degree of freedom. We illustrate this aspect for the case of two-photon transitions. It has been shown that the dynamical factors in the two-photon transition rate are either symmetric (for transitions to states which have symmetries corresponding to the spherical $l = 0, 2$ symmetries) or antisymmetric ($l = 1$) for the exchange of the photon frequencies [11]. This can imply that states with a crystal symmetry which corresponds to the spherical $l = 1$ symmetry turn out to be forbidden in the case of one-beam spectroscopy. In this way an additional selection rule

can occur. Therefore, the possibility of studying absorption with either one or two beams can be used in order to determine the symmetry of excited states. In general, in multiphoton transitions, permutation symmetry of the photons affects the polarization dependence by making some dynamical factors vanish, which can sometimes lead to additional selection rules.

All the aforementioned aspects demonstrate the richness of multiphoton phenomena. However, there are some experimental problems which have to be settled [12]. For instance in two-photon spectroscopy, in order to profit from the flexability of the technique, two light sources are needed, one of which should be tunable. Generally, as two-photon phenomena are second-order effects, the two-photon absorption coefficient is much smaller as compared to the one-photon one, and at least one of the light sources should be a high-power laser. In order to measure the two-photon absorption coefficient, it is necessary to detect a change in transmission. As this change is small with respect to the background, signal-to-noise problems can occur. The absorption can be increased by using higher power densities for either of the two sources, because the number of absorbed photons is proportional to the intensities of both light sources. It is interesting to compare the Raman effect to the two-photon absorption. In the Raman effect, which is also a second-order effect, one photon is absorbed and one emitted. Though two photons are involved in both processes, two-photon absorption requires a more difficult technique than Raman experiments. The Raman measurement is simpler: it only requires one light source, and, instead of measuring an absorption coefficient, one just has to detect the emitted photon. In addition, the order of magnitude of the two effects is considerably different [12]. In fact, in two-photon absorption the transition probability is proportional to the occupation numbers of both sources, whereas in the Raman effect it is

proportional only to that of one source, as one of the photons is now emitted.

From a theoretical point of view there are some peculiar problems which have to be addressed. The formula for the two-photon transition rate, which is obtained from second-order time-dependent perturbation theory, contains a summation over all the eigenstates of the system (intermediate states). As these states are in general unknown, the calculation of the transition rate is complicated, and can be carried out exactly only for simple systems such as the hydrogen atom. It is therefore often necessary to adopt models in which it is possible to calculate the eigenstates. As these models may introduce non-local potentials, particular care must be taken in the coupling to the electromagnetic field in order to preserve gauge-invariance of the physical properties. Another problem consists in the determination of the polarization dependence of the transitions. This problem is strongly related to the permutation symmetry of the photons, which can make some dynamical factors vanish.

## 1.2 Present contribution

In this thesis we will be concerned with some peculiar aspects of multiphoton transitions in solids. In order to study different aspects, we have chosen to consider two types of materials among those which are presently studied experimentally. For the first system we consider, we perform a calculation of the two-photon absorption spectrum for given polarizations. In this case, we have to consider the problem of summing over intermediate states. In the second system, we are interested in the polarization dependence of three-photon transitions. As a framework which includes the cases in which three or more photons are absorbed is lacking, we develop a general symmetry analysis.

As a first application, we have studied two-photon transitions in GaAs-$Ga_{1-x}Al_xAs$ quantum wells (QW's). These systems consist of a central GaAs layer sandwiched between two layers of $Ga_{1-x}Al_xAs$. Because of the smaller band gap of GaAs, the electrons in the conduction band as well as the holes in the valence band are mainly confined in the GaAs layer. The confinement of the carriers can be accounted for by including abrupt potential barriers in the effective mass Hamiltonian. Because of the quantization of the energy levels in the growth direction, the energy dispersion consists of a two-dimensional subband structure.

The motivation of this study is twofold. Firstly, two-photon transitions in QW's have recently been studied experimentally [13, 14]. Photoluminescence excitation spectra have been provided for polarization of the radiation in the layer planes and along the growth direction. The spectra for the two non-equivalent polarizations are considerably different reflecting the anisotropy of the QW system. The shape of the absorption curve, the energies at which new subband-subband transitions occur, as well as the excitonic effects differ considerably for the two polarizations. In this thesis, we will be concerned with the interpretation of those experimental spectra.

Secondly, the problem of the summation over the intermediate states appears to be an interesting challenge in the QW system. Different kinds of problems occur. First of all a two-band approximation is adopted in order to describe the quantum well system. In order to maintain gauge-invariance, the electromagnetic field is coupled to the current of the quantum system. Because of non-local effects, it turns out that the usual $\mathbf{A} \cdot \mathbf{p}$ interaction gives different results. We will calculate the transition rate with different interaction Hamiltonians pointing out this effect. Furthermore, we have used different techniques to perform the

summation over intermediate states. In the case of subband-subband transitions we have developed a new formulation based on distribution theory which allows us to perform the summation over all the states of our model Hamiltonian. Another technique is used in the calculation of the transition rate to exciton states. We apply successfully a new variational calculation which gives the transition rate without requiring a precise knowledge of all the eigenstates of the system [15].

In experiments on alkali halides three-photon spectroscopy has been used to detect excitonic transitions [16, 17, 18]. It has been possible to excite lines which were neither observable in one- nor in two-photon spectroscopy. These recent experimental observations have been the motivation for the second application of this thesis. In fact, these experiments called for a better understanding of the selection rules and the polarization dependence of three-photon transitions. We cope with this problem developing a symmetry analysis which gives the polarization dependence of multiphoton transitions for any crystal point group. Particular emphasis is given to the cases in which some or all of the absorbed photons have equal polarizations or frequencies. We show that the dynamical factors which appear in the $n$-photon transition rate transform like irreducible representations of the permutation group of $n$ elements. It is thus possible to predict which dynamical factors vanish when some or all of the photon frequencies are equal. In some cases, permutation symmetry of the photons can lead to more stringent selection rules, in addition to dipole and geometrical selection rules. Application of our theory to the case of three-photon transitions in alkali halides gives an interpretation of the absorption spectra.

The thesis is organized as follows. In Chapter 2, we give a brief discussion of different methods which can be used to cope with the problem of the interme-

diate states. We also point out the problem of gauge-invariance and describe in which way gauge-invariance of the physical properties can be preserved in the case of model Hamiltonians which contain non-local potentials. In Chapter 3, we develop a general symmetry analysis which gives the polarization dependence and the dynamical factors for multiphoton transitions. The applications to quantum wells and alkali halides are given in Chapter 4 and Chapter 5, respectively. Concluding remarks can be found in Chapter 6.

# Chapter 2

# Problem of intermediate states

In this chapter we will consider theoretical problems which occur in the calculation of multiphoton transition rates. We will consider the case of two-photon transitions, which is the simplest one and already contains the main difficulties. The two-photon transition rate can be obtained from second-order perturbation theory. The transition amplitude contains a sum over all the intermediate states of the system. The presence of this sum is the main difference with respect to one-photon transitions. For the calculation of the one-photon transition rate, only a good description of the initial and final states is required, whereas, for the two-photon transition rate, it is necessary to have access to a complete set of intermediate states. In the case of intermediate resonance, the contributions of all non-resonant intermediate states are small, and accurate results can be obtained retaining in the sum only the resonant state.

In the first calculations of two-photon interband transition rates in solids, only one virtual intermediate band was considered [19, 20]. Following Loudon [21], who pointed out that electronic transitions must produce exciton states, Mahan calculated two-photon transition rates to exciton states in a two-band

model [22]. He assumed that the intermediate states are exciton states which are related to the same bands as the final exciton state. Within this model the exciton states are described by a hydrogen-like effective mass theory, and, therefore, it has been possible to consider all the intermediate exciton states related to the considered bands. Mahan's calculations were successful in explaining many experimental results. The effect due to remote bands could evidently be neglected because of the energy denominators in the two-photon transition rate.

As a complete description of all intermediate states is often impossible, the usual procedure is to consider only a limited number of states. These states are assumed to give the relevant contribution to the transition rate. In this way, only a limited number of states have to be described by the theory. However, this procedure gives rise to a gauge question.

## 2.1 Question of gauge

It is known that the choice of the gauge determines the explicit form of the electron-photon interaction, although, of course, the physical quantities are independent of this choice. Commonly used interaction forms are $-\mathbf{A}\cdot\mathbf{p}e/mc$ and $-\mathbf{E}\cdot\mathbf{x}e$, which are named velocity gauge and length gauge, respectively. In first-order perturbation, the equivalence of the two expressions can easily be demonstrated using the resonance condition which relates the energy separation between initial and final state to the photon energy. In second-order perturbation, the equivalence can still be shown provided also the completeness of the set of intermediate states is used explicitly [23]. The demonstration has been extended to all orders of perturbation theory [24]. Finally, the gauge-invariance has been proved for a general gauge transformation to all orders in perturbation

theory [25].

Bassani, Forney, and Quattropani calculated the $1s$–$2s$ two-photon transition rate in hydrogen verifying explicitly that the transition rate is independent of whether the velocity or length gauge is used [26]. The whole set of eigenfunctions of the hydrogen atom were taken as intermediate states. They showed that summations over part of this set yield results which differ by orders of magnitude for the two gauges. Thus, although the calculated transition rate is gauge-invariant if the sum is carried out over the complete set, the partial contribution of the same intermediate states are not equal for different interaction forms. This is an important question in connection with the problem of using incomplete basis sets, as is usually done for calculations in solids.

As in most problems in physics one does not have the luxury of a complete set of exact eigenfunctions, it is important to address the problem of obtaining gauge-invariant results when only a part of the eigenstates are known. An important contribution in this direction has been given by Robinson [27]. He proposed an approximation scheme in which gauge-invariant transition rates can be calculated even if only a limited number of intermediate states are known. His scheme relies on one free parameter and therefore its application is not straightforward. However, he showed that only a very limited number of intermediate states and one external parameter are necessary to reproduce the transition rate as a function of the photon frequencies, provided one works in a gauge-invariant scheme. An important message which one should retain from Robinson's contribution is that, whatever approximation is used, it is important to work in a gauge-invariant scheme.

In order to perform explicit calculations of transition rates in solids, the many-body Hamiltonian is usually abandoned and an effective Hamiltonian,

which we will call model Hamiltonian, is promoted to replace it. All the eigenstates of the model Hamiltonian are assumed to be more or less known (in order to satisfy this condition it is often necessary to reduce the Hilbert space to the one spanned by the eigenstates which are effectively known). Since model Hamiltonians may contain nonlocal potentials, particular attention must be paid to the coupling to the electromagnetic field. Starace has shown that, in order to preserve gauge-invariance, the electromagnetic field should be coupled to the current of the model Hamiltonian [28]. This brings to a new interaction form, $\mathbf{A} \cdot \mathbf{v}e/c$, where $\mathbf{v}$ is the velocity, which we will refer to as the current gauge. In the case of model Hamiltonians containing only local potentials, $\mathbf{v} = \mathbf{p}/m$, and the current gauge turns out to be equivalent to the usual velocity gauge. Girlanda, Quattropani and Schwendimann have generalized the results of Starace for the treatment of multiphoton transitions [29]. Such non local effects have been studied in bulk semiconductors for electromagnetic transitions to exciton states [29] and for interband transitions in the presence of an external magnetic field [30].

## 2.2 Methods to perform the sum over intermediate states

We assume now that we have decided which model Hamiltonian is relevant for the physical problem we are interested in and that the coupling question has been settled. We are thus left with the problem of performing the sum over the intermediate states.

### Explicit summation

We first suppose that the exact eigenfunctions are explicitly known. In this case, the matrix elements can be calculated explicitly. The sum can then be performed, e.g. analogously as has been done for the hydrogen atom [26]. If the intermediate states are continuum states, the sum can be turned into an integral and no particular problems arise. It may occur that intermediate as well as initial or final states happen to be continuum states. In this case the summation is more complicated. In Chapter 4, we will treat such a problem within the formalism of distribution theory.

In the more general situation only a limited number of eigenstates are explicitly known. The other eigenstates, which we feel cannot be omitted in our basis set, are only known implicitly through the eigenvalue equation. Although the complete solution of the eigenvalue problem is often possible, it is in practice a too difficult task. It is therefore important to develop summation methods which do not require a precise knowledge of all the eigenstates.

### Green function method

One way out of this problem is to use the method of Green functions. The transition amplitude can be expressed as a matrix element between initial and final state replacing the sum over intermediate state by a Green function [22, 31]. In simple systems such as the hydrogen atom, the Green function is known and the transition rate can be expressed as an integral [22]. This method seems unpractible to be extended to more complicated systems. Within the Green function formalism, it can be shown that the transition amplitude can be expressed as a matrix element of the final state and one particular state which is solution of a nonhomogeneous equation [32]. Baroni and Quattropani have de-

scribed a numerical technique to solve this equation [31]. The method has been applied to the hydrogen atom but can be extended to treat more complicated systems. A technique based on Green functions has also been used in connection with multiphoton ionization processes in atoms [33].

### Variational method

Another, much more efficient, procedure, which we will refer to as the variational method, has recently been put forward by Quattropani and Binggeli [15]. This method deserves a detailed description. A variational basis set is chosen, which can eventually be enlarged in order to approach completeness. The Hamiltonian is diagonalized in the usual way on this variational basis. Now, the variational eigenstates and their corresponding variational energies are used as if they were the true ones in the calculation of the transition rate. The procedure is repeated enlarging the basis set until convergence is reached. The method has been shown to give very accurate results in the case of the $1s$–$2s$ two-photon transition in the hydrogen atom [15]. It has been shown that the correct results are obtained independently of the form of the interaction Hamiltonian or of the type of variational basis set.

The advantages of such a method are evident. Firstly, it is not necessary to have a precise knowledge of the exact eigenstates. In fact, the variational method gives a good description only of the lowest eigenstates. Although not all the eigenstates are known, the transition rate converges rapidly. Secondly, the matrix elements which appear in the transition amplitude are particularly simple to calculate. In fact, instead of evaluating matrix elements between the exact eigenstates, which can be extremely complicated, it is now possible to choose a convenient variational basis, which simplifies considerably the calculation of the

matrix elements.

In Chapter 4, we will apply this method to the case of exciton states in quantum well structures. Again we find rapid convergence of the transition rate, independently of the chosen basis set.

From the theoretical point of view it is an interesting problem to understand the underlying reasons for the effectiveness of this method [34]. The method turns out to be particularly easy to apply and therefore extremely useful, mainly because of two pleasant features. First, it does not seem to depend critically on the choice of the set of wave functions on which the Hamiltonian is diagonalized. Second, convergence is rapidly achieved. Both of these properties can easily be understood. In fact, the condition which has to be satisfied in order to achieve convergence of the transition rate is that one particular state is described accurately by the chosen basis set. In the following we give the formal derivation and apply it to the case of the $1s$-$2s$ two-photon transition in hydrogen.

In general, quantities which are given by second order perturbation contain summations over intermediate states. For instance, in order to calculate the rate of a two-photon transition from an initial state $\psi_i$ to a final state $\psi_f$, we must evaluate summations such as in

$$T_{if}(\omega) = \sum_n \frac{\langle \psi_f | p | \psi_n \rangle \langle \psi_n | p | \psi_i \rangle}{E_n - E_i - \hbar\omega}, \tag{2.1}$$

where $\psi_n$ are eigenstates of energy $E_n$, $p$ is the momentum operator, $E_i$ the energy of the initial state, and $\omega$ one of the photon frequencies. The full transition rate is proportional to $T_{if}(\omega_1) + T_{if}(\omega_2)$, where $\omega_1$ and $\omega_2$ are the frequencies of the radiation beams.

Following the procedure of Dalgarno and Lewis [35], we study the solution

$\phi(\psi_i, \omega)$ of the non-homogeneous equation

$$(H - E_i - \hbar\omega)|\phi\rangle = p|\psi_i\rangle. \tag{2.2}$$

The solution of this equation gives the result of (2.1) without performing the summation over the intermediate states:

$$T_{if} = \langle\psi_f|p|\phi\rangle \tag{2.3}$$

Another remarkable property is that the normalized state

$$\phi_N = \phi/\langle\phi|\phi\rangle^{1/2}, \tag{2.4}$$

satisfies

$$T_{if} = \frac{\langle\psi_f|p|\phi_N\rangle\langle\phi_N|p|\psi_i\rangle}{\langle\phi_N|H|\phi_N\rangle - E_i - \hbar\omega}. \tag{2.5}$$

In order to obtain the exact result for $T_{if}$, it is therefore sufficient to consider in the summation (2.1) only one particular state $\phi_N$, provided that the energy in the denominator is replaced by the diagonal matrix element of the Hamiltonian on that state.

We note that $\phi$ is a function of the initial state $\psi_i$ and the frequency $\omega$. The same state $\phi$ can therefore be used for different final states $\psi_f$. The particular state that satisfies (2.5) is not necessarily unique. Another state of this kind can be obtained, when one considers the solution of the differential equation obtained by replacing $\psi_i$ by $\psi_f$ in (2.2).

The result obtained can be generalized. We consider a finite set of states among which we have included $\phi$. We consider the eigenvectors $\varphi_j$ which diagonalize the Hamiltonian eigenvalue problem on this basis:

$$\langle\varphi_j|H|\varphi_{j'}\rangle = \lambda_j\delta_{jj'}, \qquad \langle\varphi_j|\varphi_{j'}\rangle = \delta_{jj'}. \tag{2.6}$$

As $\phi$ is contained in the basis set, it is possible to express it as

$$\phi = \sum_j a_j \varphi_j. \tag{2.7}$$

If we substitute expression (2.7) for $\phi$ in the differential equation (2.2) and project on $|\varphi_j\rangle$, we obtain for the $a_j$:

$$(\lambda_j - E_i - \hbar\omega) a_j = \langle \varphi_j | p | \psi_i \rangle. \tag{2.8}$$

We now evaluate

$$T'_{if} = \sum_j \frac{\langle \psi_f | p | \varphi_j \rangle \langle \varphi_j | p | \psi_i \rangle}{\lambda_j - E_i - \hbar\omega}, \tag{2.9}$$

where we have summed over the solutions $\varphi_j$ and replaced the energy $E_n$ of (2.1) by $\lambda_j$. With the use of (2.8), and then of (2.7) and (2.3), we show that the result so obtained is the same as that in (2.1):

$$T'_{if} = \sum_j \langle \psi_f | p | \varphi_j \rangle a_j = \langle \psi_f | p | \phi \rangle = T_{if} \tag{2.10}$$

In conclusion, we have shown that if the transition rate is calculated as in (2.9), replacing the true eigenfunctions with a finite number of wavefunctions which diagonalize the Hamiltonian and the energies by the eigenvalues of the finite matrix problem, the exact result is obtained, provided that the particular state $\phi$ is included among the functions in the finite basis set.

In practice, we do not know the state $\phi$. However, if we are able to choose a basis set which gives an accurate description of this state, we can obtain approximate values for the transition rate which can be very accurate. The theorems exposed here, allow us to acquire a better insight in the kind of conditions which are required to achieve convergence.

In order to illustrate the considerations exposed above, we now consider some well-known cases. As a first example, we consider the Thomas-Reiche-Kuhn sum

rule in hydrogen [36], which states that the sum of all oscillator strengths for transitions from a state $\psi_i$ is equal to one. In atomic units:

$$\sum_n \frac{4|\langle\psi_n|p_z|\psi_i\rangle|^2}{E_n - E_i} = 1, \tag{2.11}$$

which can be cast in the form (2.1) with $\psi_f = \psi_i$ and $\omega = 0$. This case is particularly interesting as the differential equation (2.2) can be solved exactly, if $\psi_i$ is the ground state. The solution is given by

$$\phi(r) = \frac{1}{\sqrt{3}} Y_{10} r e^{-r}, \tag{2.12}$$

where $Y_{10}$ is a spherical harmonic. Hence, it is sufficient to include the state (2.12) in the finite basis set, in order to obtain exactly 1, when the sum rule is evaluated as in (2.9). We note the state $\phi$ is not unique. In fact, if we add to $\phi$ a state which is proportional to the ground state, we obtain another state which satisfies Eq. (2.2).

As a second, more interesting, example is the $1s$-$2s$ transition in hydrogen. The transition rate is given by a sum of two terms as in (2.1), with $\omega = \omega_1$ and $\omega = \omega_2$, respectively. Quattropani and Binggeli [15] have shown that the transition rates converge rapidly to the correct results [26] when a variational set of $p$-type functions of the type

$$\psi_j(r) = Y_{10} r e^{-\gamma_j r} \tag{2.13}$$

is chosen, where the exponents $\gamma_j$ are chosen in a geometrical series. We have also performed such a calculation using 10 wavefunctions. The results, in the same units used in Ref. [26], are reported in Table I. Comparison to the exact results shows excellent agreement.

**Tabel I.** – Comparison between the variational and the exact calculation of the $1s$–$2s$ two-photon transition probability in hydrogen. We have used the basis set (2.13) with $1/\gamma_j = r_0 q^{j-5}$, for $j = 1, 2, ...10$, where $r_0 = 1$ (atomic units) and $q = 1.2$.

| $\omega_1$ | Variational | Exact |
|---|---|---|
| 0.3750 | 11.780483 | 11.780483 |
| 0.5250 | 14.731873 | 14.731873 |
| 0.6750 | 41.148411 | 41.148411 |
| 0.6875 | 49.687778 | 49.687778 |
| 0.7000 | 62.659474 | 62.659474 |
| 0.7125 | 84.525170 | 84.525170 |
| 0.7250 | 128.683525 | 128.683525 |
| 0.7375 | 262.165418 | 262.165419 |
| 0.7475 | 1334.32609 | 1334.32614 |

We have not yet been able to find an exact solution of Eq. (2.2) in this case. However, if we use the basis set given in (2.13) we can plot an approximate solution of the particular states $\phi_N(\psi_{1s}, \omega_1)$ and $\phi_N(\psi_{1s}, \omega_2)$ by using the coefficients as obtained with (2.8).

In Fig. 2.1, we plot the radial part of the functions $\phi_N(\psi_{1s}, \omega)$ for different values of $\omega$. In order to evaluate the $1s$-$2s$ two-photon transition rate, two particular states have to be considered, one for each photon frequency. The values of the two frequencies are related because of the resonance condition $\hbar\omega_1 + \hbar\omega_2 = 3/4$ Ry. From Fig. 2.1, we note that as $\omega$ increases the average

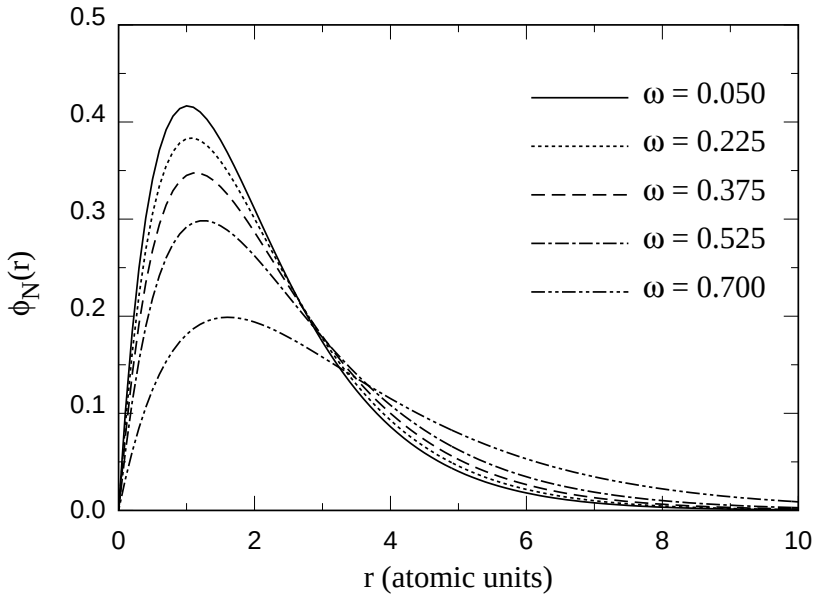


**Figure 2.1.** – Radial part of the state $\phi_N(\psi_{1s}, \omega)$ for different values of $\omega$. The frequencies $\omega$ are given in Rydberg.

radius increases. This can be understood by observing that the homogeneous equation of (2.2) corresponds to the hydrogen Schrödinger equation at an energy $E_{1s} + \hbar\omega$. The rather smooth behaviour of this state for frequencies in the range $0 < \hbar\omega < 0.75$ Ry. explains the good convergence properties of the method when a basis such as in (2.13) is used. Note that in the limiting case of $\omega = 0$, we recover the particular state (2.12) of the sum rule case.

Further work on this subject is still in progress.

# Chapter 3

# Polarization dependence

An important problem in multiphoton transitions is the polarization dependence of the transition rate. In contrast to the problem discussed in the previous chapter which required a calculation, the polarization dependence is obtained from a symmetry analysis and will depend on the symmetry group of the system under investigation.

In the most simplest cases, there is a given polarization dependence for transitions to states of a given symmetry, i.e., all transitions to states of that symmetry have the same polarization dependence. In this case, the calculation of the actual value of the transition rate and the determination of its polarization dependence are uncorrelated problems. In fact, the transition rate can be separated into a geometrical factor which contains the polarization dependence and a dynamical factor which contains the transition matrix elements [11]. Only the latter is dependent on the photon frequencies. However, this is not generally the case.

In general, the transition rate is not separable and the polarization dependence contains dynamical parameters which have different values for different

excited states of the same symmetry [37, 38, 39]. Only the number of dynamical parameters which appear in the transition rate is determined by the symmetry of the excited state. The number of dynamical parameters in the case of small point groups is generally larger than in the case of point groups of higher symmetry [37]. When the number of absorbed photons increases, generally the number of dynamical parameters increases as well [37, 38].

These dynamical parameters, which are usually unknown, are taken as free parameters and therefore a precise symmetry identification of the excited state from polarization measurements only is often difficult in multiphoton transitions. However, there is another aspect which turns out to be particularly useful in this respect. The additional degree of freedom of using photons from different beams or from the same beam, can be used to gain more information on the symmetry of excited states.

We present in this chapter a general procedure which gives the polarization dependence of multiphoton transitions. We devote particular attention to the cases in which the absorbed photons are of equal polarization or frequency. We show that the dynamical factors in the $n$-photon transition rate transform under permutation of the photon frequencies like basis-functions of irreducible representations of the permutation group of $n$ elements [40]. This implies that if some or all of the involved photons are of equal frequency, some of the dynamical factors may vanish. If for transitions to states of a particular symmetry all the dynamical factors vanish, additional selection rules occur. For example, in the case of two-photon absorption, it is known that the dynamical factors are either symmetric or antisymmetric for exchange of the photon frequencies [11]. Antisymmetric dynamical factors vanish when the absorbed photons have equal frequencies. In this case, excited states of a particular symmetry whose

transition rate contains only antisymmetric dynamical factors are forbidden. In the present analysis we show that this additional selection rule found in the case of two-photon transitions is related to the permutation symmetry of the photon frequencies and develop a general framework which allows us to deduce similar rules for cases in which more photons are absorbed. In general, permutation symmetry reduces the number of non-vanishing dynamical factors and therefore simplifies the polarization dependence. The polarization dependence turns out to be the same for all excited states of the same given symmetry if all dynamical factors but one vanish. The symmetry analysis shows that particular irreducible representations of the permutation group are associated to the allowed irreducible representations of the point group. Thus it is possible to study the symmetry of the excited states by analysing how the number of dynamical parameters in the polarization dependence varies when some or eventually all the absorbed photons are of equal frequency.

In particular we show that, when the photons are taken of equal energy *or* of equal polarization, the dipole selection rules are affected in the *same* way. The relation between the transformation properties for separate permutations of the photon frequencies and polarizations is given by the condition that the transition rate is invariant if frequencies *and* polarizations are permuted simultaneously. The invariance under permutation of all the photon quantum numbers of the electron-photon interaction is a consequence of the Bosonic character of the photons.

In the next sections, the general analysis is derived and then applied to the case of two-, three- and four-photon transitions. A general procedure is described which gives the polarization dependence for any crystal point group. In Chapter 5, this analysis is applied to the case of three-photon transitions in alkali halides

in order to interpret recent experimental spectra. The results of this chapter will be published soon [41], whereas those of Chapter 5 appeared in Ref. [42].

## 3.1 Symmetry analysis of the transition rate

The $n$-photon transition rate can be obtained from time-dependent perturbation theory. We are interested in the transition rate from the ground state of the system $|0\rangle$ to a final state $f_\nu^\alpha$ which belongs to the $\nu$th row of the representation $\alpha$ of the point group. In the dipole approximation, the transition rate is proportional to

$$\sum_\nu \left| \sum_\sigma O_\sigma \langle f_\nu^\alpha \mid \boldsymbol{\epsilon}_1^* \cdot \mathbf{P}\, \Lambda(\omega_2 + ... + \omega_n) ... \boldsymbol{\epsilon}_{n-1}^* \cdot \mathbf{P}\, \Lambda(\omega_n)\, \boldsymbol{\epsilon}_n^* \cdot \mathbf{P} \mid 0 \rangle \right|^2, \tag{3.1}$$

where the $\Lambda$ are symmetry invariant operators

$$\Lambda(\omega) = \sum_k \frac{\mid \psi_k \rangle \langle \psi_k \mid}{E_k - E_0 - \hbar\omega}, \tag{3.2}$$

the total momentum operator $\mathbf{P}$ is given by $\mathbf{P} = \sum_i \mathbf{p}_i$, and $\boldsymbol{\epsilon}_j$ and $\omega_j$ $(j = 1, ...n)$ represent the polarization vector and the frequency of the $j$th photon, respectively. The operator $O_\sigma$ permutes all the indices of the polarizations and frequencies. The sum over $\sigma$ in (3.1) stands for the sum over all the $n!$ permutations of $n$ indices. Because of this sum the expression is symmetric for a permutation of the photon indices.

We consider the operator in the matrix element in (3.1) for one particular permutation: suppose for simplicity the identity. The transition operators in (3.1) transform in the same way as $P_{i_1} P_{i_2} ... P_{i_n}$, where $i_k$ for $k = 1, ..n$ indicates the component of each momentum operator. The order in which the momentum operators appear is relevant because of the presence of the $\Lambda$ operators. These transition operators transform as a $3^n$-dimensional representation $R$ of the point

group as well as of the permutation group. Moreover, as permutation operators and symmetry operators of the point group commute, the transition operators also transform as a $3^n$-dimensional representation of the group which is obtained as a direct product of the point group and the permutation group. The representation $R$ can therefore be decomposed into the irreducible representations of this direct product group, which are direct products of the irreducible representations of the point group and the permutation group. Expression (3.1) can be rewritten by decomposing the transition operators into operators $T^{(\alpha'\beta)}_{\nu'\lambda}$, which transform as the $\nu'$th row of the irreducible representation $\alpha'$ of the point group under space operators and as the $\lambda$th row of the the irreducible representation $\beta$ of the permutation group under permutations of the component indices $i_k$. Expression (3.1) reads now

$$\sum_{\nu}\left|\sum_{\sigma} O_\sigma \sum_{n,(\alpha'\beta)} \sum_{\nu'=1}^{l_{\alpha'}} \sum_{\lambda=1}^{l_\beta} [\phi^{n,(\alpha'\beta)}_{\nu'\lambda}(\boldsymbol{\epsilon}_1,...\boldsymbol{\epsilon}_n)]^* \langle f^\alpha_\nu \mid T^{n,(\alpha'\beta)}_{\nu'\lambda}(\omega_1,...\omega_n) \mid 0\rangle\right|^2, \quad (3.3)$$

where the index $n$ labels identical representations $(\alpha'\beta)$ which can occur more than once and where $l_{\alpha'}$ and $l_\beta$ are the dimensions of the representations $\alpha'$ and $\beta$, respectively. The $\phi$'s are expressions of the polarization vectors,

$$\phi^{n,(\alpha\beta)}_{\nu\lambda}(\boldsymbol{\epsilon}_1,...\boldsymbol{\epsilon}_n) = \sum_{i_1,...i_n} c^{n,(\alpha\beta),\nu\lambda}_{i_1...i_n} \epsilon_{1i_1}...\epsilon_{ni_n}, \quad (3.4)$$

where the $c^{n,(\alpha\beta),\nu\lambda}_{i_1...i_n}$ are the analogous of the Clebsch-Gordan coefficients. With the use of the Wigner-Eckart theorem, we derive that the transition operators must have the same symmetry as the final state, and the above expression simplifies to

$$\sum_{\nu}\left|\sum_{\sigma} O_\sigma \sum_{n,\beta} \sum_{\lambda=1}^{l_\beta} [\phi^{n,(\alpha\beta)}_{\nu,\lambda}(\boldsymbol{\epsilon}_1,...\boldsymbol{\epsilon}_n)]^* \langle f^\alpha \mid\mid T^{n,(\alpha\beta)}_{\lambda}(\omega_1,...\omega_n) \mid\mid 0\rangle\right|^2, \quad (3.5)$$

where standard notation has been used for the reduced matrix elements. Because of the scalar products in (3.1), the $\phi$'s have the same transformation properties as the $T$'s. We note that as the different $\epsilon_{ki_k}$ are labelled by the photon index $k$, a permutation of the component indices $i_k$ yields the same result as the same permutation of the photon indices $k$. Thus the $\phi$'s transform under the operators $O_\sigma$ according to the irreducible representation $\beta$ of the permutation group. On the other hand the $T_\lambda^{n,(\alpha\beta)}$ do not transform as any irreducible representation when the indices of the photon frequencies are permuted. However, if the effect of the $O_\sigma$ on the $\phi$'s in (3.5) is worked out, it can be seen that the $T$'s are projected on the same irreducible representation $\beta$ to which the $\phi$'s belong. A detailed derivation is given in Appendix A. We obtain:

$$\sum_\nu \left| \sum_{n,\beta} \sum_{\lambda=1}^{l_\beta} [\phi_{\nu,\lambda}^{n,(\alpha\beta)}(\boldsymbol{\epsilon}_1, \ldots \boldsymbol{\epsilon}_n)]^* D_\lambda^{n,(\alpha\beta)}(\omega_1, \ldots \omega_n) \right|^2 , \tag{3.6}$$

where the $D_\lambda^{n,(\alpha\beta)}$ are the projected $T$'s. The explicit expression of the $D_\lambda^{n,(\alpha\beta)}$ as a function of the $T$'s is given in Appendix A.

Some important remarks can be made on the result (3.6). First, according to the symmetry $\alpha$ of the excited state not only the polarization dependence is different, as was expected [37, 38], but in general also the associated permutation symmetries $\beta$ are different. In fact, in the decomposition of the transition operator into the irreducible representations of the product group, product representations are found which relate representations of the permutation group to representations of the point group.

Second, in the polarization dependence of the transition rate, a certain number of dynamical factors $D$ can appear. These factors have different values for different excited states of a given symmetry. If more than one dynamical factor appears in (3.6) the polarization dependence is not dependent on symmetry

alone and contains $N_\alpha - 1$ dynamical parameters, where $N_\alpha$ is the number of dynamical factors in (3.6). The number $N_\alpha$ corresponds to the number of times the representation $\alpha$ appears in the decomposition of the representation $R$ of the transition operators into the irreducible representations of the point group. If $N_\alpha = 1$, the transition rate is a simple product of geometrical and dynamical factors and the polarization dependence of the transition rate is the same for all final states of symmetry $\alpha$.

Third, expression (3.6) shows that the dynamical factors transform under permutations of the frequencies according to irreducible representations of the permutation group of $n$ elements. This result is very useful in order to determine which dynamical factors vanish when some or all the photons have the same frequency. This aspect is analysed in detail in the next section for the cases of two-, three-, and four-photon transitions.

Fourth, the transformation properties of the dynamical factors $D$ under permutation of the photon frequencies are exactly the same as those of the corresponding geometrical factors $\phi$ under permutations of the photon polarizations. In fact, because of this property the whole expression (3.6) is still invariant for permutation of all the photon indices, although the projector $\sum_\sigma O_\sigma$ does not appear explicitly any more. The fact that the transition rate is symmetric under permutation of the photon indices follows directly from the Bosonic character of the photons. The formulation in Eq. (3.6) is useful because it emphasizes the transformation properties of geometrical and dynamical factors separately. For instance, in two-photon transitions, if the dynamical factor vanishes for equal frequencies, we know that the corresponding geometrical factor vanishes for equal polarizations.

We conclude this section with some remarks on the $n$-photon transition rate

(3.1). This formula is obtained by supposing that the absorption occurs taking one photon from each of the $n$ beams which are focused on the sample. The total energy which is needed to reach the final state corresponds to the sum of all the photon energies. If some of the beams have equal energy (but not necessarily equal polarization), it is also possible to reach the final state by taking two photons from the same beam. Because of this possibility additional terms appear within the square modulus of formula (3.1) for the transition rate. These other terms, which are omitted in (3.1), can be analysed in the same way. When this occurs the polarization dependence of the transition rate can be dependent on the relative intensities and phases of the electromagnetic fields of the radiation beams.

We have analysed explicitly the case of $n$-photon absorption processes. If a photon is emitted as occurs for example in hyper-Raman scattering [43] or in difference-frequency generation [9], the polarization vector of the emitted photon has to be replaced by its complex conjugate and its frequency $\omega$ by $-\omega$.

We note that all the conclusions of this chapter are based on an analysis of the transition rate (3.1) in the dipole approximation. In this approximation the only relevant quantum numbers of the photons are their frequencies and polarization vectors, as their wave vectors do not appear in formula (3.1). Nevertheless, the analysis can be applied to derive selection rules for longitudinal and transversal excitations, e.g. the longitudinal exciton (LE) and the transverse polaritons (TP). In this case the interaction with the electromagnetic radiation yields a symmetry reduction with respect to the symmetry of the point group. The polarization dependence can be found analogously by decomposing the excited state in components which are parallel (for LE) or perpendicular (for TP) to the total wave vector [44].

## 3.2 Application to two-, three-, and four-photon transitions

In this section we apply the theory to the cases of two-, three- and four-photon transitions with a particular emphasis on the effects due to permutation symmetry. We will first take as symmetry group of the system the full spherical group $O(3)$, which includes all proper and improper rotations in three dimensions. As $O(3)$ contains all the crystal point groups, the results for a particular point group follow easily making use of compatibility relations. For the point groups we will use the notation of Koster *et al.* [45]. We will study in detail the point groups $O_h$, $T_d$ and $C_{6v}$, which correspond to the cubic, zincblende and wurtzite structure, respectively. We will limit ourselves to the case of $n$-photon absorption processes from the crystal ground state.

### 3.2.1 Two-photon transitions

The polarization dependence of two-photon transitions has been studied for all the crystal point groups. It is well known that dynamical factors can either be symmetric or antisymmetric for the exchange of the photon frequencies [11]. A tabulation of all possible cases can be found in the paper by Inoue and Toyozawa [37]. In this subsection, we apply our formulation in order to recover these results and to illustrate the procedure in a simple case. As we will show, our procedure is particularly useful in the more complicated cases in which three or more photons are absorbed.

The transition operators transform as $P_{i_1} P_{i_2}$ and form a 9-dimensional representation $R$ of the group $O(3)$, of the permutation group of two elements $S_2$ and of the product group $O(3) \otimes S_2$. We decompose the representation $R$ into

irreducible representations of these three groups:

$$O(3) \quad : \qquad R \to D_0^+ \oplus D_1^+ \oplus D_2^+, \tag{3.7}$$

$$S_2 \quad : \qquad R \to 6\tilde{\Gamma}_1^+ \oplus 3\tilde{\Gamma}_1^-, \tag{3.8}$$

$$O(3) \otimes S_2 \quad : \qquad R \to D_0^+ \cdot \tilde{\Gamma}_1^+ \oplus D_1^+ \cdot \tilde{\Gamma}_1^- \oplus D_2^+ \cdot \tilde{\Gamma}_1^+, \tag{3.9}$$

where the $D_j^{\pm}$'s represent the well known irreducible representations of $O(3)$ and $\tilde{\Gamma}_1^+$ and $\tilde{\Gamma}_1^-$ are the onedimensional symmetric and antisymmetric representations of $S_2$, respectively. We will denote the representations of the permutation groups by $\tilde{\Gamma}_k^{\pm}$, where $k$ is the dimensionality of the representation and the sign indicates whether the representation has a positive or negative character for the exchange of two elements. The representations of $O(3) \otimes S_2$ have been indicated as products of representations of its subgroups. We note that the representation of highest angular momentum transforms necessarily as the total symmetric representation of the permutation group.

Lets consider for example the case of the point group $O_h$. By use of compatibility tables we deduce from Eqs. (3.7) and (3.9):

$$O_h \quad : \qquad R \to \Gamma_1^+ \oplus \Gamma_3^+ \oplus \Gamma_4^+ \oplus \Gamma_5^+, \tag{3.10}$$

$$O_h \otimes S_2 \quad : \qquad R \to \Gamma_1^+ \cdot \tilde{\Gamma}_1^+ \oplus \Gamma_3^+ \cdot \tilde{\Gamma}_1^+ \oplus \Gamma_4^+ \cdot \tilde{\Gamma}_1^- \oplus \Gamma_5^+ \cdot \tilde{\Gamma}_1^+. \tag{3.11}$$

All symmetries of the point group appear just once in the decomposition of $R$ into the irreducible representations of $O_h$ and therefore the polarization dependence is the same for all transitions to states of a given symmetry. Only the dynamical factors of transitions to $\Gamma_4^+$ states are antisymmetric with respect to the exchange of the frequencies. In the case of two radiation beams of equal frequency, transitions to $\Gamma_4^+$ states are forbidden. We note that the additional terms which appear in the transition rate because of the possibility of absorbing

two photons of the same beam, vanish for the same reason. Another important remark is that also the geometrical factor of $\Gamma_4^+$ transitions is antisymmetric for the exchange of the two polarization vectors. Hence, in the case of two beams of different frequency but equal polarization, $\Gamma_4^+$ states cannot be detected. Of course, in the case of one-beam two-photon spectroscopy (equal frequency and equal polarization) the transition rate vanishes as well.

For the point group $T_d$, the conclusions are identical to the case of $O_h$ apart from the fact that parity is no longer a good quantum number. In fact in two-photon spectroscopy it is possible to excite states which are also excited in one-photon spectroscopy (states of $\Gamma_5$ symmetry):

$$T_d \quad : \qquad R \to \Gamma_1 \oplus \Gamma_3 \oplus \Gamma_4 \oplus \Gamma_5, \tag{3.12}$$

$$T_d \otimes S_2 \quad : \qquad R \to \Gamma_1 \cdot \tilde{\Gamma}_1^+ \oplus \Gamma_3 \cdot \tilde{\Gamma}_1^+ \oplus \Gamma_4 \cdot \tilde{\Gamma}_1^- \oplus \Gamma_5 \cdot \tilde{\Gamma}_1^+. \tag{3.13}$$

As another example we consider the group $C_{6v}$ which is the point group of the wurzite structure. We find:

$$C_{6v} \quad : \qquad R \to 2\Gamma_1 \oplus \Gamma_2 \oplus 2\Gamma_5 \oplus \Gamma_6, \tag{3.14}$$

$$C_{6v} \otimes S_2 \quad : \qquad R \to 2\Gamma_1 \cdot \tilde{\Gamma}_1^+ \oplus \Gamma_2 \cdot \tilde{\Gamma}_1^- \oplus \Gamma_5 \cdot \tilde{\Gamma}_1^+ \oplus \Gamma_5 \cdot \tilde{\Gamma}_1^- \oplus \Gamma_6 \cdot \tilde{\Gamma}_1^+. \tag{3.15}$$

For this point group it is not always possible to express the transition rate as a simple product of dynamical and geometrical factors. In the case of excited states of $\Gamma_1$ or $\Gamma_5$ symmetry, there are two dynamical factors and therefore one dynamical parameter appears in the polarization dependence. The transition rates of $\Gamma_2$ and $\Gamma_6$ contain just one dynamical factor and their polarization dependence is thus independent of dynamical parameters. In the case of photons of equal frequency, transitions to $\Gamma_2$ states are forbidden analogously to the case

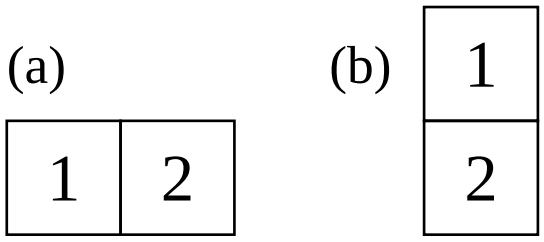


**Figure 3.1.** – Young diagrams for the projectors on the rows of the irreducible representations of the permutation group of two elements $S_2$: (a) $\tilde{\Gamma}_1^+$, the symmetric representation, and (b) $\tilde{\Gamma}_1^-$, the antisymmetric representation.

of transitions to $\Gamma_4^+$ states in $O_h$. For $\Gamma_1$ transitions the two dynamical factors are both symmetric for the exchange of frequencies, whereas for $\Gamma_5$ transitions one is symmetric and the other antisymmetric. In the case of photons of equal frequency, the polarization dependence of transitions to $\Gamma_1$ states will therefore still contain one dynamical parameter. On the other hand, for $\Gamma_5$ transitions, the antisymmetric dynamical factor vanishes and the polarization dependence will thus be identical for all $\Gamma_5$ states. Care must be taken in the transition rate of $\Gamma_5$ states in the case of two beams of equal frequency. Now the symmetric geometrical and dynamical factors which correspond to the case of two photons being absorbed from the same beam do not vanish and must be accounted for in the polarization dependence.

In order to use a handy formulation we introduce Young diagrams which represent projectors on the rows of the representations of the permutation group [40]. The representations of $S_2$ are one-dimensional and can be represented as

in Fig. 3.1. The projectors associated to the diagrams act by first taking the symmetric part with respect to the indices which are contained in the horizontal boxes and then the antisymmetric part with respect to those which appear in the same vertical column. It is evident that the result will vanish if the Young projector is applied on expressions which are invariant for exchanges of indices which appear in the same column.

### 3.2.2 Three-photon transitions

Recently there has been an increased interest in the use of three-photon spectroscopy to investigate electronic states in crystals [18]. Since there are many allowed states, the understanding of the polarization dependence of the transitions is particularly useful. For the case of absorption processes of three photons of equal frequency and polarization, the polarization dependence has been tabulated for all crystal point groups [38]. As already pointed out [42], Ref. [46] contains incorrect statements.

We start our analysis as in the case of two-photon transitions with the full spherical group $O(3)$. The transition operators transform as a 27-dimensional representation of $O(3)$, of $S_3$ and of $O(3) \otimes S_3$:

$$O(3) \quad : \qquad R \to D_0^- \oplus 3D_1^- \oplus 2D_2^- \oplus D_3^- , \tag{3.16}$$

$$S_3 \quad : \qquad R \to 10\tilde{\Gamma}_1^+ \oplus 8\tilde{\Gamma}_2 \oplus \tilde{\Gamma}_1^- , \tag{3.17}$$

$$O(3) \otimes S_3 \quad : \qquad R \to D_0^- \cdot \tilde{\Gamma}_1^- \oplus D_1^- \cdot \tilde{\Gamma}_1^+ \oplus D_1^- \cdot \tilde{\Gamma}_2 \oplus D_2^- \cdot \tilde{\Gamma}_2 \oplus D_3^- \cdot \tilde{\Gamma}_1^+ . \tag{3.18}$$

The permutation group of three elements $S_3$ has three kinds of irreducible representations: the symmetric representation $\tilde{\Gamma}_1^+$, the antisymmetric representation $\tilde{\Gamma}_1^-$ and a twodimensional representation $\tilde{\Gamma}_2$. The associated Young diagrams

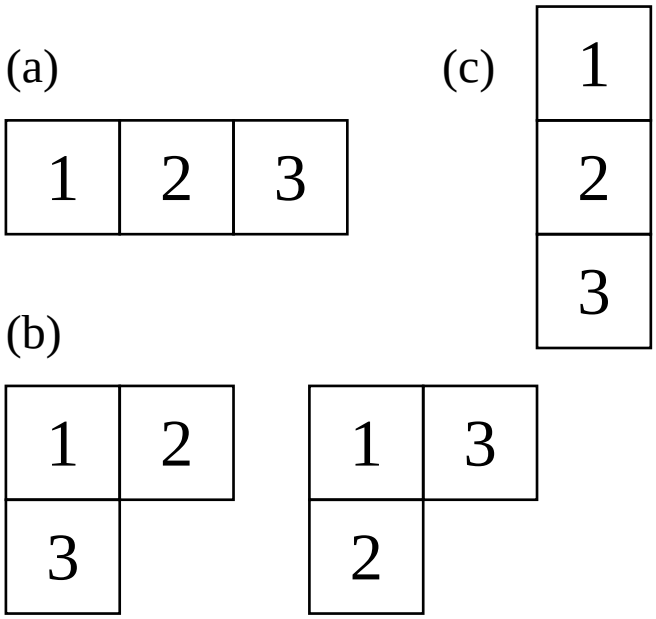


**Figure 3.2.** – Young diagrams for the projectors on the rows of the irreducible representations of the permutation group of three elements $S_3$: (a) $\tilde{\Gamma}_1^+$, the symmetric representation, (b) $\tilde{\Gamma}_2$, the twodimensional representation, and (c) $\tilde{\Gamma}_1^-$, the antisymmetric representation.

are given in Fig. 3.2. Dynamical or geometrical factors which transform as $\tilde{\Gamma}_1^+$ do not vanish even if the three absorbed photons are equal. On the other hand dynamical (geometrical) factors which transform as $\tilde{\Gamma}_1^-$ vanish unless the three photons have three different frequencies (polarizations). In the case of the $\tilde{\Gamma}_2$ representation there are two dynamical factors which appear together and transform according to the two rows of the representation. The rows which are defined by the projectors in Fig. 3.2 represent one possible choice. If the frequencies of the three involved photons are taken to be equal both of the $\tilde{\Gamma}_2$ dynamical factors vanish. In fact, if the dynamical factors are chosen to transform as defined by the projectors in Fig. 3.2 the first is antisymmetric for the exchange of the frequencies of photon 1 and photon 3, whereas the second for the exchange of the frequencies of photon 1 and photon 2. If only two frequencies are equal, for instance those of photon 1 and photon 2, the first dynamical factor contributes whereas the second vanishes. The same reasoning applies for the geometrical factors in the case of equal polarizations. From Eq. (3.18), we see how the dynamical factors in the transition rates of states of a given symmetry transform under permutations. In particular the transition rate of states of $D_1^-$ symmetry contains 3 dynamical factors; one which transforms as $\tilde{\Gamma}_1^+$ and two as $\tilde{\Gamma}_2$. In the case of photons of equal frequency the nonvanishing dynamical factors are deduced as discussed above.

In the following part of this subsection we illustrate our analysis in the case of the $O_h$, $T_d$ and $C_{6v}$ point groups. The polarization dependence for these groups is given in Appendix B. An analogue analysis can be carried out for any point group.

For the $O_h$ point group the transition operator transforms as

$$O_h \quad : \qquad R \rightarrow \quad \Gamma_1^- \oplus \Gamma_2^- \oplus 2\Gamma_3^- \oplus 4\Gamma_4^- \oplus 3\Gamma_5^-, \tag{3.19}$$

$$O_h \otimes S_3 \quad : \qquad R \rightarrow \quad \Gamma_1^- \cdot \tilde{\Gamma}_1^- \oplus \Gamma_2^- \cdot \tilde{\Gamma}_1^+ \oplus \Gamma_3^- \cdot \tilde{\Gamma}_2 \oplus 2\Gamma_4^- \cdot \tilde{\Gamma}_1^+ \\ \oplus \Gamma_4^- \cdot \tilde{\Gamma}_2 \oplus \Gamma_5^- \cdot \tilde{\Gamma}_1^+ \oplus \Gamma_5^- \cdot \tilde{\Gamma}_2. \tag{3.20}$$

If only one radiation beam is used, only states of $\Gamma_2^-$, $\Gamma_4^-$ and $\Gamma_5^-$ symmetry can be excited. The polarization dependence of $\Gamma_2^-$ and $\Gamma_5^-$ states have only one dynamical factor and thus contain no dynamical parameters. In the case of $\Gamma_4^-$ transitions, there is one dynamical parameter as the representation $\Gamma_4^- \cdot \tilde{\Gamma}_1^+$ appears twice in the decomposition of $R$. If two beams are used, also $\Gamma_3^-$ states are observable. The polarization dependence of $\Gamma_2^-$ transitions still has no dynamical parameters, whereas those of $\Gamma_4^-$ and $\Gamma_5^-$ acquire one parameter more. Finally with three photons of different frequency and polarization it is also possible to observe the $\Gamma_1^-$ states. In the latter case the number of dynamical factors which occur in the polarization dependence of transitions to states of a given symmetry is given by the number of times that symmetry appears in the decomposition of $R$: 1 for $\Gamma_1^-$ and $\Gamma_2^-$, 2 for $\Gamma_3^-$, 4 for $\Gamma_4^-$, and 3 for $\Gamma_5^-$.

The representation $R$ of transition operators decomposes as follows into irreducible representations of $T_d$ and $T_d \otimes S_3$:

$$T_d \quad : \qquad R \rightarrow \quad \Gamma_1 \oplus \Gamma_2 \oplus 2\Gamma_3 \oplus 3\Gamma_4 \oplus 4\Gamma_5, \tag{3.21}$$

$$T_d \otimes S_3 \quad : \qquad R \rightarrow \quad \Gamma_1 \cdot \tilde{\Gamma}_1^+ \oplus \Gamma_2 \cdot \tilde{\Gamma}_1^- \oplus \Gamma_3 \cdot \tilde{\Gamma}_2 \oplus \Gamma_4 \cdot \tilde{\Gamma}_1^+ \\ \oplus \Gamma_4 \cdot \tilde{\Gamma}_2 \oplus 2\Gamma_5 \cdot \tilde{\Gamma}_1^+ \oplus \Gamma_5 \cdot \tilde{\Gamma}_2. \tag{3.22}$$

Knowing the relation between permutation symmetry and point group symmetry it is now simple to deduce as above the number of nonvanishing dynamical factors for each possible configuration of the photons. In particular we note that for three photons of equal frequency $\Gamma_1$, $\Gamma_4$ and $\Gamma_5$ states can be excited. We note that $\Gamma_5$ states are observable in *one*-beam spectroscopy either absorbing one, two or three photons.

As a final example, we give the decomposition of $R$ for the $C_{6v}$ point group:

$$C_{6v} \quad : \qquad R \to \quad 4\Gamma_1 \oplus 3\Gamma_2 \oplus \Gamma_3 \oplus \Gamma_4 \oplus 6\Gamma_5 \oplus 3\Gamma_6, \tag{3.23}$$

$$\begin{aligned} C_{6v} \otimes S_3 \quad : \qquad R \to \quad & 2\Gamma_1 \cdot \tilde{\Gamma}_1^+ \oplus \Gamma_1 \cdot \tilde{\Gamma}_2 \oplus \Gamma_2 \cdot \tilde{\Gamma}_1^- \oplus \Gamma_2 \cdot \tilde{\Gamma}_2 \\ & \oplus \Gamma_3 \cdot \tilde{\Gamma}_1^+ \oplus \Gamma_4 \cdot \tilde{\Gamma}_1^+ \oplus 2\Gamma_5 \cdot \tilde{\Gamma}_1^+ \oplus 2\Gamma_5 \cdot \tilde{\Gamma}_2 \\ & \oplus \Gamma_6 \cdot \tilde{\Gamma}_1^+ \oplus \Gamma_6 \cdot \tilde{\Gamma}_2. \end{aligned} \tag{3.24}$$

Representations of $C_{6v}$ are either onedimensional, like $\Gamma_1$, $\Gamma_2$, $\Gamma_3$ and $\Gamma_4$, or twodimensional like $\Gamma_5$ and $\Gamma_6$. Because of the lower symmetry of $C_{6v}$ with respect to the cubic groups, there are now many dynamical parameters, as much as 5 for $\Gamma_5$ transitions. If the absorbed photons are all of equal frequency (or polarization), all states but those of $\Gamma_2$ symmetry are observable. In this case, $\Gamma_3$, $\Gamma_4$ and $\Gamma_6$ transitions have a polarization dependence with no dynamical parameters, whereas $\Gamma_1$ and $\Gamma_5$ transitions have a polarization dependence with one dynamical parameter.

### 3.2.3 Four-photon transitions

In this subsection we present the results of our symmetry analysis for four-photon transitions. We only discuss the case of the $O(3)$ point group. The transition operators transform as an 81-dimensional representation of $O(3)$, of $S_4$ and of $O(3) \otimes S_4$:

$$O(3) \quad : \qquad R \to \quad 3D_0^+ \oplus 6D_1^+ \oplus 6D_2^+ \oplus 3D_3^- \oplus D_4^-, \tag{3.25}$$

$$S_4 \quad : \qquad R \to \quad 15\tilde{\Gamma}_1^+ \oplus 15\tilde{\Gamma}_3^+ \oplus 6\tilde{\Gamma}_2 \oplus 3\tilde{\Gamma}_3^-, \tag{3.26}$$

$$\begin{aligned} O(3) \otimes S_4 \quad : \qquad R \to \quad & D_0^+ \cdot \tilde{\Gamma}_1^+ \oplus D_0^+ \cdot \tilde{\Gamma}_2 \oplus D_1^+ \cdot \tilde{\Gamma}_3^+ \oplus D_1^+ \cdot \tilde{\Gamma}_3^- \oplus D_2^+ \cdot \tilde{\Gamma}_1^+ \\ & \oplus D_2^+ \cdot \tilde{\Gamma}_2 \oplus D_2^+ \cdot \tilde{\Gamma}_3^+ \oplus D_3^+ \cdot \tilde{\Gamma}_3^+ \oplus D_4^+ \cdot \tilde{\Gamma}_1^+. \end{aligned} \tag{3.27}$$

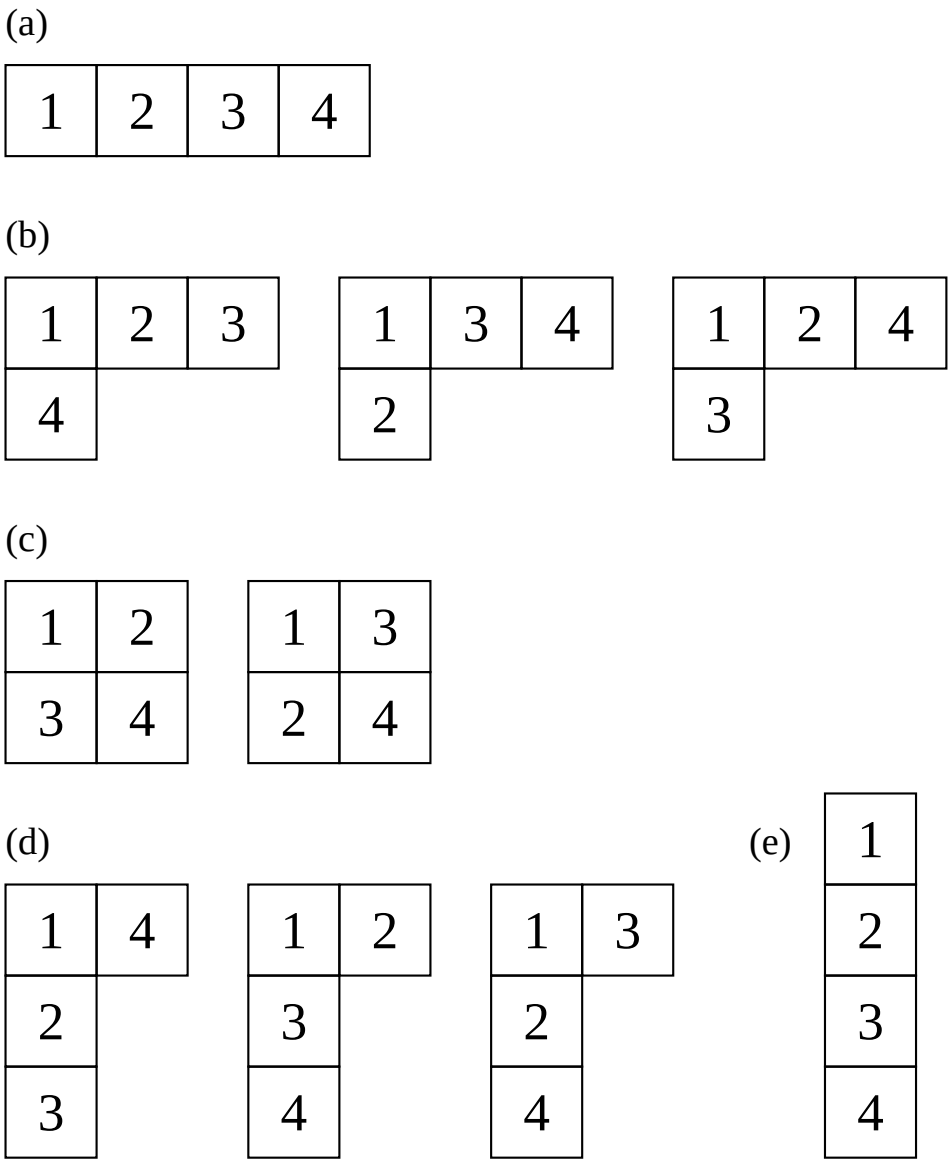


**Figure 3.3.** – Young diagrams for the projectors on the rows of the irreducible representations of the permutation group of four elements $S_4$: (a) $\tilde{\Gamma}_1^+$, (b) $\tilde{\Gamma}_3^+$, (c) $\tilde{\Gamma}_2$, (d) $\tilde{\Gamma}_3^-$, and (e) $\tilde{\Gamma}_1^-$.

The Young diagrams for $S_4$ are given in Fig. 3.3. From Fig. 3.3 we can deduce the transformation properties of the dynamical factors and identify the nonvanishing ones in the case of photons of equal frequency. Only the $\tilde{\Gamma}_1^+$ representation is nonvanishing if all the frequencies are equal. We thus deduce that in the case of one beam spectroscopy, only states of $D_0^+$, $D_2^+$ and $D_4^+$ can be detected. As another example, if we take the frequencies of photons 1 and 2 to be equal and at the same time the frequencies of photons 3 and 4 to be equal to each other but different with respect to those of photons 1 and 2, we see that only the dynamical factors which transform as $\tilde{\Gamma}_1^+$ and one of the two which transform as $\tilde{\Gamma}_2$ do not vanish.

## 3.3 General remarks

The polarization dependence which has been described here is complete, i.e., it gives the full dependence on the polarization vectors for a given point group. However, it is often possible to go beyond the most general polarization dependence because of additional physical information. For example, if it is known that only particular intermediate states are important in the absorption process, a more detailed description of the polarization dependence can be given using two- [22] or three-band [47] models. As another example, if the final states are well described in a spherical model, the polarization dependence will rather be as for the $O(3)$ group instead of as for the crystal point group, i.e., because of additional information we know that some of the crystal dynamical parameters are very small.

For some point groups, final states of different spatial symmetry can be degenerate because of time-reversal symmetry. In this case, the absorption rate is

given by the sum of the transition rates of each of the states which are degenerate. The dynamical parameters which appear in the single expressions can be related to each other because of time-reversal symmetry. Sometimes, for example in the case of Wannier exciton states, different states of different symmetry turn out to be almost degenerate [11]. Analogously as for the time-reversal degeneracy the transition rate is obtained as a sum of different contributions. In this respect, Refs. [44] and [11] are particularly interesting.

Additional selection rules can occur because of the fact that the electromagnetic radiation can only excite the singlet component of exciton states. This property is independent on the number of photons participating in the process. Although the spin is not a good quantum number, the mixing because of the spin-orbit interaction between singlet and triplet states is often very weak. The mixing can be increased by external magnetic fields [17].

## 3.4 Related problems

### Molecular systems

It is worth while to note that all the results presented here can also be applied to atomic and molecular gases. The same analysis can be carried out considering the point group of a molecular system. Finally, the transition rate is obtained by averaging the directions of the polarization vectors over the whole solid angle. In this way, only expressions of the polarization vectors which are spherically invariant are maintained. Operatively this can be done by expressing the $\phi$ which appear in Eq. (3.6) for a particular molecular point group as linear combinations of expressions $R_{lm}$ which transform in the same way as the spherical harmonics $Y_{lm}$. The products $R^*_{l'm'}R_{lm}$ which occur after the square modulus has been

taken, can again be decomposed into linear combinations of $R'_{lm}$ which also transform as spherical harmonics. When the spherical average is taken all the $R'_{lm}$ vanish except those transforming as $Y_{00}$. In this way a procedure is provided which produces analogue results as alternative methods in which the average over the whole solid is taken in the beginning of the analysis [48, 49, 50]. In particular our procedure can be useful if, for some reason, a full spherical average is not required.

**Related applications**

Here, we have considered multiphoton absorption processes from the crystal ground state. The same analysis can be extended to cope with transitions between states of all possible symmetries, as has been done in the case of two-photon transitions by Bader and Gold [39]. If initial and final state transform as $\Gamma_i$ and $\Gamma_f$ of the point group, respectively, the transition operators which transform as one of the representations in the product $\Gamma_f^* \otimes \Gamma_i$ will be active. The number of nonvanishing dynamical factors depends on the number of photons of equal frequency and can be determined as for transitions from the ground state. Other processes, related to higher-order susceptibilities $\chi^{(n)}$, such as sum-frequency or difference-frequency generation [43], can also be described by formulae which are similar to that of Eq. (3.1). In this case final and initial state are the crystal ground state. In order to have non-vanishing $\chi^{(n)}$ there must be a transition operator which transforms as the representation $\Gamma_1$. Moreover, if some of the involved photons are of equal frequency at least one of the $\Gamma_1$ dynamical factors should not be vanishing.

# Chapter 4

# Two-photon transitions in quantum wells

## 4.1 Introduction to quantum wells

Owing to continuous developments and improvements of crystal growth techniques, such as molecular beam epitaxy (MBE) [51], nowadays it is possible to obtain high quality heterostructures composed of alternating semiconductor layers. Because of the possibility of varying within large bounds the width, the composition and the doping concentration of the layers, the study of such structures has attracted considerable interest from an experimental as well as from a theoretical point of view. Moreover, the possibility of varying artificially the physical properties is a major advantage for applications in electronic devices. The width of the layers can be varied from several angstrom to several hundred angstroms and can be controlled on an atomic scale, yielding abrupt interfaces between different semiconductors. The background impurity concentration is low, and intrinsic phenomena dominate the luminescence spectra [52].

The most widely studied heterostructure is the GaAs-$Ga_{1-x}Al_xAs$ superlattice. In this system the bandgap, which increases with the aluminum concentration $x$, changes from one layer to another. The electrons in the conduction band as well as the holes in the valence band are mainly confined in the GaAs layers, because the bandgap discontinuity is distributed between conduction (65%) and valence band (35%). When the barriers are sufficiently thick that coupling between different wells can be neglected, one deals with a single quantum well. This is the case studied in this chapter.

A good description of the electronic states in QW's can be given within the effective mass approach, which has been extended to the QW system. The bandgap discontinuity is accounted for by introducing square-well potentials for the electrons as well as for the holes. Because of the different band parameters of well and barrier materials, particular boundary conditions, which conserve the average current through the interfaces, have to be introduced [53, 54].

The square-well potential produces a quantization of the electronic levels for the motion along the growth axis ($z$-axis). As long as the quantization energy is lower than the barrier potential, the levels are discrete and the electron is mainly confined in the well. The motion in the planes can be characterized by a two-dimensional wavevector $\mathbf{k}$, which reflects the translational invariance in the planes. The energy dispersion therefore consists in a two-dimensional band structure, in which a subband is related to each discrete level arising from the quantization of the motion in the $z$ direction. The motion of an electron in the conduction band is very similar to the problem of a particle-in-a-box, as the conduction band is only spin-degenerate. On the other hand, the valence band, which, in the bulk, is fourfold degenerate at the centre of the Brillouin zone, has a more complicated dispersion in the QW. Firstly, the degeneracy between

heavy and light holes is lifted by the confinement potential. Secondly, the subband dipersion is characterized by strong non-parabolicities [54, 55], which occur because of mixing effects between heavy and light holes.

Effective mass approaches have allowed to understand the linear absorption spectrum, which is strongly characterized by excitonic features. In fact, it has been possible to give a quantitative explanation of intrinsic properties, such as binding energies and oscillator strengths of excitons [56]. Also extrinsic properties such as binding energies of donors [57] or acceptors [58] can be calculated within an effective-mass-like scheme.

In this chapter, we will be concerned with two-photon transitions in GaAs-$Ga_{1-x}Al_xAs$ QW's. Recently considerable attention has been paid to two-photon spectroscopy to investigate electronic properties in QW's [59, 13, 14, 60]. Simultaneously, there has been also a growing interest for the theoretical understanding of two-photon absorption [61, 62, 63, 64, 65]. The selection rules and the shape of the absorption curve for subband-subband transitions were predicted to be strongly dependent on the polarization of the radiation beam [61, 62, 65]. Photoluminescence excitation experiments [13, 14] have provided two-photon spectra which confirmed the theoretical predictions for the subband-subband absorption. Moreover excitonic structure was observed, which differed for polarization in the layer planes or along the growth axis. In the experiment by Tai *et al.* [13], excitonic structure was detected only for $z$-polarization, whereas the experiment of Catalano *et al.* [14] reported excitonic peaks for $z$- as well as for $x$-polarization. The excitonic peaks observable with $x$- and $z$-polarization were attributed to transitions to exciton states of $p$- and $s$-symmetry, respectively.

Excitonic effects have recently been considered by Shimizu [63], who estimated two-photon transition rates of exciton states for the case of photon ener-

gies close to half the band-gap. In Shimizu's calculation the excitons are taken to be purely two-dimensional and the sum over the intermediate states is avoided assuming constant energy denominators in the two-photon transition rate which is obtained from second order perturbation theory. Shimizu has found significant transition rates for excitons of $s$-symmetry in the case of $z$-polarization and negligible transition rates for excitons of $p$-symmetry in the case of $x$-polarization. This result seems to support the experiment of Tai *et al.* [13], but it is not clear to what extent the calculations of Shimizu are independent of the involved approximations.

In this chapter we calculate two-photon transition rates in QW's. We will adopt a two-band model within the effective-mass approach in order to describe the electronic levels of the conduction and the valence band. We will mainly be concerned with the effects due to confinement and will therefore neglect effects due to the particular boundary conditions or to the mixing between heavy and light holes in the valence band. We first study the subband-subband transition rate in QW's with infinite barriers. We give the selection rules for $x$- and $z$-polarization. Then, the effect of finite barriers on the absorption spectrum is investigated. We consider the contribution due to continuum states to the two-photon transition rate in QW's. Unlike in the case of one-photon absorption, we show that in two-photon spectroscopy continuum states can contribute significantly to absorption even for transition energies below the band-gap of the barrier material. In order to treat accurately the QW continuum, we have developed a new mathematical formulation, based on the formalism of distribution theory, in which the continuum states are extended in the direction of the growth axis.

In the last section of this chapter we calculate the two-photon transition

rates of discrete excitonic states in order to compare our results with experimental spectra. As the experiments seem to yield controversial results for the excitonic effects, we go beyond the simplified model by Shimizu [63]. Firstly, we describe the three-dimensional character of the exciton states within a model which is an extension of the model proposed by Bastard *et al.* [66]. In our model the exciton wave function is separable in the **r**-coordinates and is expected to describe the exciton state accurately as long as the exciton radius is comparable to the QW width [66]. Secondly, in the calculation of the two-photon transition rate we take the sum over the intermediate states explicitly into account, using a variational procedure which has been shown to be accurate in the case of two-photon transitions in the hydrogen atom [15]. In this sum, interaction matrix elements between ground and exciton states as well as between different exciton states occur. We note that our model is more flexible than Shimizu's as it does not make approximations on the photon energies. In fact we are able to calculate transition rates also for photons of different energy. We will show how the transition rate is enhanced when the energy of one photon approaches energies of the order of the subband separation, while the other photon has an energy of the order of the band-gap.

Throughout the whole chapter particular emphasis is given to the way the electromagnetic radiation is coupled to the QW system. When model Hamiltonians are used, care has to be taken in the definition of the electromagnetic coupling in order to maintain gauge-invariance of the physical properties [28, 29]. In the present theory we adopt a two-band model, and in this approximation nonlocal potentials are introduced. Since our aim is to calculate gauge-invariant transition rates in spite of the two-band approximation, we use the current gauge to couple the quantum well system to the electromagnetic field. We note that

there is no gauge transformation which transforms the $\mathbf{A} \cdot \mathbf{p}$ interaction into the current gauge. For comparison, we always calculate the two-photon transition rate also with the $\mathbf{A} \cdot \mathbf{p}$ interaction and discuss the differences. The difference between the two results can be looked at as an estimate of the error due to the two-band approximation [62, 65].

The results presented in this chapter have been published in Refs. [62], [65] and [67].

## 4.2 Subband-subband transitions

### 4.2.1 Two-photon transition rate

We consider two-photon transitions between the valence and the conduction band in a single quantum well structure. We adopt a simple effective mass model, assuming infinite barriers and parabolic bands. In order to describe semiconductors such as GaAs, we consider heavy holes as well as light holes, but we neglect valence band mixing. Thus, we describe our system with the one-particle effective mass Hamiltonian given by

$$H = \sum_{n_c,\mathbf{k}} E^{ck}_{n_c} |\psi^{c\mathbf{k}}_{n_c}\rangle\langle\psi^{c\mathbf{k}}_{n_c}| + \sum_{n_v,\mathbf{k}} E^{vk}_{n_v} |\psi^{v\mathbf{k}}_{n_v}\rangle\langle\psi^{v\mathbf{k}}_{n_v}|, \tag{4.1}$$

where $E^{ck}_{n_c}$ and $E^{vk}_{n_v}$ are the energy eigenvalues and $\psi^{c\mathbf{k}}_{n_c}$ and $\psi^{v,\mathbf{k}}_{n_v}$ the eigenstates of conduction and valence band. The wave vector $\mathbf{k}$ is a good quantum number and reflects the translational symmetry in the QW plane. The confinement potential yields subbands which are labelled with the particle-in-a-box quantum number $n$. For each wave vector $\mathbf{k}$, the full electronic wave function of energy $E^{ck}_n = E^{c0}_n + \hbar^2 k^2/(2m_c)$, related to the conduction envelope function $f^c_n$, is given by

$$\psi^{c\mathbf{k}}_n(\mathbf{r}) = f^c_n(z)\phi^c_{\mathbf{k}}(\mathbf{r}), \tag{4.2}$$

where $\phi^c_{\mathbf{k}}$ are bulk Bloch functions of the conduction band characterized by a three-dimensional wave vector ($\mathbf{k}$,0). The $f^c_n$ are normalized to one:

$$\int dz\, [f^c_n(z)]^* f^c_{n'}(z) = \delta_{nn'}. \tag{4.3}$$

Wave functions of the valence band are treated analogously. We consider first a single valence band with an effective mass $m_v$.

The interaction Hamiltonian obtained by coupling the electromagnetic radiation to the current is given, up to quadratic terms in the vector potential, by [28]

$$H_J^{int} = -\frac{e}{c}\mathbf{A}\cdot\mathbf{v} + \frac{1}{2i\hbar}\left(\frac{e}{c}\right)^2 \mathbf{A}\cdot[\mathbf{r}, \mathbf{A}\cdot\mathbf{v}], \tag{4.4}$$

where the velocity operator is defined by

$$\mathbf{v} = \frac{1}{i\hbar}[\mathbf{r}, H]. \tag{4.5}$$

We shall refer to $H_J^{int}$ of (4.4) as the interaction Hamiltonian in the current gauge. The usual form of the interaction Hamiltonian, to which we shall refer as the $\mathbf{A}\cdot\mathbf{p}$ interaction,

$$\hat{H}^{int} = -\frac{e}{m_0 c}\mathbf{A}\cdot\mathbf{p} + \frac{1}{2m_0}\left(\frac{e}{c}\right)^2 A^2, \tag{4.6}$$

is recovered, when $\mathbf{v} = \mathbf{p}/m_0$ as is the case for Hamiltonians containing only local potentials [29].

In our case, $\mathbf{v}$ is different from $\mathbf{p}/m_0$, as can be shown following the lines of Ref. [29], and the interaction form (4.4) has to be used in order to obtain a gauge independent transition rate. The interaction (4.6) cannot be obtained neither from (4.1) through the minimal coupling procedure nor from (4.4) through a gauge transformation due to the presence of a nonlocal potential in (4.1), not commuting with the position operator $\mathbf{r}$.

Our aim is to evaluate the two-photon transition rate from the ground state of the system using as interaction the Hamiltonian (4.4). We also perform the analogous calculation with the interaction $\hat{H}^{int}$ (4.6), and show explicitly the differences between the two approaches. The two-photon transition rate in an electromagnetic field of vector potential

$$\mathbf{A} = A_1 e^{i\omega_1 t}\boldsymbol{\epsilon}_1 + A_2 e^{i\omega_2 t}\boldsymbol{\epsilon}_2 + c.\ c.\ , \tag{4.7}$$

can be obtained from second order perturbation theory:

$$W_J^{2ph}(\boldsymbol{\epsilon}_1,\boldsymbol{\epsilon}_2;\hbar\omega_1,\hbar\omega_2) = \frac{2\pi}{\hbar}\left(\frac{e}{c}\right)^4 (A_1A_2)^2 \frac{S}{(2\pi)^2}\int d\mathbf{k}\sum_f\sum_i \Big|(1+P_{12})$$

$$\times\Big[\sum_\mu \frac{\langle\psi_f^{c\mathbf{k}}|\boldsymbol{\epsilon}_1\cdot\mathbf{v}|\psi^{\mu\mathbf{k}}\rangle\langle\psi^{\mu\mathbf{k}}|\boldsymbol{\epsilon}_2\cdot\mathbf{v}|\psi_i^{v\mathbf{k}}\rangle}{E^{\mu\mathbf{k}}-E_i^{v\mathbf{k}}-\hbar\omega_2} - \frac{1}{2i\hbar}(\langle\psi_f^{c\mathbf{k}}|\boldsymbol{\epsilon}_1\cdot\mathbf{r}|\psi^{\mu\mathbf{k}}\rangle\langle\psi^{\mu\mathbf{k}}|\boldsymbol{\epsilon}_2\cdot\mathbf{v}|\psi_i^{v\mathbf{k}}\rangle$$

$$-\langle\psi_f^{c\mathbf{k}}|\boldsymbol{\epsilon}_2\cdot\mathbf{v}|\psi^{\mu\mathbf{k}}\rangle\langle\psi^{\mu\mathbf{k}}|\boldsymbol{\epsilon}_1\cdot\mathbf{r}|\psi_i^{v\mathbf{k}}\rangle)\Big]\Big|^2 \delta(E_f^{ck}-E_i^{vk}-\hbar\omega_1-\hbar\omega_2), \tag{4.8}$$

where $S$ is the surface of the QW system in the $xy$-plane and where the operator $P_{12}$ interchanges the photon indices. The sum over the states $\psi^{\mu\mathbf{k}}$ stands for a sum over all eigenstates of our model Hamiltonian. In the case of $\hat{H}^{int}$, $\mathbf{v}$ in Eq. (4.8) has to be replaced by $\mathbf{p}/m_0$ and the second term in the square brackets should be disregarded. In Eq. (4.8) interband as well as intraband matrix elements appear.

The two-photon transition rate of (4.8) gives the probability per unit time of absorbing a total energy of $\hbar\omega_1+\hbar\omega_2$, i.e. one photon from each radiation beam. The formula is valid as long as the photon energies are different. In fact, for photons of equal energy both photons can also be absorbed from the same radiation beam and formula (4.8) is inadequate. Actually, the absolute values of the transition rate for photons of equal energy and polarization, as we shall consider in the following, have to be increased by a factor 4 because of this effect. In the case of photons of equal energy, but different polarization the transition rate is not simply related to formula (4.8).

We express the interband matrix elements of $\mathbf{v}$ and $\mathbf{p}/m_0$, which appear in (4.8), in terms of the matrix element of momentum between conduction and

valence-band zone-centre Bloch functions $\mathbf{p}_{cv}$:

$$\begin{aligned}\langle\psi_n^{c\mathbf{k}}|\boldsymbol{\epsilon}\cdot\mathbf{p}|\psi_{n'}^{v\mathbf{k}}\rangle &= \delta_{nn'}\,\boldsymbol{\epsilon}\cdot\mathbf{p}_{cv},\\ \langle\psi_n^{c\mathbf{k}}|\boldsymbol{\epsilon}\cdot\mathbf{v}|\psi_{n'}^{v\mathbf{k}}\rangle &= \frac{E_n^{ck}-E_{n'}^{vk}}{E_g+\hbar^2k^2/(2\mu)}\delta_{nn'}\,\boldsymbol{\epsilon}\cdot\mathbf{p}_{cv}/m_0,\end{aligned} \tag{4.9}$$

where $E_g$ is the band gap, $\mu$ is the conduction-valence-band reduced mass, and $m_0$ is the free electron mass. The second equation of (4.9) has been obtained using the fact that $\mathbf{p}/m_0 = [\mathbf{r}, H_b]/(i\hbar)$, where $H_b$ is the bulk Hamiltonian, is valid for bulk Bloch functions. In fact, $\mathbf{p}_{cv}$ in Eqs. (4.9) should be calculated between Bloch functions of wave vector $\mathbf{k}$. We will neglect the dependence of this parameter on $\mathbf{k}$. This approximation affects the results obtained with the two interaction Hamiltonians in the same way. We note that, if effects due to the lack of inversion symmetry are negligible, $\mathbf{p}_{cv}$ depends only quadratically on $\mathbf{k}$.

The reduced mass $\mu$ as well as the matrix element $\mathbf{p}_{cv}$ are different for heavy holes or light holes. The matrix elements $\mathbf{p}_{cvh}$ and $\mathbf{p}_{cvl}$ for heavy and light holes, respectively, are however related by Clebsch-Gordan coefficients. We give them for $x$- and $z$-polarization:

$$\begin{aligned}\textstyle\sum_s(\hat{\mathbf{x}}\cdot\mathbf{p}_{cvh})^2 &= P^2,\\ \textstyle\sum_s(\hat{\mathbf{x}}\cdot\mathbf{p}_{cvl})^2 &= P^2/3,\\ \textstyle\sum_s(\hat{\mathbf{z}}\cdot\mathbf{p}_{cvh})^2 &= 0,\\ \textstyle\sum_s(\hat{\mathbf{z}}\cdot\mathbf{p}_{cvl})^2 &= 4P^2/3,\end{aligned} \tag{4.10}$$

where we have summed over the spin states and where $P = \langle s|p_x|X\rangle$ is the momentum matrix element between spinless conduction and valence zone-centre Bloch states.

We remark that Eqs. (4.9) provide a stringent selection rule on interband

transitions due to the fact that the particle-in-a-box envelope functions are mass independent and therefore orthogonal for different principal quantum number $n$. These selection rules limit the number of intermediate states in Eq. (4.8) to be considered to two.

We calculate the two-photon transition rate for two beams of equal polarization ($\boldsymbol{\epsilon}_1 = \boldsymbol{\epsilon}_2$) and equal photon energy ($\hbar\omega_1 = \hbar\omega_2$) in two cases for which different selection rules occur: for photons polarized in the layer planes ($x$-direction) and along the growth axis ($z$-direction). The intraband matrix elements of $\mathbf{v}$ and $\mathbf{p}/m_0$ are equal, for $x$- as well as for $z$-polarization. For $x$-polarization, only diagonal matrix elements do not vanish. We calculate the intraband matrix elements of the velocity and the momentum operator up to the first order in $\mathbf{k}$. We give them for conduction states:

$$\langle \psi_n^{c\mathbf{k}} | \hat{\mathbf{x}} \cdot \mathbf{v} | \psi_n^{c\mathbf{k}} \rangle = \langle \psi_n^{c\mathbf{k}} | \hat{\mathbf{x}} \cdot \mathbf{p}/m_0 | \psi_n^{c\mathbf{k}} \rangle = \hat{\mathbf{x}} \cdot \hbar\mathbf{k}/m_c. \tag{4.11}$$

Analogous expressions are valid for valence states. In the two-photon transition rate (4.8) also diagonal matrix elements of $\mathbf{r}$ occur. These matrix elements are not well defined and diverge as the size of the QW system in the $x$-direction. However, they appear only in differences, which are well defined and which are vanishing up to the first order in $\mathbf{k}$:

$$\langle \psi^{c\mathbf{k}} | \hat{\mathbf{x}} \cdot \mathbf{r} | \psi^{c\mathbf{k}} \rangle - \langle \psi^{v\mathbf{k}} | \hat{\mathbf{x}} \cdot \mathbf{r} | \psi^{v\mathbf{k}} \rangle = 0. \tag{4.12}$$

For $z$-polarization the intraband matrix elements couple only states of opposite parity. For the conduction states, we obtain

$$\begin{aligned} &\langle \psi_n^{c\mathbf{k}} | \hat{\mathbf{z}} \cdot \mathbf{v} | \psi_{n'}^{c\mathbf{k}} \rangle = \langle \psi_n^{c\mathbf{k}} | \hat{\mathbf{z}} \cdot \mathbf{p}/m_0 | \psi_{n'}^{c\mathbf{k}} \rangle = \langle f_n^c | p_z/m_c | f_{n'}^c \rangle, \\ &\langle \psi_n^{c\mathbf{k}} | \hat{\mathbf{z}} \cdot \mathbf{r} | \psi_{n'}^{c\mathbf{k}} \rangle = \langle f_n^c | z | f_{n'}^c \rangle, \end{aligned} \tag{4.13}$$

where

$$\langle f_n^c|p_z/m_c|f_{n'}^c\rangle = \frac{4i\hbar}{m_c L}\frac{nn'}{n^2-n'^2},$$
$$\langle f_n^c|z|f_{n'}^c\rangle = \frac{8L}{\pi^2}\frac{nn'}{[n^2-n'^2]^2}, \tag{4.14}$$

$L$ being the well width. Analogous expressions are valid for matrix elements between valence states. As the interband matrix elements (4.9) allow transitions only between states of same parity, two-photon transitions occur between states of opposite parity. From Eqs. (4.13) we see that, in the case of $z$-polarization, the intraband matrix elements between full electronic wave functions (4.2) reduce to matrix elements between envelope functions. We notice that the selection rules for the electronic transitions do not depend on the choice of the interaction Hamiltonian.

With the matrix elements of Eqs. (4.9), (4.11) and (4.13) the two-photon transition rate (4.8) can be obtained in a close form for the current interaction as well as for the $\mathbf{A}\cdot\mathbf{p}$ interaction. Transition rates with the interaction $\hat{H}^{int}$ have previously been calculated by Spector [61]. His results differ considerably from ours since this author did not consider valence band states when performing the sum over intermediate states.

### 4.2.2 Results and discussion

In Fig. 4.1(a) we plot $W_J^{2ph}(\boldsymbol{\epsilon}_1 = \boldsymbol{\epsilon}_2; \omega_1 = \omega_2)$ as a function of transition energy for radiation polarized in the plane perpendicular to the growth axis ($z$-axis) of the quantum well. In the calculations we have taken $m_c = 0.067m_0$, $m_{HH} = 0.377m_0$, $m_{LH} = 0.0905m_0$, $E_g = 1.521$ eV [68] and $P^2/m_0 = 12.85$ eV [69]. In the case of $x$-polarization the possible two-photon transitions are those with $\Delta n = 0$. The transition rate grows with the transition energy and has

a discontinuous derivative for each subband-subband transition with $\Delta n = 0$, i.e. for $2\hbar\omega_1 = E_n^{c0} - E_n^{v0}$. The fact that $W_J^{2ph}$ is continuous at the onsets of new subband-subband transitions, is due to the linear dependence of the dipole matrix elements on the wave vector $\mathbf{k}$. The onset of the absorption occurs in correspondence to the transition between the first conduction subband C1 and the first hole subband HH1.

In Fig. 4.1(b), we plot the transition rate under the same conditions as in the previous case, but for $z$-polarization. In this configuration only transitions with odd $\Delta n$ contribute to the absorption coefficient. The above selection rule is due to the form of the interaction which couples only subbands of different parity with respect to the reflection $z \to -z$. By symmetry, only light holes interact with radiation polarized in the $z$-direction and so the onset of absorption corresponds to the transition from the lowest conduction subband C1 to the second light hole subband LH2. The transition LH1-C2 occurs at higher energy because the light hole effective mass is larger than the conduction band mass. The onset of absorption is shifted towards higher energies when compared with the case of $x$-polarization.

The transition rate for $z$-polarization is much more structured as compared to the previous case. A step in $W_J^{2ph}$ occurs in correspondence to each subband-subband transition with photon frequency $2\hbar\omega_1 = E_n^{c0} - E_{n'}^{v0}$, where $\Delta n = n - n'$ is odd. In fact, the intraband dipole matrix elements for $z$-polarization are $\mathbf{k}$-independent giving rise to the step structure in $W_J^{2ph}$ as indicated in Fig. 4.1(b). For both polarizations the difference between the results obtained with the two interaction Hamiltonians is only quantitative.

Although the results in Fig. 4.1 do not include excitonic effects a qualitative comparison with the experimental spectra of Tai *et al.* [13] is possible. In this

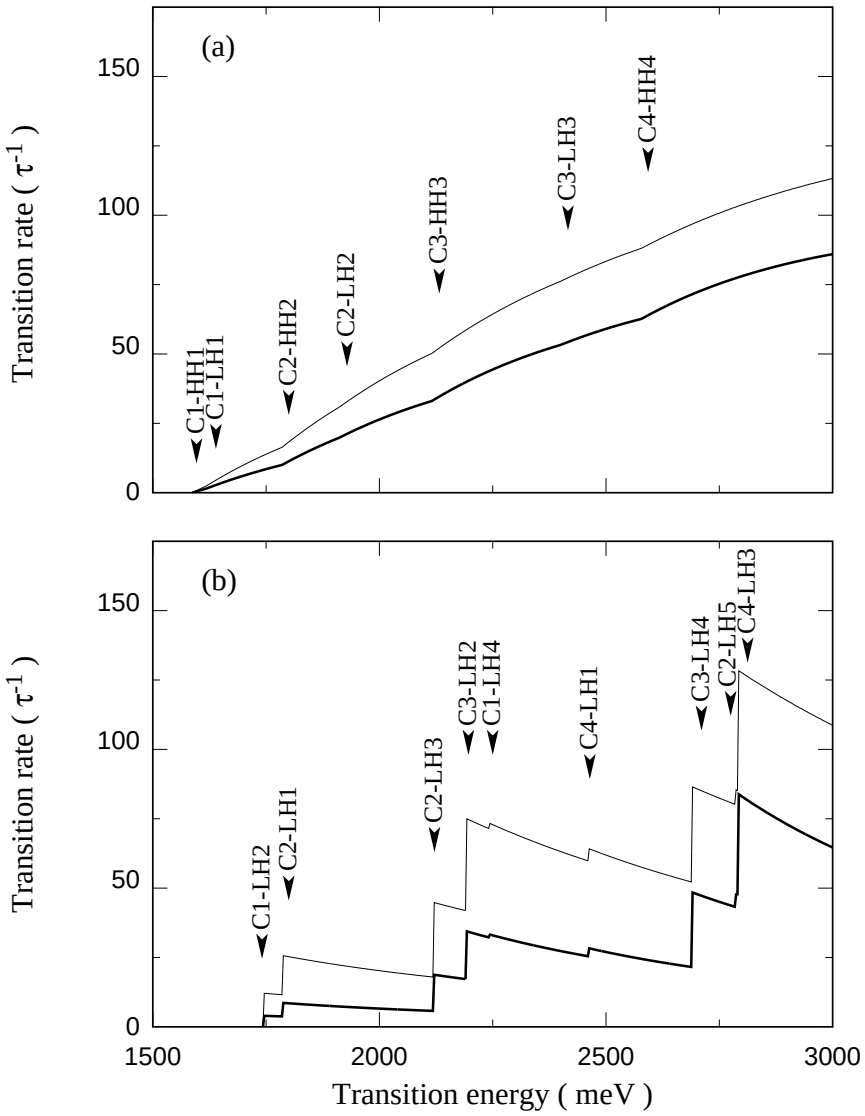


**Figure 4.1.** – Two-photon transition rate $W_J^{2ph}(\boldsymbol{\epsilon}_1 = \boldsymbol{\epsilon}_2; \omega_1 = \omega_2)$ versus transition energy for $x$- (a) and $z$-polarization (b) in a 100 Å GaAs quantum well (thick curves). The transition rate is expressed in the unit $\tau^{-1} = (e/c)^4 (A_1 A_2)^2 S/m_0\hbar^3$. For comparison, we also plot the transition rate calculated with the $\mathbf{A} \cdot \mathbf{p}$ interaction (thin curves).

experiment only a small energy region has been investigated, but the absorption of $x$- and $z$-polarized radiation has been analysed separately. They indeed find that the onset of absorption is at higher energies for $z$-polarization than for $x$-polarization. For $z$-polarization, under the excitonic peaks, which dominate the spectrum, it is possible to recognize a step structure. For $x$-polarization, no excitonic effects are detected except a little feature at the transition onset. The absorption structure shows a linear dependence on transition energy with discontinuities in the derivative at the onsets of new subband-subband transitions. At this stage, agreement with our theoretical results is therefore fairly good.

To deduce the absorption coefficient from our transition rates it is important to define the direction of the photon wave vector with respect to the quantum well system. Our calculations have been performed supposing the radiation intensity constant over all the system. The results are so valid for a thin sample. For radiation propagating in the $z$-direction (growth axis) the absorption coefficient is adimensional and proportional to the transition rate, $S$ being the surface of the quantum well system in the $xy$-plane. Our thin-slab approximation is valid as long as the well width $L$ is small compared to the wavelength of the radiation. On the other hand, for radiation propagating along the $x$-direction, the absorption coefficient has the dimensions of an inverse length and absorption will depend on the length of the sample in the $x$-direction following an exponential law. In this case, the absorption coefficient is proportional to the derivative of the transition rate with respect to the length of the sample in the $x$-direction.

## 4.3 Effect of continuum states

In this section, we give an estimation of the contribution due to continuum states to the two-photon transition rate in QW's. Unlike in the case of one-photon absorption, it is not possible to rule out this effect on the basis of simple arguments. We indeed show that continuum states can contribute significantly to absorption even for transition energies below the band-gap of the barrier material. For these transition energies the subband-subband transition rate is obtained by summing over contributions due to two kinds of transitions. *(i)* Transitions between discrete states. Apart from a shift of the absorption edges to lower energies, the contribution due to these transitions is expected to be similar to the transition rates found in the case of infinite barriers [61, 62]. *(ii)* Transitions between discrete and continuum states. We stress that the contribution of the latter kind of transitions is peculiar for quantum wells with finite barriers. The QW continuum has been treated within a mathematical formulation, based on the formalism of distribution theory, which allows for extended states in the direction of the growth axis.

Continuum-continuum transitions, which occur for transition energies above the band-gap of the barrier material have not been considered here. We remark that the absorption due to this type of transitions is no more independent of the size of the QW system in the $z$-direction and assumes a three-dimensional character.

### 4.3.1 One-photon transition rate

It is useful to consider first the effect of the continuum on one-photon absorption. The study of the interband matrix elements is important to understand the

features obtained for the two-photon transition rate. The effective-mass equation for the conduction envelope functions $f^c(z)$ is given by

$$[\frac{p_z^2}{2m_c} + U_c(z)]f^c(z) = (E^c - E_g)f^c(z), \tag{4.15}$$

where $m_c$ is the effective mass of the conduction band and where the energy values are refered to the top of the valence band. The confinement potential $U_c$ in (4.15), due to band-gap discontinuity in the conduction band, is given by

$$U_c(z) = \begin{cases} 0 & \text{for } |z| \leq L/2 \\ V_c & \text{for } |z| > L/2 \end{cases}, \tag{4.16}$$

where $L$ is the well width. The valence band is treated analogously. In order to cope with GaAs-$Al_xGa_{1-x}As$ quantum wells, heavy holes as well as light holes are considered, but mixing is neglected. We consider neither the effective-mass mismatch between well and barrier material, nor non-parabolicity effects.

For energies $E < V_c$, we find a finite number of discrete solutions of Eq. (4.15). The eigenfunctions of these discrete states are trigonometric functions inside the well and decreasing exponentials outside. They are normalized as in Eq. (4.3). For each energy $E > V_c$, there are two solutions of different parity with respect to the reflection in the $z = 0$ plane. These states represent the continuum of the conduction subbands. We give these eigenfunctions of energy $E^c$ and of definite parity explicitly:

$$f^c_{E+}(z) = \begin{cases} G\cos(gz + \delta^+) & \text{for } z \geq L/2 \\ A^+\cos(kz) & \text{for } |z| \leq L/2 \\ G\cos(-gz + \delta^+) & \text{for } z \leq -L/2 \end{cases}, \tag{4.17}$$

$$f^c_{E-}(z) = \begin{cases} G\cos(gz + \delta^-) & \text{for } z \geq L/2 \\ A^-\sin(kz) & \text{for } |z| \leq L/2 \\ -G\cos(-gz + \delta^-) & \text{for } z \leq -L/2 \end{cases}, \tag{4.18}$$

where the parameters $A$ and $\delta$ can be obtained by imposing the boundary conditions at $z = L/2$ and where

$$\begin{aligned} k &= [2m_c(E^c - E_g)/\hbar^2]^{1/2}, \\ g &= [2m_c(E^c - E_g - V_c)/\hbar^2]^{1/2}, \\ G &= [m_c/(\pi\hbar^2 g)]^{1/2}. \end{aligned} \tag{4.19}$$

The choice of parameter $G$ is such that the normalization of these functions is

$$\int dz\, [f^c_{E\sigma}(z)]^* f^c_{E'\sigma'}(z) = \delta(E - E')\delta_{\sigma\sigma'}, \tag{4.20}$$

where the parity with respect to reflection has been indicated by $\sigma$. We notice that the onset of the continuum depends on $\mathbf{k}$ and occurs at $V_c + \hbar^2 k^2/(2m_c)$.

From first order perturbation theory, the one-photon transition rate, in an electromagnetic field $\mathbf{A}$ of frequency $\omega$ and polarization $\boldsymbol{\epsilon}$, is given by

$$W_J^{1ph}(\boldsymbol{\epsilon}; \hbar\omega) = \frac{2\pi}{\hbar}\left(\frac{e}{c}\right)^2 A^2 \frac{S}{(2\pi)^2} \sum_i \sum_f \int d\mathbf{k}\, |\langle \psi_f^{c\mathbf{k}} | \boldsymbol{\epsilon}\cdot\mathbf{v} | \psi_i^{v\mathbf{k}} \rangle|^2 \delta(E_f^{c\mathbf{k}} - E_i^{v\mathbf{k}} - \hbar\omega), \tag{4.21}$$

where $S$ is the surface of the QW system in the $xy$-plane. The sum over the initial states $\psi_i^{v\mathbf{k}}$ stands for a sum over all valence states, discrete as well as continuum. In the case of continuum states, the sum has to be replaced by an integral over energy. The states $\psi_f^{c\mathbf{k}}$ represent analogously all final conduction states. In the case of interaction $\hat{H}^{int}$, $\mathbf{v}$ in Eq. (4.21) has to be replaced by $\mathbf{p}/m_0$.

The interband matrix elements of $\mathbf{v}$ and $\mathbf{p}/m_0$, which appear in (4.21), are similar to those of Eq. (4.9):

$$\begin{aligned} \langle \psi_n^{c\mathbf{k}} | \boldsymbol{\epsilon}\cdot\mathbf{p} | \psi_{n'}^{v\mathbf{k}} \rangle &= \langle f_n^c | f_{n'}^v \rangle\, \boldsymbol{\epsilon}\cdot\mathbf{p}_{cv}, \\ \langle \psi_n^{c\mathbf{k}} | \boldsymbol{\epsilon}\cdot\mathbf{v} | \psi_{n'}^{v\mathbf{k}} \rangle &= \frac{E_n^{ck} - E_{n'}^{vk}}{E_g + \hbar^2 k^2/(2\mu)} \langle f_n^c | f_{n'}^v \rangle\, \boldsymbol{\epsilon}\cdot\mathbf{p}_{cv}/m_0, \end{aligned} \tag{4.22}$$

where the indices $n$ and $n'$ represent now discrete as well as continuum states. From Eq. (4.22) we see that transitions are allowed between all valence and conduction states of same parity. In contrast with the case of infinite barriers, the envelope functions of valence and conduction states are now different. In fact, the $\Delta n = 0$ rule for transitions between discrete subbands, which occurs in QW's with infinite barriers, is no more strictly valid.

In Fig. 4.2, we report the one-photon transition rate for energies below the band-gap of the barrier material in a 100 Å GaAs-$Al_{0.4}Ga_{0.6}As$ QW. The band-gap discontinuity is given by $\Delta E_g = 1247x$ meV [70] and we take $V_c/\Delta E_g = 0.65$. The transition rates are calculated with the two interaction Hamiltonians, for photons polarized along the $x$- and $z$-axis. Because of the two-dimensional Brillouin zone, a step occurs in the transition rate in correspondence to new allowed subband-subband transitions. For $x$-polarization, transitions occur between conduction and valence subbands of same parity, for light holes as well as for heavy holes. The onset of absorption due to transitions from the valence continuum to the first conduction subband occurs in this model at 1730 meV, and that due to transitions from the first heavy hole subband to the conduction continuum at 1853 meV. For $z$-polarization only light holes are active. The onset of absorption due to transitions from valence continuum to discrete conduction states occurs at the same energy as for $x$-polarization. The onset of transitions from discrete light hole to continuum conduction states occurs at 1869 meV. We notice from Fig. 4.2 that the contribution of transitions from valence or to conduction continuum states is small and their absorption edges are not evidently marked. The continuum contribution becomes larger if the photon energy increases. In fact, the largest contribution to the absorption due to the continuum involves the highest discrete subbands. The overall continuum contributions are expected to

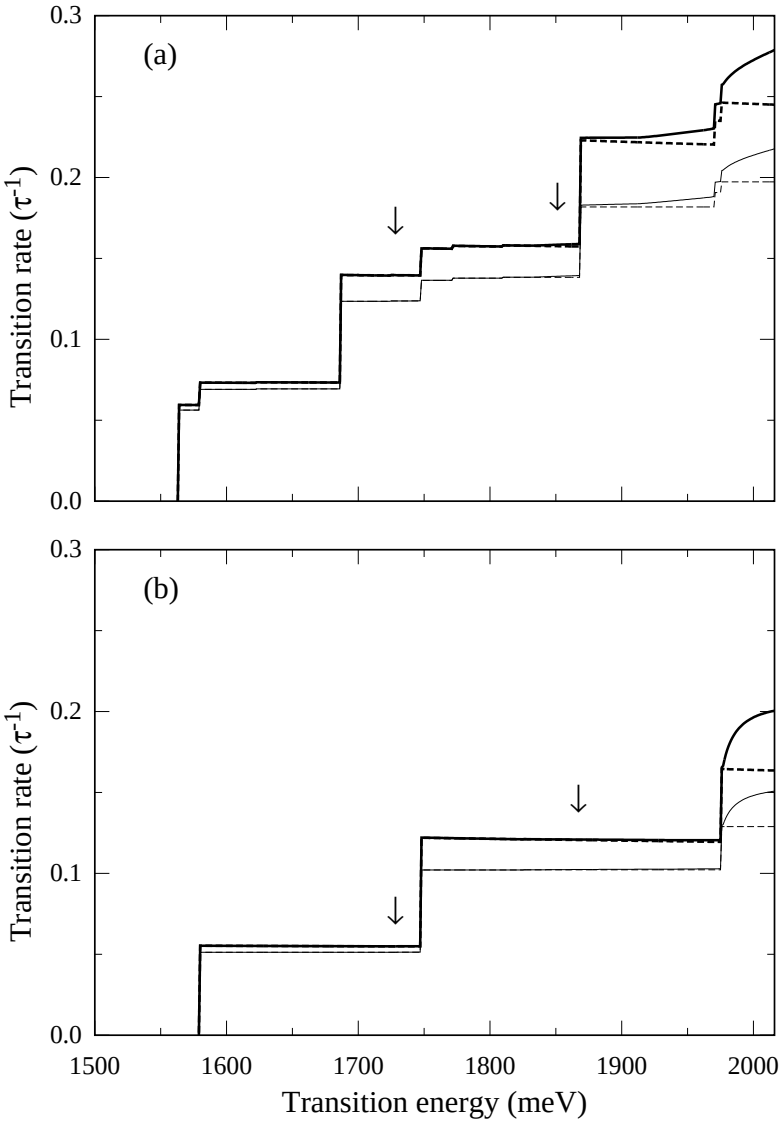


**Figure 4.2.** – One-photon transition rate vs transition energy in a 100 Å GaAs-$Ga_{0.6}Al_{0.4}As$ QW for (a) $x$- and (b) $z$-polarization. Dashed curves represent the rate obtained considering only transitions between discrete subbands. The calculations are performed in the current gauge (thick curves) as well as with the $\mathbf{A}\cdot\mathbf{p}$ interaction (thin curves). The unit of the transition rate is $\tau^{-1} = (eA/c)^2 P^2 S/m_0\hbar^3$. The arrows indicate the onset of transitions from the valence or to conduction continuum states.

be small as, in the case of equal effective masses and band-gap discontinuities in conduction and valence band, these contributions vanish. In fact, in this case, the discrete states $f^c$ are orthogonal to the continuum $f^v$, being both eigenstates of identical effective mass Hamiltonians. The same is true for continuum conduction and discrete valence states. For both polarizations the difference between the results obtained with the two interaction Hamiltonians is again only quantitative.

### 4.3.2 Two-photon transition rate

The two-photon transition rate is given by Eq. (4.8) where the sum over the states $\psi^{\mu\mathbf{k}}$ stands now for a sum over all discrete and continuum states of valence and conduction band. We calculate the two-photon transition rate for $x$- and $z$-polarization.

Analogously as for infinite barriers, the intraband matrix elements of $\mathbf{v}$ and $\mathbf{p}/m_0$ are equal for $x$- as well as for $z$-polarization. For $x$-polarization, the matrix elements between discrete states are as given in Eq. (4.11): only diagonal matrix elements do not vanish. We give them for continuum conduction states:

$$\langle\psi_E^{c\mathbf{k}}|\hat{\mathbf{x}}\cdot\mathbf{v}|\psi_{E'}^{c\mathbf{k}}\rangle = \langle\psi_E^{c\mathbf{k}}|\hat{\mathbf{x}}\cdot\mathbf{p}/m_0|\psi_{E'}^{c\mathbf{k}}\rangle = \hat{\mathbf{x}}\cdot\hbar\mathbf{k}/m_c\,\delta(E-E'). \tag{4.23}$$

Analogous expressions are valid for valence states. The intraband matrix elements (4.11) and (4.23) allow to eliminate the sum over the intermediate states $\psi^{\mu\mathbf{k}}$ in (4.8), which considerably simplifies the expression for the transition rate. The only matrix elements that govern the selection rules are the interband ones and therefore the same selection rules as for one-photon transitions are obtained.

For $z$-polarization the intraband matrix elements are given by Eq. (4.13), where now the indices $n$ and $n'$ indicate discrete states as well as continuum

states. In this case the sum over the intermediate states $\psi^{\mu\mathbf{k}}$ in (4.8) remains and all discrete as well as continuum states of valence and conduction band have to be considered. In the case of matrix elements between discrete states or between a continuum and a discrete state, matrix elements (4.13) are easy to calculate. However, for matrix elements between continuum states a more involved analysis is necessary. These matrix elements as well as the interband matrix elements (4.22) between continuum valence and continuum conduction states can all be obtained by explicit calculations and are given in Appendix C.

We note that the sum over the intermediate states $\psi^{\mu\mathbf{k}}$, which in the case of continuum states has to be replaced by an integral, allows us to use wave functions which are normalized as in Eq. (4.20). The distribution formalism is well defined as long as final or initial states are discrete. We have checked that the same results for the transition rate are obtained by discretizing the continuum introducing sufficiently distant infinite barriers. In the case of continuum-continuum transitions the transition rate calculated within the formalism of distribution theory diverges, which is an indication of the fact that the result depends on the size of the QW system in the $z$ direction.

In Fig. 4.3, we present the two-photon transition rate for absorption of equal photons of $x$- and $z$-polarization in a 100 Å GaAs-$Al_{0.4}Ga_{0.6}As$ QW. We also give the contribution to the absorption due to the only discrete subbands; in this case all intermediate states are taken into account but only discrete final and initial states are considered. These latter curves, obtained without the contributions due to the continuum, are similar to those obtained in the case of infinite barriers, apart form an overall shift towards lower energies. Because of the fact that all continuum states are degenerate with a state of opposite parity, the onset of continuum transitions occurs at the same energies as in one-photon

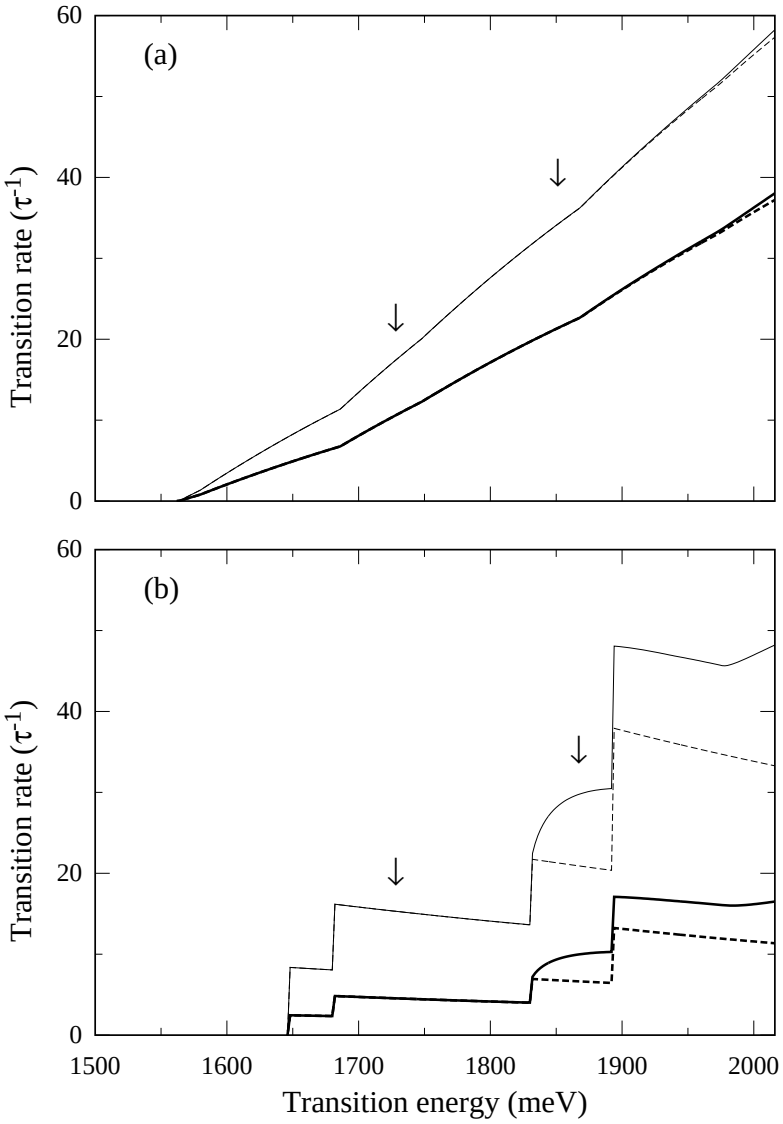


**Figure 4.3.** – Two-photon transition rate for equal photons vs transition energy in a 100 Å GaAs-$Ga_{0.6}Al_{0.4}As$ QW for (a) $x$- and (b) $z$-polarization. Dashed curves represent the rate obtained considering only transitions between discrete subbands. The calculations are performed in the current gauge (thick curves) as well as with the $\mathbf{A}\cdot\mathbf{p}$ interaction (thin curves). The unit of the transition rate is $\tau^{-1} = (e/c)^4(A_1A_2)^2S/m_0\hbar^3$. The arrows indicate the onset of transitions from the valence or to conduction continuum states.

transitions. We find that the two interaction Hamiltonians yield qualitatively similar results, for $x$- as well as for $z$-polarization.

In the case of $x$-polarization, we find that the continuum contribution to the transition rate is negligible. As for one-photon transitions, this contribution vanishes in the case of equal masses and band discontinuities in conduction and valence band. Moreover, from the intraband matrix elements (4.11) and (4.23) we see that transitions are forbidden at the centre of the Brillouin zone. Thus, the effect is even less evident than in the case of one-photon transitions.

For $z$-polarization, the matrix elements which govern the selection rules are different than in one-photon interactions, and the effect of the continuum is not vanishing for equal masses and band discontinuities in valence and conduction band. In fact, the effect of the continuum is much larger as compared to the case of $x$-polarization. It is important to notice that, although the onset of the continuum absorption occurs at relatively low transition energies, its contribution becomes substantial in correspondence of transitions from the valence continuum to the higher discrete conduction subbands. We note that this contribution is much larger than the absorption due to transitions from discrete valence states to continuum conduction states. This asymmetry is due to the fact that the band discontinuity is smaller in the valence than in the conduction band.

Only two photoluminescence excitation experiments on two-photon absorption in QW's have been performed up to now [13, 14]. In the experiment of Ref. [13] only limited energy regions have been studied and it is therefore not possible to identify the effect due to the continuum. In the experiment of Ref. [14] absorption is studied in a much larger energy region. However, only the energy region where only transitions between discrete subbands occur is investigated. Comparison with experiment is therefore not possible at the moment

as absorption spectra in the energy region where the continuum is expected to contribute are not available.

In the present calculations we have not considered effects due to the non-parabolicity of the bands. This effect is relevant at the photon energies for which absorption in the continuum occurs. We expect the non-parabolicity of the bands to shift the onset of this absorption towards lower energies. Moreover the overall absorption in the continuum is expected to be larger because of the increase in the joint density of states due to the flattening of the bands.

In conclusion, the relevant result of this study is that the relative contribution due to the continuum states strongly depends on the polarization of the radiation beam. The continuum contribution turns out to be negligible for $x$-polarization, whereas in the case of $z$-polarization the continuum contribution is important and of the same order of magnitude as that due to transitions between discrete states. Moreover, in the latter case, it is also important to observe that, although the onset of transitions which involve continuum states occurs at rather low transition energies, their contribution to absorption becomes significant only at relatively much higher transition energies.

## 4.4 Excitonic effects

In this section we calculate two-photon transition rates of exciton states in GaAs QW's for varying well widths. Experimentally it has been found that excitonic effects for $x$- and $z$-polarization differ substantially [13]. In the case of $z$-polarization the large peaks which dominate the absorption spectra have been interpreted as transitions to excitons of $s$-symmetry. On the other hand in the case of $x$-polarization no peaks have been observed, and the little feature observed at the transition onset has been attributed to excitons of $p$-symmetry [13].

In the present theory, the excitonic states are described in the effective-mass approximation and are obtained variationally assuming wave functions which are separable in the $\mathbf{r}$-coordinates. The two-photon transition rate is calculated taking explicitly into account the sum over all the intermediate states, using a variational procedure [15]. We calculate transition rates of excitons of $s$-symmetry as well as of $p$-symmetry.

In the calculations mixing effects due to the complicated valence band structure have been neglected. The selection rules we obtain are therefore the same as those obtained by Shimizu [63]. Recently, a symmetry analysis has been presented which gives two-photon selection rules for transitions to excitons in quantum wells when valence-band mixing is considered [64]. However, even in one-photon spectroscopy excitonic transitions which are only allowed by valence-band mixing generally have a significant smaller oscillator strength [71].

We first describe the model we have used to determine the excitonic states. The two-photon transition rates of $s$- and $p$-excitons are then calculated with two different interaction Hamiltonians and presented as a function of the well

width. Finally, the absorption spectrum is obtained for both polarizations by adding the excitonic effects to the subband-subband absorption and is compared to experiment.

### 4.4.1 Excitonic states

The exciton states are calculated variationally in a simple effective-mass model appropriate to a GaAs QW system [66]. The exciton Hamiltonian acts on a wave function $\psi$ which is a function of the $z$-coordinates, $z_e$ and $z_h$, and of the relative in-plane coordinates $(\rho, \phi)$ of hole and electron:

$$H = \frac{p_{z_e}^2}{2m_e} + \frac{p_{z_h}^2}{2m_h} - \frac{\hbar^2}{2\mu}\nabla_{\parallel}^2 - \frac{e^2}{\epsilon[\rho^2 + (z_e - z_h)^2]^{1/2}} + V_{conf}(z_e) + V_{conf}(z_h), \quad (4.24)$$

where $m_e$, $m_h$ are the electron and hole effective masses governing the motion along the confined direction, and where $\mu$ is the parallel reduced mass, which describes the in-plane motion of the exciton. The potentials $V_{conf}$ confine the motion of holes and electrons in the well: $|z| \leq L/2$, where $L$ is the well width. The Coulomb potential is screened by the dielectric constant $\epsilon$. We neglect the coupling between different subbands and take the wave function to be separable. The rotation symmetry around the $z$-axis allows to consider eigenstates of definite angular momentum $m$:

$$\psi^{n_e,n_h,m}(\rho, \phi, z_e, z_h) = f_{n_e}^c(z_e) f_{n_h}^v(z_h) R_{|m|}(\rho) \frac{e^{im\phi}}{(2\pi)^{1/2}}, \quad (4.25)$$

where the $f_{n_e}^c(z)$ and $f_{n_h}^v(z)$ are QW-eigenfunctions of the conduction and valence band, respectively, in absence of the Coulomb potential. The indices $n_e$ and $n_h$ indicate the considered subbands of conduction and valence band, respectively, and represent together with the angular momentum the quantum numbers of the exciton states in our model. The radial functions are obtained

by a symmetry adapted expansion in decreasing exponentials:

$$R_{|m|}(\rho) = \rho^{|m|} \sum_{k=1}^{N} A_k \, e^{-\alpha_k \rho}, \tag{4.26}$$

where the exponents $\alpha_k$ are chosen to cover a large physical region. Using the standard variational method, the eigenvalue problem can be turned into a set of coupled linear algebraic equations for the $A_k$. The calculation of the matrix elements of the exciton kinetic energy is straightforward and can be carried out analytically. The matrix elements of the Coulomb potential are more complicated. The calculation of the latter matrix elements can be simplified using the following integral expression for the Coulomb potential which decouples $z$ and $\rho$ coordinates:

$$\frac{1}{[\rho^2 + (z_e - z_h)^2]^{1/2}} = \int_0^\infty ds \; e^{-|z_e - z_h| s} \, J_0(\rho s), \tag{4.27}$$

where $J_0$ is a Bessel function. In this way all integrals over the coordinates can be carried out analytically [72]. Only the final integral of Eq. (4.27) is evaluated numerically. Provided the basis is chosen large enough these calculations yield excitonic binding energies and wave functions for the lowest state as well as for the first excited states of a given set of quantum numbers.

For the conduction band we have taken an isotropic effective mass $m_e = 0.067 m_0$ [68]. We have neglected valence band mixing, i.e., we have kept only the diagonal terms of the Luttinger Hamiltonian [73]. The effective masses in the valence band can be expressed in terms of the Luttinger parameters [74] as $m_0/m^z_{HH} = \gamma_1 - 2\gamma_2$ and $m_0/m^z_{LH} = \gamma_1 + 2\gamma_2$ for the motion along the $z$-axis, and as $m_0/m^{\|}_{HH} = \gamma_1 + \gamma_2$ and $m_0/m^{\|}_{LH} = \gamma_1 - \gamma_2$ for the in-plane motion, for heavy and light holes, respectively. In the numerical calculations we have taken $\gamma_1 = 6.85$ and $\gamma_2 = 2.1$ [68]. For the dielectric constant we have taken $\epsilon = 12.56$ [68].

The present description of the exciton states accounts qualitatively correctly for the three-dimensional character of the wave function of $s$- ($m = 0$) and $p$-excitons ($m = \pm 1$). Bastard *et al.* [66] have shown that the choice of taking a wave function which is separable in the **r**-coordinates is appropriate as long as the exciton radius is comparable to the well width, which is the case for the well width range we considered (50Å$\leq L \leq$200Å). We also would like to point out that, in contrast to the purely two-dimensional excitonic series [75], the energy and the wave function of the $p$-excitons are not directly related to the lowest $s$-exciton, and a separate calculation will be needed to obtain them. This aspect is important as inspection of the result by Shimizu [63] shows that the ratio between the transition rate of $s$-excitons and $p$-excitons depends on the ratio between the square values of the $s$ wave function and of the derivative of the $p$ wave function at $\rho = 0$.

### 4.4.2 Two-photon transition rate

In our model the QW system is represented by a two-band model with in addition a Coulomb interaction between the excited electron in one of the conduction subbands and the hole which is left in one of the valence subbands. In order to obtain gauge-invariant transition rates the electromagnetic field must be coupled to the current of the QW system [29]. It has been shown that this is equivalent to the coupling in the length gauge [29]. For an electromagnetic field of vector potential **A** as given in Eq. (4.7), the two-photon transition rate of a discrete exciton state, determined by the set of quantum numbers $\beta = (n_e, n_h, m, \nu)$, where $\nu$ is the principal quantum number, can be obtained from second order

perturbation theory [29]:

$$W_{0\to\beta} = \frac{2\pi}{\hbar}\left(\frac{e}{c}\right)^4 (A_1A_2)^2 \left|(1+P_{12})\sum_{\beta'}\frac{\langle\beta|\omega_1\boldsymbol{\epsilon}_1\cdot\mathbf{r}|\beta'\rangle\langle\beta'|\omega_2\boldsymbol{\epsilon}_2\cdot\mathbf{r}|0\rangle}{E_{\beta'}-E_0-\hbar\omega_2}\right|^2 \times\delta(E_\beta-E_0-\hbar\omega_1-\hbar\omega_2), \quad (4.28)$$

where $|0\rangle$ is the crystal ground state and $\mathbf{r}$ the position operator. The sum over $\beta'$ stands for a sum over all the excitonic eigenstates of our model Hamiltonian, including bound as well as continuum excitonic states. When the electromagnetic field and the QW system are coupled with the $\mathbf{A}\cdot\mathbf{p}$ interaction Hamiltonian, the transition rate is obtained from Eq. (4.28) by replacing $\omega\mathbf{r}$ by $\mathbf{p}/m_0$, where $m_0$ is the free electron mass.

The major difficulty in the evaluation of transition rate (4.28) is the sum over all the intermediate states $\beta'$. In fact, whereas the lowest exciton states can be well determined by the variational procedure described in the previous section, the continuum exciton states are unknown and a different calculation is needed to obtain them. However, Quattropani and Binggeli [15] have shown that in the case of the hydrogen atom it is not necessary to know all the continuum states in order to calculate accurately the two-photon transition rate. The procedure consists in calculating the transition rate by replacing the sum over the exact eigenstates $\beta'$ by a sum over the states which diagonalize the Hamiltonian on the variational basis. This procedure is repeated increasing the number of wave functions in the variational basis until convergence is reached. The same method has also been used successfully for the calculation of the polarizability in silicon, which also derives from a second order expression [76]. We will use this method in the present calculations. In order to test the convergence of the method, we have repeated all the calculations of this paper using a complete basis of generalized orthogonal Laguerre polynomials instead of the exponentials of Eq.

(4.26) [77]:

$$R_{|m|}(\rho) = \rho^{|m|} e^{-\rho/a} \sum_{k=0}^{N} A_k \; L_k^{(2m+1)}(2\rho/a), \tag{4.29}$$

where the length unit $a$ has been chosen of the order of the exciton in-plane radius. The results obtained with this basis also converge and converge to the same results obtained with the basis of exponentials.

We notice that in Eq. (4.28) matrix elements between the crystal ground state and an intermediate exciton state $\beta'$ as well as matrix elements between two exciton states $\beta$ and $\beta'$ occur. We consider first the former matrix elements:

$$\begin{aligned} \langle m, n_e, n_h, \nu | \boldsymbol{\epsilon} \cdot \mathbf{r} | 0 \rangle &= -\frac{i\hbar}{E_g} \langle m, n_e, n_h, \nu | \boldsymbol{\epsilon} \cdot \mathbf{p}/m_0 | 0 \rangle, \\ \langle m, n_e, n_h, \nu | \boldsymbol{\epsilon} \cdot \mathbf{p}/m_0 | 0 \rangle &= S^{1/2} \frac{\boldsymbol{\epsilon} \cdot \mathbf{p}_{cv}}{m_0} \frac{R_0(\rho = 0)}{(2\pi)^{1/2}} \delta_{n_e n_h} \delta_{m0}, \end{aligned} \tag{4.30}$$

where $E_g$ is the band-gap, $S$ the surface of the QW system in the $xy$-plane, and $\mathbf{p}_{cv}$ the matrix element of momentum between zone-centre Bloch functions of conduction and valence band. From Eqs. (4.30) we notice that the only allowed intermediate states are of $s$-symmetry, independently of the final exciton state. Moreover we recover the $n_e = n_h$ rule for one-photon transitions, which is valid in the case of infinite barriers [78].

The position as well as the momentum operator can couple only excitons with orbital angular momenta $|m - m'| \leq 1$. Knowing that intermediate states are of symmetry $m = 0$, we deduce that allowed final states have $m = 0, \pm 1$, which correspond to $s$- and $p$-excitons. We first consider the matrix elements in the case $m = m'$, which occur in the calculation of the transition rate of exciton states of $s$-symmetry:

$$\langle m, n'_e, n'_h, \nu' | \boldsymbol{\epsilon} \cdot \mathbf{r} | m, n_e, n_h, \nu \rangle =$$

$$\epsilon_z[\delta_{n'_h n_h}\langle f^c_{n'_e}|z|f^c_{n_e}\rangle - \delta_{n'_e n_e}\langle f^v_{n_h}|z|f^v_{n'_h}\rangle]\int_0^\infty d\rho\ \rho R'_{|m|}(\rho)R_{|m|}(\rho). \quad (4.31)$$

The matrix elements of $\mathbf{p}/m_0$ can be obtained from (4.31) by replacing $z$ with $p_z/m_e$ and $-p_z/m_h$ in the matrix elements between the QW-states $f_n$ of conduction and valence band, respectively. These matrix elements of $z$ and $p_z$ are given in Eqs. (4.14). Because of matrix elements (4.30) intermediate states have $m = 0$, and final $s$-excitons are therefore reachable only if at least one of the two polarization vectors has a component along the $z$-axis. In the sum over the intermediate states $n_e = n_h$, therefore the matrix elements between the QW-states $f_n(z)$ imply that only $s$-excitons which belong to subbands of different parity with respect to the $z \to -z$ reflection are allowed [63].

The matrix elements between excitons with $|m - m'| = 1$, which appear in (4.28) in the case of transitions to exciton states of $p$-symmetry, are given by:

$$\begin{gathered}\langle m \pm 1, n'_e, n'_h, \nu'|\boldsymbol{\epsilon}\cdot\mathbf{r}|m, n_e, n_h, \nu\rangle = \\ \frac{1}{2}(\epsilon_x \mp i\epsilon_y)\delta_{n'_e n_e}\delta_{n'_h n_h}\int_0^\infty d\rho\ \rho^2 R_{|m\pm1|}(\rho)R_{|m|}(\rho),\end{gathered} \quad (4.32)$$

$$\begin{gathered}\langle m \pm 1, n'_e, n'_h, \nu'|\boldsymbol{\epsilon}\cdot\mathbf{p}/m_0|m, n_e, n_h, \nu\rangle = \\ \frac{-i\hbar}{2\mu}(\epsilon_x \mp i\epsilon_y)\delta_{n'_e n_e}\delta_{n'_h n_h}\int_0^\infty d\rho\ R_{|m\pm1|}(\rho)[\rho\frac{\partial}{\partial\rho}R_{|m|}(\rho) \mp mR_{|m|}].\end{gathered}$$

Keeping in mind that intermediate states are of $s$-symmetry and are related to subbands with $n_e = n_h$, we see directly from (4.32) that in order to reach $p$-type final states at least one of the polarization vectors must have a component in the layer planes. Secondly, we notice that the only allowed exciton states of $p$-symmetry must have $n_e = n_h$. We therefore recover the selection rules found in Ref. [63].

As we have seen, the matrix elements of $\mathbf{p}_{cv}$ for different polarizations are re-

lated by Clebsch-Gordan coefficients and can all be expressed in terms of the matrix element of momentum between spinless conduction and valence band zone-centre Bloch functions: $P = \langle s|p_x|X\rangle$. In particular, in the case of transitions from heavy-hole subbands the matrix element $\mathbf{p}_{cv}$ vanishes for $z$-polarization.

In Fig. 4.4 we present two-photon transition rates of (a) ground as well as of (b) first-excited exciton states of $s$-symmetry as a function of the well width $L$. The C1-LH2 excitons are associated to the first conduction and second light-hole subband, and the C2-LH1 excitons are defined analogously. The absorbed photons are of equal energy and of $z$-polarization. It is important to notice how the transition rate increases for decreasing well widths. This effect is mainly due to the increasing inter-exciton matrix elements (4.31) which are proportional to the reciprocal of $L$. A second effect which increases the transition rate is that for decreasing well widths the photon energy which corresponds to a half of the energy of the excited exciton approaches the energy of the intermediate resonant level C1-LH1. The increase for decreasing well widths is analogous to the increase of the subband-subband transition rate which corresponds to the transition rate of the exciton continuum [62, 65]. We notice that the transition rate of the $1s$ C2-LH1 state is slightly larger than the transition rate of the $1s$ C1-LH2 state. In fact, in the former case, the transition energy is larger and hence, in the case of absorbed photons of equal energy, the photon energy is nearer to the resonant energy of C1-HH1. In the bulk limit the energy separation between the C1-LH2 and the C2-LH1 excitons vanishes and so does the difference between their transition rates. The transition rate of $2s$ excited states, reported in Fig. 4.4(b), follows the same behaviour as the rate to the ground states, but is about an order of magnitude smaller.

We note that for decreasing well width we do not obtain the transition rate

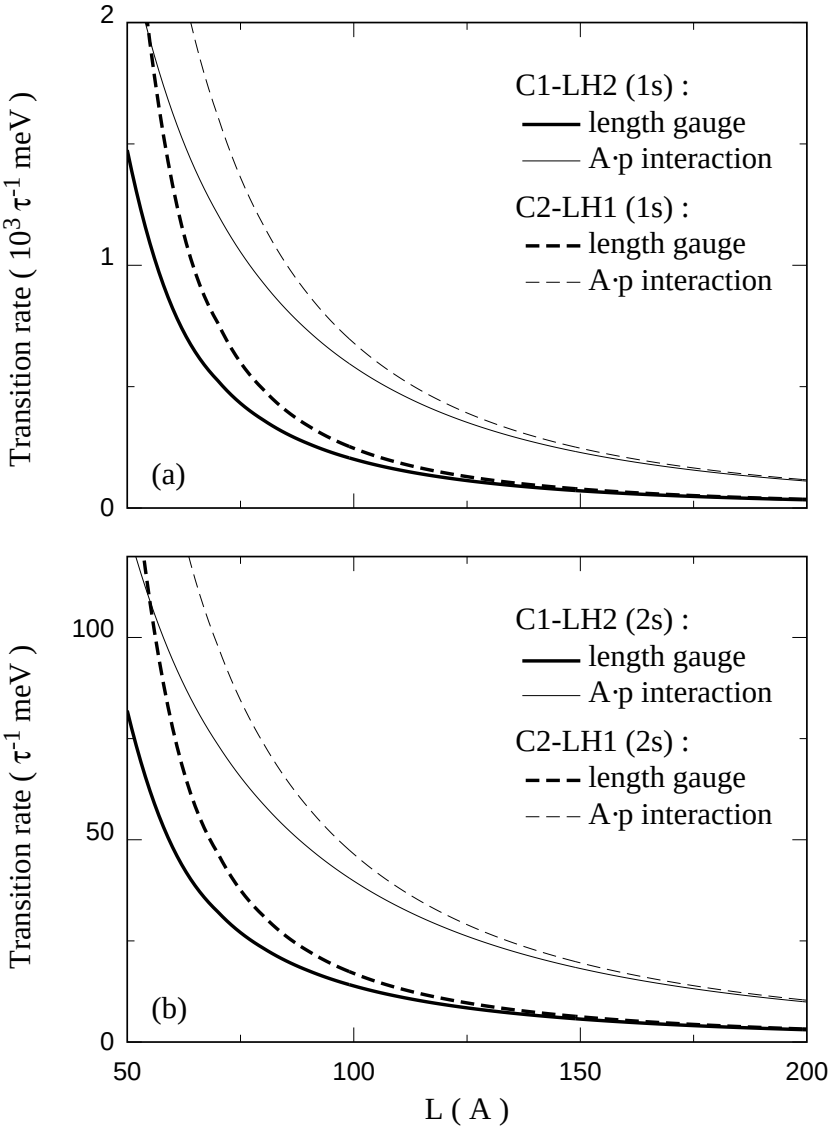


**Figure 4.4.** – Two-photon transition rate of (a) $1s$ and (b) $2s$, C1-LH2 and C2-LH1 exciton states in GaAs quantum wells as function of the well width. The absorbed photons are of the same energy and of $z$-polarization. The transition rate is expressed in the unit $\tau^{-1} = (e/c)^4 (A_1 A_2)^2 S/m_0\hbar^3$. Gauge-invariant results are obtained in the length gauge (thick lines). For comparison the same transition rates are calculated in the $\mathbf{A} \cdot \mathbf{p}$ interaction (thin lines).

of two-dimensional exciton states. In fact the transition energy diverges for decreasing well width because of the increase of the QW quantization energy. In more realistic calculations which account for finite barriers one of the subbands to which the exciton is associated moves out of the quantum well at sufficiently narrow well widths. This type of exciton which is in part associated to a discrete subband and in part to the continuum of the QW subbands is not described by the present calculations, which describe only excitons related to two discrete subbands.

In Fig. 4.4 we also report the transition rates as obtained in the $\mathbf{A} \cdot \mathbf{p}$ interaction. The two calculations yield different absolute values for the rates but the same relative behaviour is found, in agreement with previous results [62, 65]. With respect to previous bulk calculations [29], a larger difference between the two results is found. We attribute this larger difference to the fact that in the bulk only the relative small binding energy of the exciton is described in the effective mass approximation, whereas for excitons in QW's also the quantization energy of the subbands is accounted for.

In Fig. 4.5 we report transition rates of the $p$-type C1-HH1 and C1-LH1 excitons. The absorbed photons are taken of equal energy and of $x$-polarization. In our model $p$-type exciton states with $m = 1$ and $m = -1$ are degenerate. The transition rate presented in Fig. 4.5 is the sum of the transition rates of these two exciton states. The first important remark is that the transition rate is about two orders of magnitude smaller than the transition rate of $1s$ excitons. Second, the transition rate is almost independent of the well width. In fact, in this case the matrix elements (4.32) do not depend strongly on the well width $L$.

Also in this case, we have performed the calculations in the $\mathbf{A} \cdot \mathbf{p}$ interaction:

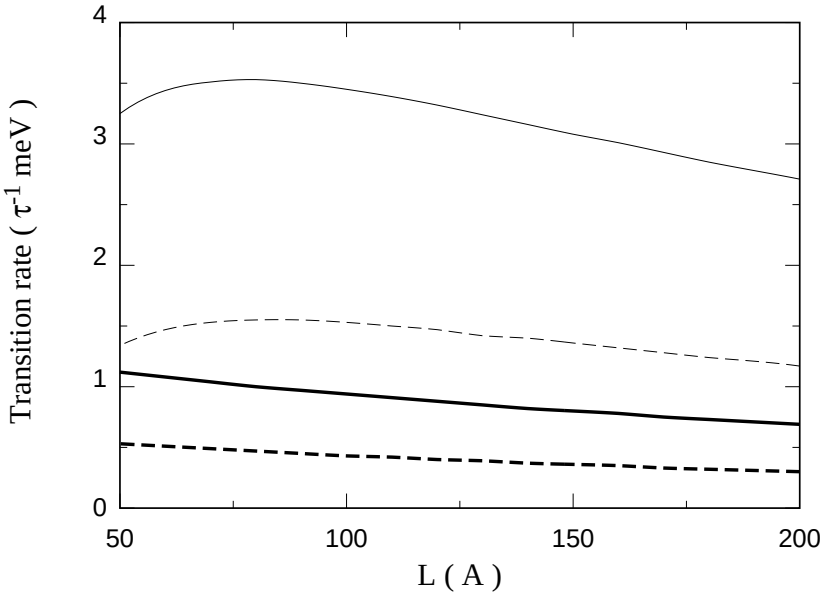


**Figure 4.5.** – Two-photon transition rate of $p$-type C1-HH1 (solid lines) and C1-LH1 (dashed) exciton states in GaAs quantum wells as a function of the well width. The absorbed photons are of the same energy and of $x$-polarization. The transition rate is obtained in the length gauge (thick lines), and in the $\mathbf{A} \cdot \mathbf{p}$ interaction (thin lines).

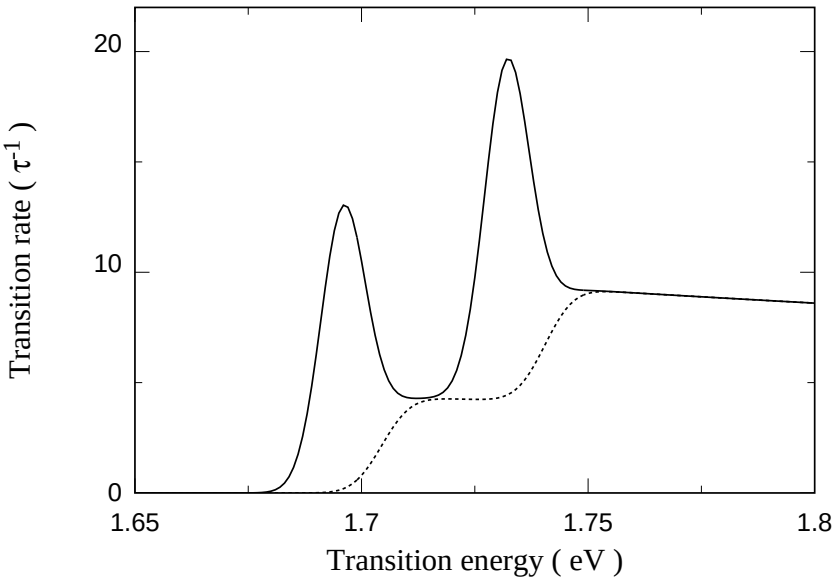


**Figure 4.6.** – Two-photon transition rate versus transition energy in a 110 Å QW in the case of equal photons of $z$-polarization. Transitions to $s$-type C1-LH2 and C2-LH1 excitons as well as between the associated subbands are considered. An overall Gaussian broadening with $\sigma = 5$ meV has been used.

the same conclusions as above apply. For narrow wells the two gauges seem to have a different behaviour. However, this difference is not meaningful and originates from the fact that the effective mass assumption that the envelope function is slowly varying with respect to the Bloch function breaks down for narrow well widths. In fact, this property has extensively been used calculating matrix elements of the momentum and position operators and relating them to each other. We expect that when different behaviour is found the limit of such calculations is reached.

In order to estimate if the peaks corresponding to $s$-excitons and $p$-excitons are observable we compare the exciton transition rates to their relative subband-subband transition rate [62]. The transition rate of the subband-subband continuum is given in units of $\tau^{-1} = (e/c)^4 (A_1 A_2)^2 S/m_0 \hbar^3$. On the other hand the transition rate of an exciton state, which is a discrete state, is expressed in the unit $\tau^{-1}$ meV, and corresponds to the area of the exciton peak. We assume an overall Gaussian broadening with $\sigma = 5$ meV. This seems to be realistic as can be deduced from the linewidth of the excitons [13, 14]. In Fig. 4.6 we plot the transition rate versus the transition energy in the case of $z$-polarization for a QW of 110 Å. The subband-subband transition rate, which has been obtained in the previous sections, is step-like with steps occuring at the C1-LH2 and C2-LH1 transition edges. The corresponding $s$-type exciton peaks have been added. The area of these peaks is determined by the present calculations. As can be seen from Fig. 4.6, it turns out that the excitonic effects mark the absorption spectrum with important features. Good agreement is found with the photoluminescence excitation experiment of Tai *et al.* [13]. The absolute energies at which the transitions occur in Fig. 4.6 are different from the experimental situation [13] because of the fact that the subband levels have been determined using the infinite barrier approximation. We note that in Fig. 4.6 the excitonic enhancement of the continuum has been neglected.

In Fig. 4.7 we plot the transition rate versus the transition energy in the case of $x$-polarization for a 40 Å QW. The subband-subband transition rate now vanishes at the transition-edge and grows linearly for increasing transition energies. The onset of absorption occurs at the C1-HH1 transition edge. In this case only $p$-type excitons can be excited. The C1-HH1 exciton peak has been added to the subband-subband transition rate in the same way as we have done

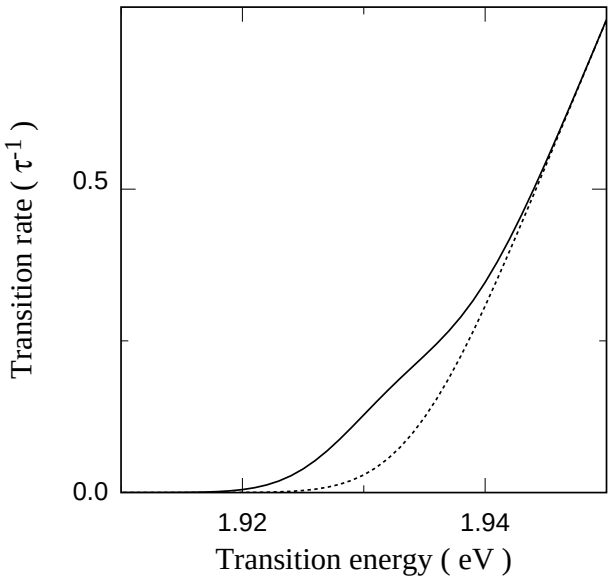


**Figure 4.7.** – Two-photon transition rate versus transition energy in a 40 Å QW in the case of equal photons of $x$-polarization. Transitions to $p$-type C1-HH1 excitons as well as between the associated subbands are considered. An overall Gaussian broadening with a $\sigma = 5$ meV has been used.

in the case of $z$-polarization. As can be seen from Fig. 4.7 the transition rate of the $p$-exciton is small and the exciton is hardly observable. In the experiment of Tai *et al.* [13] a particular feature was observed at the transition edge and was attributed to the $p$-exciton. The result of Fig. 4.7 shows that this feature can indeed be interpreted as an excitonic effect.

In the experiment of Catalano *et al.* [14] distinct excitonic peaks have been observed for $x$-polarization. These peaks are found at the transition edges of C2-HH2 and C2-LH2. We have calculated the transition rates of the $p$-type excitons which belong to these transition edges and found them to be as small as or even smaller than those presented in Fig. 4.5. If we use a broadening much smaller than 10 meV, the excitonic peaks are more visible. However, in this case, we are still not able to explain with the present theory the large area of these peaks which has been found in Ref. [14].

The origin of the large difference between transition rates of $s$-type and $p$-type excitons can be understood in part by analysing the subband-subband transition rate [62]. The exciton states can be built using the near-edge subband states. In the case of $z$-polarization ($s$-excitons) the transition rate of these states does not vanish at the centre of the Brillouin zone, whereas for $x$-polarization ($p$-excitons) it does. Moreover $p$-excitons are less bound and therefore the subband states which contribute most to the $p$ wave functions are states of small wave vector, which have negligible transition rate. This case is the analogue of second-kind transitions in bulk systems [37].

In Fig. 4.8 we present transition rates of the $1s$ C1-LH2 and C2-LH1 exciton states in a 100 Å GaAs QW for varying relative energy of the photons. The transition energy is kept fixed and is different for the two excitons. The photon energy varies from an energy which corresponds to a half of the transition

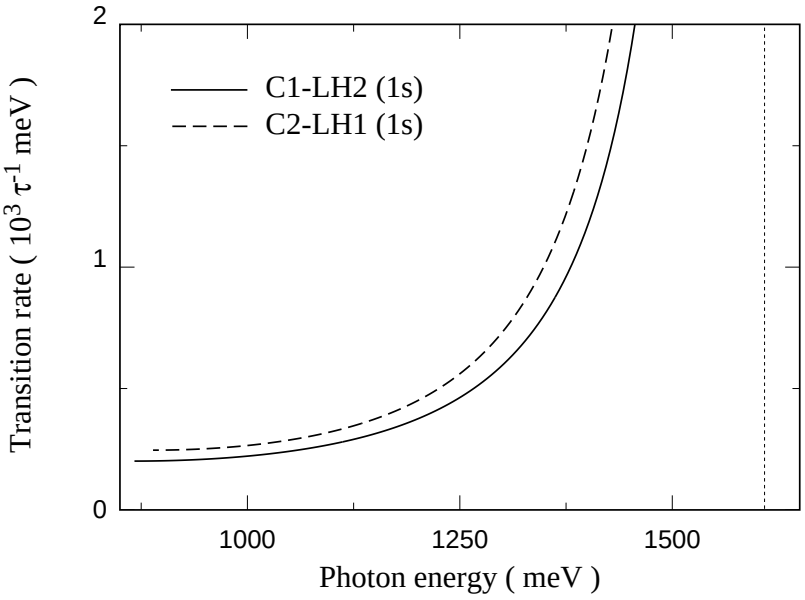


**Figure 4.8.** – Two-photon transition rate of $1s$ C1-LH2 (solid line) and C2-LH1 (dashed) exciton states in a 100 Å GaAs quantum well as a function of the energy of one of the photons. The absorbed photons are of $z$-polarization. The resonant energy of the intermediate state $1s$ C1-LH1 is indicated by a vertical dotted line.

energy to the energy of the $1s$ C1-LH1 exciton, which is a resonant intermediate state for both excitonic transitions. The transition rate of both excitons is strongly enhanced when one of the photon energies approaches the resonant energy. Near the resonance the transition rate is proportional to the reciprocal of the square of the energy separation between the photon energy and the energy of the intermediate state.

In conclusion, for $s$-type excitons, which are allowed for $z$-polarization, we have found that the transition rates are so large that the excitons appear as distinct peaks in the absorption spectrum. On the other hand, in the case of $p$-excitons, which are allowed for $x$-polarization, we have found rather small transition rates. In this case, excitonic effects are not expected to appear as distinct peaks but rather as particular features at the transition-edges. This kind of excitonic effect has indeed been observed [13]. These results confirm a previous calculation in a simplified model [63] and are in agreement with experiment [13].

# Chapter 5

# Interpretation of three-photon spectra in alkali halides

Recently, it has been possible to obtain three-photon spectra in alkali halides [3, 16, 17, 18]. The possibility of varying the total absorbed wavevector without changing the transition energy, makes of multiphoton spectroscopy a particularly valuable tool for the study of the $k$-dispersion of the polariton. In crystal which have an inversion centre, such as alkali halides, two-photon spectroscopy cannot be used to detect polariton states because of the parity selection rule. However, in three-photon spectroscopy, the parity selection rule is the same as in one-photon spectroscopy, and the polariton states can again be excited. In fact, with this technique it has been possible to measure the dispersion of the upper polariton and the longitudinal exciton in $O_h$ alkali halides [3]. Moreover, in three-photon spectroscopy also states with symmetry different from the dipole can be observed.

We consider interaction processes in which three photons of equal frequency

are absorbed. There are three types of selection rules. Dipole selection rules are determined by considering the direct product of the irriducible representations of the photons. Only transitions to final states belonging to this product are allowed. Geometrical selection rules arise when the polarizations of the photons make the geometrical factor of the transition vanish. Finally, when the photons are of equal energy the symmetrization of the interaction operator provides additional selection rules, as we have seen in Chapter 3. We illustrate these selection rules for excitonic transitions in alkali halides in order to interpret recent experiments [16, 17, 18].

In the case of two-photon transitions, it has been shown that for an $O_h$ point group it is always possible to factorize the transition probability into a dynamical and a geometrical factor [11]. In three-photon transitions, however, even in the case of photons of equal energy, there exist transitions whose polarization dependence is not fully determined by symmetry and contains a dynamical parameter [38]. We discuss how this parameter can be measured. Finally we consider the effect of a magnetic field in the three non-equivalent principal directions and interpret the available experimental results.

## 5.1 Excitonic transitions in alkali halides

In the $O_h$ point group, the polarization of the photon transforms according to the $\Gamma_4^-$ representation. The representation of a dipole allowed final state must belong to the triple direct product of $\Gamma_4^-$, as obtained in Eq. (3.19):

$$\mathbf{p} \otimes \mathbf{p} \otimes \mathbf{p} = \Gamma_1^- \oplus \Gamma_2^- \oplus 2\Gamma_3^- \oplus 4\Gamma_4^- \oplus 3\Gamma_5^- . \tag{5.1}$$

The corresponding polarization dependence has been given in Appendix B.

As the experiments of Refs. [16, 17, 18] are performed with photons of equal frequency, we must keep only the fully symmetric representations, i.e. those which in Eq. (3.20) are related to the $\tilde{\Gamma}_1^+$ representation of the permutation group $S_3$. This gives

$$S[\mathbf{p}\otimes\mathbf{p}\otimes\mathbf{p}] = \Gamma_2^- \oplus 2\Gamma_4^- \oplus \Gamma_5^-. \tag{5.2}$$

We notice that, even in the case of equal photons, three-photon spectroscopy allows more transitions than in one-photon processes, where only $\Gamma_4^-$ states can be excited. The symmetrized expressions of the polarization vectors that are left are also given in Appendix B.

We remark that the representations $\Gamma_2^-$ and $\Gamma_5^-$ occur only once in the symmetrized product. This implies that the polarization dependence in the transition probability to states of these symmetries is completely determined: the dynamical and geometrical factors are separable for $\Gamma_2^-$ and $\Gamma_5^-$ final states. We give the geometrical factors of the transition probability to states of these symmetries:

$$G_2(\boldsymbol{\epsilon}_1,\boldsymbol{\epsilon}_2,\boldsymbol{\epsilon}_3) = |\phi_2|^2, \tag{5.3}$$

$$G_5(\boldsymbol{\epsilon}_1,\boldsymbol{\epsilon}_2,\boldsymbol{\epsilon}_3) = |\phi_{5yz}^{(1)}|^2 + |\phi_{5zx}^{(1)}|^2 + |\phi_{5xy}^{(1)}|^2, \tag{5.4}$$

where the $\phi$'s are those of Eqs. (B.1)–(B.4).

The $\Gamma_4^-$ representation appears twice in the decomposition (5.2), giving rise to two different reduced matrix elements in the transition probability to final states of $\Gamma_4^-$ symmetry. Now it is no longer possible to separate dynamical and geometrical factors, contrary to some statements made in literature [46]. The polarization dependence contains one dynamical parameter $\lambda$ which depends on the final state considered:

$$G_4(\boldsymbol{\epsilon}_1,\boldsymbol{\epsilon}_2,\boldsymbol{\epsilon}_3) = |\phi_{4x}^{(1)} + \lambda\phi_{4x}^{(2)}|^2 + |\phi_{4y}^{(1)} + \lambda\phi_{4y}^{(2)}|^2 + |\phi_{4z}^{(1)} + \lambda\phi_{4z}^{(2)}|^2. \tag{5.5}$$

The same expressions have been obtained by Bobrysheva and Moskalenko in the particular case of three photons of equal frequency and polarization [38]. The formulae (B.1)–(B.4) are also valid for photons from different beams, which may have different polarizations, provided they are of the same frequency. However, in this case, the transition amplitude must be summed over all possible processes, in which, e.g., all three photons are taken from the same beam, or two photons from the same beam and the third one from another beam. In the case of spherical symmetry the dynamical parameter in (5.5) is fixed by symmetry, $\lambda = \sqrt{2/3}$, and the polarization dependence becomes

$$G_4^{sph}(\boldsymbol{\epsilon}_1, \boldsymbol{\epsilon}_2, \boldsymbol{\epsilon}_3) = \frac{1}{9}||(\boldsymbol{\epsilon}_1 \cdot \boldsymbol{\epsilon}_2)\boldsymbol{\epsilon}_3 + (\boldsymbol{\epsilon}_3 \cdot \boldsymbol{\epsilon}_1)\boldsymbol{\epsilon}_2 + (\boldsymbol{\epsilon}_2 \cdot \boldsymbol{\epsilon}_3)\boldsymbol{\epsilon}_1||^2. \tag{5.6}$$

We emphasize that all formulae we have obtained are valid for whatever state of polarization, i.e. even for complex polarization vectors. In particular, formula (5.6) contains factors of the type $\boldsymbol{\epsilon}_1 \cdot \boldsymbol{\epsilon}_2$ [not $\boldsymbol{\epsilon}_1^* \cdot \boldsymbol{\epsilon}_2$]. These factor make expression (5.6) vanish for circularly polarized photons with the same polarization vectors. This is analogous to the case of two-photon transitions, where transitions to states of $\Gamma_1^+$ symmetry are forbidden for photons of the same circular polarization [79]. In the case of Raman processes, on the other hand, one of the photons is emitted, and factors of the type $\boldsymbol{\epsilon}_1^* \cdot \boldsymbol{\epsilon}_2$ will appear in the polarization dependence.

Excitonic transitions in alkali halides have been studied since a long time. We analyse the symmetry of the excitons starting from the band structure [80, 81]. At the centre of the Brillouin zone, the valence band, arising from halogen $p$-states, is split by the spin-orbit interaction into an uppermost band of $\Gamma_8^-$ symmetry and a lower-lying band of $\Gamma_6^-$ symmetry. The lowest conduction band arises from alkali $s$-states and has $\Gamma_6^+$ symmetry at the $\Gamma$ point. The symmetry

of the $s$-excitons related to these bands is given by

$$\begin{aligned} \Gamma_6^+ \oplus \Gamma_8^- &= \Gamma_3^- \oplus \Gamma_4^- \oplus \Gamma_5^-, \\ \Gamma_6^+ \oplus \Gamma_6^- &= \Gamma_1^- \oplus \Gamma_4^-. \end{aligned} \tag{5.7}$$

The $\Gamma_4^-$ states are allowed in one-photon transitions and give rise to a pronounced doublet structure at the fundamental absorption edge, which is observed in most alkali halides [82]. The relative oscillator strengths of these peaks have been studied in detail by Onodera and Toyozawa [83]. They have also shown that the $\Gamma_3^-$ and the $\Gamma_5^-$ states are pure spin triplets (paraexcitons). The $\Gamma_5^-$ state is dipole allowed in three-photon spectroscopy, but its oscillator strength would be zero in the absence of the spin-orbit interaction, and is therefore expected to be very small. Indeed only recently Beerwerth and Fröhlich have observed paraexciton states in KI by three-photon spectroscopy and have measured an oscillator strength which is three order of magnitude smaller as compared with the $\Gamma_4^-$ lines [17].

In CsCl-type halides there is another low-lying conduction band, which arises mainly from alkali $d$-states and has $\Gamma_8^+$ symmetry [81]. At the fundamental absorption edge of these alkali halides one finds, besides the ($\Gamma_6^+$,$\Gamma_8^-$) excitons, additional structure due to the ($\Gamma_8^+$,$\Gamma_8^-$) excitons [82]:

$$\Gamma_8^+ \otimes \Gamma_8^- = \Gamma_1^- \oplus \Gamma_2^- \oplus \Gamma_3^- \oplus 2\Gamma_4^- \oplus 2\Gamma_5^-. \tag{5.8}$$

In CsI, the two additional $\Gamma_4^-$ lines have been observed in one- [82] as well as in three-photon [16, 18] spectroscopy. According to the selection rules of Eq. (5.2), states of $\Gamma_2^-$ and $\Gamma_5^-$ symmetry are allowed in addition to $\Gamma_4^-$. The two $\Gamma_5^-$ states of (5.8) have been observed in Refs. [16, 18]. We remark that the observed polarization dependence of the $\Gamma_4^-$ and $\Gamma_5^-$ lines is in agreement with Eqs. (5.4) and (5.5). We consider these expressions for a laser beam aligned along a crystal

axis, $\boldsymbol{\epsilon} = (\epsilon_x, \epsilon_y, 0)$:

$$G_4(\boldsymbol{\epsilon}) = |\epsilon_x|^2|\epsilon_x^2 + \sqrt{3/2}\lambda\epsilon_y^2|^2 + |\epsilon_y|^2|\epsilon_y^2 + \sqrt{3/2}\lambda\epsilon_x^2|^2, \tag{5.9}$$

$$G_5(\boldsymbol{\epsilon}) = \frac{3}{2}|\epsilon_x|^2|\epsilon_y|^2. \tag{5.10}$$

The $\Gamma_5^-$ lines are observable in circular polarization as well as in linear polarization, unless the latter is along a crystal axis. The $\Gamma_4^-$ lines are instead strongly suppressed in circular polarization if the dynamical parameter $\lambda$ is near to its spherical value:

$$G_4(\sigma^\pm) = \frac{3}{8}|\lambda - \sqrt{2/3}|^2. \tag{5.11}$$

In fact, in order to make the $\Gamma_5^-$ line observable, circular polarization has been used to suppress the $\Gamma_4^-$ line which belongs together with the adjacent $\Gamma_5^-$ line to the spherical $F = 3$ multiplet [18].

The dynamical parameters $\lambda$ in the polarization dependence of the $\Gamma_4^-$ lines can be determined for example by taking the ratio of the peak values with linear and with circular polarization. In order to reduce the influence of experimental errors, $\lambda$ can be better deduced by considering the $\Gamma_4^-$-$\Gamma_5^-$ peak to peak ratio for the two polarizations. For linear polarization with $\tilde{\boldsymbol{\epsilon}} = (1/\sqrt{2}, 1/\sqrt{2}, 0)$ the relevant ratio is

$$\frac{G_4(\sigma^\pm)}{G_5(\sigma^\pm)}\frac{G_5(\tilde{\boldsymbol{\epsilon}})}{G_4(\tilde{\boldsymbol{\epsilon}})} = \frac{|\lambda - \sqrt{2/3}|^2}{|\lambda + \sqrt{2/3}|^2}. \tag{5.12}$$

This ratio depends in a sensitive way on the deviation of $\lambda$ from its spherical value.

Among the ($\Gamma_8^+$,$\Gamma_8^-$) excitons there is also one exciton of $\Gamma_2^-$ symmetry. Although allowed in three-photon spectroscopy, this excitonic line has not yet been observed. In fact, for identical photons, Eq. (5.3) gives $G_2 = 6|\epsilon_x|^2|\epsilon_y|^2|\epsilon_z|^2$, and the geometrical factor of this line vanishes unless the absorbed photons have

a polarization component along the three cubic axes. To estimate the energy position of this line it is useful to consider how the spherical multiplets are split by the crystal field. The $\Gamma_2^-$ state belongs together with a $\Gamma_4^-$ and a $\Gamma_5^-$ to a spherical multiplet $F = 3$. In the CsI spectrum of Ref. [18] a $\Gamma_4^-$ and a $\Gamma_5^-$ are found near to each other, which means that the crystal field splitting is small: therefore the $\Gamma_2^-$ line should also be searched in this energy region. A possible way to detect this line is to use a circularly polarized beam aligned along the $\langle 111 \rangle$ direction. In this configuration the geometrical factors are $G_2(\sigma^\pm) = 16/9$, $G_5(\sigma^\pm) = 4$, and $G_4(\sigma^\pm) = (4/3)|\lambda - \sqrt{2/3}|^2$. The adjacent strong $\Gamma_4^-$ line is therefore suppressed if $\lambda$ is near to its spherical value. Another possibility for observing this line could be to split the laser beam in three beams that enter the sample along the three cubic axes.

According to the band structure calculated by Onodera [81], the $\Gamma_2^-$ exciton state has a large triplet component. If this is indeed the case, it will be rather difficult to detect this line experimentally.

## 5.2 Effect of a magnetic field

We now investigate how the presence of a magnetic field reduces the symmetry and splits the lines that are observable in three photon spectroscopy. Because of the reduced symmetry the number of dynamical parameters in the polarization dependence increases. We use our symmetry analysis to interpret recent experimental results [16, 17, 18]. We first consider a magnetic field in the [001] direction. The symmetry group reduces from $O_h$ to $C_{4h}$. From the compatibility tables [45] we find the representations of $C_{4h}$ that are allowed in absorption processes of three photons of equal energy; the interaction operator transforms

as

$$S[\mathbf{p}\otimes\mathbf{p}\otimes\mathbf{p}] = 2\Gamma_1^- \oplus 2\Gamma_2^- \oplus 3\Gamma_3^- \oplus 3\Gamma_4^-. \tag{5.13}$$

The number $N$ of reduced matrix elements that appear in the transition probability to a state of a given symmetry is equal to the number of times that representation is found in the decomposition (5.13). The polarization dependence contains therefore a number $N-1$ of dynamical parameters. We give the polarization dependence for three-photon transitions to the states which appear in (5.13), taking the $z$-axis as the direction of the field:

$$\begin{aligned}
G_1(\boldsymbol{\epsilon}_1,\boldsymbol{\epsilon}_2,\boldsymbol{\epsilon}_3) &= |\phi_{4z}^{(1)} + \mu_1\phi_{4z}^{(2)}|^2, \\
G_2(\boldsymbol{\epsilon}_1,\boldsymbol{\epsilon}_2,\boldsymbol{\epsilon}_3) &= |\phi_2 + \mu_2\phi_{5xy}^{(1)}|^2, \\
G_3(\boldsymbol{\epsilon}_1,\boldsymbol{\epsilon}_2,\boldsymbol{\epsilon}_3) &= |\frac{1}{\sqrt{2}}(\phi_{4x}^{(1)} + i\phi_{4y}^{(1)}) + \mu_{31}\frac{1}{\sqrt{2}}(\phi_{4x}^{(2)} + i\phi_{4y}^{(2)}) \\
&\quad +\mu_{32}\frac{1}{\sqrt{2}}(\phi_{5yz}^{(1)} - i\phi_{5zx}^{(1)})|^2, \\
G_4(\boldsymbol{\epsilon}_1,\boldsymbol{\epsilon}_2,\boldsymbol{\epsilon}_3) &= |\frac{1}{\sqrt{2}}(\phi_{4x}^{(1)} - i\phi_{4y}^{(1)}) + \mu_{41}\frac{1}{\sqrt{2}}(\phi_{4x}^{(2)} - i\phi_{4y}^{(2)}) \\
&\quad +\mu_{42}\frac{1}{\sqrt{2}}(\phi_{5yz}^{(1)} + i\phi_{5zx}^{(1)})|^2.
\end{aligned} \tag{5.14}$$

In the spherical approximation the parameters $\mu_1$, $\mu_{31}$, $\mu_{41}$ are independent of the field and equal to $\sqrt{2/3}$. Moreover, for weak field, the values of these parameters coincide with $\lambda$ defined in Eq. (5.5). In a Faraday configuration, $\Gamma_1^-$ and $\Gamma_2^-$ states are forbidden, $\Gamma_3^-$ states are allowed for $\sigma^+$ polarization, and $\Gamma_4^-$ states are allowed for $\sigma^-$ polarization. In Voigt configurations all states can be excited.

A spherical $F=2$ multiplet appears in the symmetries of the ($\Gamma_6^+$,$\Gamma_8^-$) excitons and, in Cs halides, also among ($\Gamma_8^+$,$\Gamma_8^-$) excitons: this multiplet splits into $\Gamma_3^-$ and $\Gamma_5^-$ states of $O_h$. The behaviour of these $F=2$ states in a magnetic field

is analogous in the two cases. For the ($\Gamma_6^+$,$\Gamma_8^-$) excitons this has been studied experimentally in KI [17] and RbI [18], whereas for the ($\Gamma_8^+$,$\Gamma_8^-$) excitons it has been studied in CsI [16]. In a magnetic field along [001] these states split into irriducible representations of $C_{4h}$:

$$\begin{aligned} \Gamma_3^- &\rightarrow \Gamma_1^- \oplus \Gamma_2^-, \\ \Gamma_5^- &\rightarrow \Gamma_2^- \oplus \Gamma_3^- \oplus \Gamma_4^-. \end{aligned} \tag{5.15}$$

Although five lines are allowed in principle, only four are observed in the experiment [17]. The interpretation of the experimental results is as follows. The $\Gamma_3^-$ and $\Gamma_4^-$ states can be excited selectively in Faraday configuration with circular polarization $\sigma^{\pm}$. The two $\Gamma_2^-$ states can be observed in Voigt configuration. The $\Gamma_2^-$ state arising from the $\Gamma_5^-$ state of $O_h$ is allowed also in the absence of a magnetic field. The $\Gamma_2^-$ arising from $\Gamma_3^-$ is forbidden for zero magnetic field, and it acquires an appreciable oscillator strength because it is mixed by the field with the other $\Gamma_2^-$. The $\Gamma_1^-$ state also arises from the $\Gamma_3^-$ and is forbidden at zero field. At finite field, its oscillator strength remains small because there are no other nearby states of the same symmetry from which it can acquire an oscillator strength. Thus, the four observed lines correspond to $\Gamma_3^-$, $\Gamma_4^-$ and two $\Gamma_2^-$.

We note that, when the Zeeman shift is larger than the crystal field splitting of 0.1 meV (which is achieved when $B > 2T$ [18]), the states can be labelled with the quantum numbers of the full rotational symmetry: in this scheme the $\Gamma_3^-$ and $\Gamma_4^-$ states correspond to $m = \pm 1$, whereas the $\Gamma_2^-$ states correspond to $m = \pm 2$. This implies that the $m = \pm 2$ states can only be seen in the Voigt configuration, in agreement with experiment [84].

The $\Gamma_2^-$ state of $O_h$, present in the $F = 3$ multiplet but not yet detected, has $\Gamma_2^-$ symmetry in $C_{4h}$. In absence of a magnetic field, observation of this state requires a polarization component along the three cubic axes, as discussed in the

previous section. However, a magnetic field along [001] mixes this state with the state of the same symmetry arising from the decomposition of the $\Gamma_5^-$ state of $O_h$ of the same $F = 3$ multiplet (as can be seen from Eq. (5.14)). Thus the $\Gamma_2^-$ state of $O_h$ becomes allowed in the same Voigt configuration used for the detection of the $m = \pm 2$ components of the ($\Gamma_3^-$,$\Gamma_5^-$) mixed states [17]. Extrapolation to zero field would then allow to determine the energy position of the $\Gamma_2^-$ state of $O_h$. This method requires that the field-induced coupling be comparable to the crystal field splittings within the $F = 3$ multiplet.

A magnetic field in the [110] direction reduces the symmetry to $C_{2h}$. Now only two representations are allowed:

$$S[\mathbf{p} \otimes \mathbf{p} \otimes \mathbf{p}] = 4\Gamma_1^- \oplus 6\Gamma_2^-. \tag{5.16}$$

We give the polarization dependence of the transition probability to these states:

$$\begin{aligned} G_1(\boldsymbol{\epsilon}_1, \boldsymbol{\epsilon}_2, \boldsymbol{\epsilon}_3) = \quad & |\frac{1}{\sqrt{2}}(\phi_{4x}^{(1)} + \phi_{4y}^{(1)}) + \eta_{11}\frac{1}{\sqrt{2}}(\phi_{4x}^{(2)} + \phi_{4y}^{(2)}) \\ & + \eta_{12}\frac{1}{\sqrt{2}}(\phi_{5yz}^{(1)} - \phi_{5zx}^{(1)}) + \eta_{13}\phi_{5xy}^{(1)}|^2, \\ G_2(\boldsymbol{\epsilon}_1, \boldsymbol{\epsilon}_2, \boldsymbol{\epsilon}_3) = \quad & |\frac{1}{\sqrt{2}}(\phi_{4x}^{(1)} - \phi_{4y}^{(1)}) + \eta_{21}\frac{1}{\sqrt{2}}(\phi_{4x}^{(2)} - \phi_{4y}^{(2)}) \\ & + \eta_{22}\frac{1}{\sqrt{2}}(\phi_{5yz}^{(1)} + \phi_{5zx}^{(1)}) + \eta_{23}\phi_{4z}^{(1)} + \eta_{24}\phi_{4z}^{(2)} + \eta_{25}\phi_2|^2. \end{aligned} \tag{5.17}$$

As before, in the spherical approximation one has the following relations for the dynamical parameters: $\eta_{11} = \eta_{21} = \eta_{24}/\eta_{23} = \sqrt{2/3}$. In Faraday configuration, $\sigma^{\pm} = (1/2)(-1, 1, \pm\sqrt{2}i)$, only $\Gamma_2^-$ states are observable. In Voigt configuration, both $\Gamma_1^-$ and $\Gamma_2^-$ are allowed: in particular the $\Gamma_1^-$ state requires a polarization component parallel to the field.

We now apply this result to the $F = 2$ multiplet in CsI. The lines of this

multiplet split into

$$\begin{aligned} \Gamma_3^- &\to \Gamma_1^- \oplus \Gamma_2^-, \\ \Gamma_5^- &\to 2\Gamma_1^- \oplus \Gamma_2^-. \end{aligned} \tag{5.18}$$

The experiment has been performed only in the Faraday configuration [16], where two lines have been observed, one originating from the $\Gamma_5^-$ of $O_h$, the other from the $\Gamma_3^-$ line. This is in agreement with our symmetry analysis. The latter line acquires oscillator strength from the former with increasing magnetic field. We note that, in Voigt configuration, all five lines are predicted to be observable, because both the $\Gamma_1^-$ and $\Gamma_2^-$ arising from the $\Gamma_3^-$ mix with states of the same symmetry arising from $\Gamma_5^-$. This is to be compared with the case of a magnetic field along [001], where only four lines can be observed.

Like in the case of a magnetic field along [001], the $\Gamma_2^-$ of $O_h$ contained in the $F = 3$ multiplet could be observed in a Voigt configuration. In fact this state, which becomes $\Gamma_2^-$ in $C_{2h}$, mixes with states of the same symmetry arising from both $\Gamma_4^-$ and $\Gamma_5^-$ states of $O_h$.

Finally we consider a magnetic field along [111]. The symmetry group is now $C_{3i}$. The allowed states are given by

$$S[\mathbf{p} \otimes \mathbf{p} \otimes \mathbf{p}] = 4\Gamma_1^- \oplus 3\Gamma_2^- \oplus 3\Gamma_3^-, \tag{5.19}$$

and their polarization dependence is

$$\begin{aligned} G_1(\boldsymbol{\epsilon}_1, \boldsymbol{\epsilon}_2, \boldsymbol{\epsilon}_3) &= |\frac{1}{\sqrt{3}}(\phi_{4x}^{(1)} + \phi_{4y}^{(1)} + \phi_{4z}^{(1)}) + \zeta_{11}\frac{1}{\sqrt{3}}(\phi_{4x}^{(2)} + \phi_{4y}^{(2)} + \phi_{4z}^{(2)}) \\ &\quad + \zeta_{12}\frac{1}{\sqrt{3}}(\phi_{5yz}^{(1)} + \phi_{5zx}^{(1)} + \phi_{5xy}^{(1)}) + \zeta_{13}\phi_2|^2, \\ G_2(\boldsymbol{\epsilon}_1, \boldsymbol{\epsilon}_2, \boldsymbol{\epsilon}_3) &= |\frac{1}{\sqrt{3}}(\phi_{4x}^{(1)} - \omega\phi_{4y}^{(1)} + \omega^2\phi_{4z}^{(1)}) + \zeta_{21}\frac{1}{\sqrt{3}}(\phi_{4x}^{(2)} - \omega\phi_{4y}^{(2)} + \omega^2\phi_{4z}^{(2)}) \\ &\quad + \zeta_{22}\frac{1}{\sqrt{3}}(\phi_{5yz}^{(1)} - \omega\phi_{5zx}^{(1)} + \omega^2\phi_{5xy}^{(1)})|^2, \end{aligned}$$

$$G_3(\boldsymbol{\epsilon}_1,\boldsymbol{\epsilon}_2,\boldsymbol{\epsilon}_3) = |\frac{1}{\sqrt{3}}(\phi^{(1)}_{4x}+\omega^2\phi^{(1)}_{4y}-\omega\phi^{(1)}_{4z})+\zeta_{31}\frac{1}{\sqrt{3}}(\phi^{(2)}_{4x}+\omega^2\phi^{(2)}_{4y}-\omega\phi^{(2)}_{4z}) + \zeta_{32}\frac{1}{\sqrt{3}}(\phi^{(1)}_{5yz}+\omega^2\phi^{(1)}_{5zx}-\omega\phi^{(1)}_{5xy})|^2, \tag{5.20}$$

where $\omega = e^{i\pi/3}$. Again, in the case of spherical approximation, we have $\zeta_{11} = \zeta_{21} = \zeta_{31} = \sqrt{2/3}$. In a Faraday configuration,

$$\sigma^{\pm} = (1/\sqrt{2} \pm i/\sqrt{6}, -1/\sqrt{2} \pm i/\sqrt{6}, \mp 2i/\sqrt{6}), \tag{5.21}$$

only $\Gamma_1^-$ states are observable. The states of the $F = 2$ multiplet now transform as

$$\begin{aligned} \Gamma_3^- &\rightarrow \Gamma_2^- \oplus \Gamma_3^-, \\ \Gamma_5^- &\rightarrow \Gamma_1^- \oplus \Gamma_2^- \oplus \Gamma_3^-, \end{aligned} \tag{5.22}$$

and indeed, in a Faraday configuration, only one line belonging to the $\Gamma_5^-$ has been detected [16]. Also in this case it should be possible to excite all five lines in a Voigt configuration, because the $\Gamma_2^-$ and $\Gamma_3^-$ states arising from $\Gamma_3^-$ are mixed with states of the same symmetry arising from $\Gamma_5^-$.

# Chapter 6

# Conclusions

In this thesis, we have studied some aspects of multiphoton transitions providing a theoretical support to recent experimental investigations. Attention has been addressed to two particular aspects, which are representative of present research.

Two-photon spectroscopy, which is nowadays a conventional technique of investigation, is often used to gain additional information on new materials. As an example, we have studied two-photon transitions in GaAs-$Ga_{1-x}Al_xAs$ quantum wells. We have developed a theory in the framework of the effective mass approximation in order to interpret recent experimental absorption spectra [13, 14].

First we have considered the absorption due to subband-subband transitions. We have calculated two-photon transition rates within a two-band model, in which the confinement is described by infinite barriers. We have obtained the absorption spectrum for the case of polarization of the radiation beam in the layer planes ($x$-) and along the growth axis ($z$-polarization). The two spectra are very different, reflecting the anisotropy of the quantum well system. In the case of $x$-polarization, the transition rate increases linearly as a function of transition

energy. Transitions are allowed between subbands which are labelled by the same principal quantum number. On the other hand, in the case of $z$-polarization, the absorption spectrum is step-like. The steps occur at the onsets of transitions between subbands of different parity. In the approximation of infinite barriers it is possible to obtain analytical expressions for the transition rate.

We have then considered the contribution to absorption due to continuum states going beyond the approximation of infinite barriers. We have shown that transitions between discrete and continuum states can contribute substantially to the absorption rate at transition energies below the band-gap of the barrier material, in contrast to the case of one-photon absorption in which the analogous contributions are negligible. We have found that the relative contribution due to the continuum states strongly depends on the polarization of the radiation beam. The continuum contribution turns out to be negligible for $x$-polarization, whereas in the case of $z$-polarization it is important and of the same order of magnitude as that due to transitions between discrete states. However, although the onset of transitions which involve continuum states occurs at rather low energy, their contribution becomes important only at much higher energies. As far as we are concerned with transitions between the lowest subbands, this effect can be neglected.

Finally, we have calculated transition rates to discrete excitonic states and added their effect to the subband-subband absorption spectrum. We have calculated excitonic states in the effective mass approximation describing the confinement due to the well structure by infinite barriers. The exciton wave function is taken to be separable in the $\mathbf{r}$-coordinates. The transition rate is calculated taking explitly into account the sum over all the intermediate states, using a variational procedure which has been applied successfully to the hydrogen atom

[15]. For $s$-type excitons, which are allowed for $z$-polarization, we have found transition rates which are so large that the excitons appear as distinct peaks in the absorption spectrum. On the other hand, in the case of $p$-excitons, which are allowed for $x$-polarization, we have found rather small transition rates. In this case, excitonic effects are not expected to appear as distinct peaks but rather as particular features at the transition-edges. This kind of excitonic effect has indeed been observed [13]. As a conclusion of this study on two-photon transitions in quantum wells, we find that our theory is able to reproduce the main features which have been observed experimentally.

Recently, it has been possible to detect three-photon transitions to excitonic states [16, 17, 18]. The selection rules which occur in the case of three-photon transitions are different with respect to the case of one- or two-photon transitions. It is therefore often possible to detect new transitions and extract physical parameters which would be difficult to obtain otherwise. In order to provide a theoretical support to this kind of experiments, we have presented a symmetry analysis of the multiphoton transition rate of exciton states in crystals.

The symmetry analysis shows that when some of the photons are of equal frequency or polarization, additional selection rules can occur. We have therefore given a particular emphasis to the transformation properties of the transition rate under permutation of the photon indices. The transition rate is expressed as the square modulus of a sum of products of geometrical factors, which depend on the polarizations of the photons, and dynamical factors, which depend on the frequencies. We show that the geometrical as well as the dynamical factors of the $n$-photon transition rate transform as irreducible representations of the permutation group of $n$ elements under permutations of the photon polarizations and frequencies, respectively. Our formulation turns out to be particularly useful to

determine the number of nonvanishing dynamical factors in the case of absorbed photons of equal frequency. When all the dynamical parameters vanish, a new selection rule occurs in addition to the usual dipole and geometrical selection rules. We have pointed out that because of the fact that corresponding dynamical and geometrical factors belong to the same irreducible representation of the permutation group, the same additional selection rules are found if the photons are taken of equal frequency *or* of equal polarization. This property is related to the fact that the transition rate is invariant under simultaneous permutations of all the photon indices.

The theory can be applied to any point group and for any number of absorbed photons. We have considered in detail the case of two-, three- and four-photon transitions and we have analysed as examples the point groups $O_h$, $T_d$ and $C_{6v}$, which correspond to the cubic, zincblende and wurtzite structure, respectively. For these point groups we have given the polarization dependence explicitly in the case of three-photon transitions.

These symmetry considerations have been applied to alkali halides ($O_h$ symmetry) in order to interpret recent experimental results [16, 17, 18]. In the case of absorption of three photons of equal frequency, only transitions to $\Gamma_2^-$, $\Gamma_4^-$, and $\Gamma_5^-$ states are expected to be observable. The $\Gamma_4^-$ and $\Gamma_5^-$ transitions have indeed been observed and show the correct dependence on the polarization vectors of the photons. The $\Gamma_2^-$ has not yet been observed. We have discussed possible configurations in which this line could be detected.

We have considered the effect of a magnetic field in the three principal directions of the crystal. For the three different cases, we have given the polarization dependence of all allowed transitions. In the case of a spherical $F = 2$ multiplet, the analysis explains the experimental result that only four lines can be

observed with a magnetic field in a [001] direction. We also predict that all five lines should be observable in a Voigt configuration for a magnetic field along [110] or [111]. In conclusion, the number of experimentally observed lines as well as their polarization dependence is accounted for by the present symmetry analysis.

## ACKNOWLEDGMENTS

I am grateful to Prof. F. Bassani and Prof. A. Quattropani for their numerous suggestions as well as for their constant interest during the whole course of this work. The work presented in Chapter 5 has been carried out in close collaboration with L. C. Andreani, who I wish to thank for his essential contribution. I have also benefitted from interesting and fruitful discussions with A. Baldereschi, N. Binggeli, S. de Gironcoli, S. Fraizzoli, D. Fröhlich, R. Girlanda, and A. Mysyrowicz, who I all wish to thank.

I acknowledge support from the *Institut de Physique Théorique* of the *Ecole Polytechnique Fédérale de Lausanne*, as well as from the *Scuola Normale Superiore*, where a part of this work has been carried out.

# Appendix A

# Explicit expressions for the dynamical factors

The $\phi_{\nu,\lambda}^{n,(\alpha\beta)}$ in Eq. (3.5) transform as partner functions of the irreducible representation $\beta$ of the permutation group of $n$ elements:

$$O_\sigma \phi_{\nu,\lambda}^{n,(\alpha\beta)} = \sum_{\lambda'=1}^{l_\beta} M_{\lambda'\lambda}^{\beta}(\sigma) \phi_{\nu,\lambda'}^{n,(\alpha\beta)}, \tag{A.1}$$

where $M_{\lambda'\lambda}^{\beta}$ is a matrix representation of $\beta$. By inserting Eq. (A.1) in expression (3.5) we obtain expression (3.6), where

$$\begin{aligned} D_{\lambda}^{n,(\alpha\beta)}(\omega_1, ...\omega_n) &= \sum_{\lambda'=1}^{l_\beta} \sum_{\sigma} [M_{\lambda\lambda'}^{\beta}(\sigma)]^* O_\sigma \langle f^\alpha || T_{\lambda'}^{n,(\alpha\beta)}(\omega_1, ...\omega_n) || 0 \rangle \\ &= \frac{n!}{l_\beta} \sum_{\lambda'=1}^{l_\beta} \mathcal{P}_{\lambda\lambda'}^{\beta} \langle f^\alpha || T_{\lambda'}^{n,(\alpha\beta)}(\omega_1, ...\omega_n) || 0 \rangle, \end{aligned} \tag{A.2}$$

where $\mathcal{P}_{\lambda\lambda'}^{\beta}$ are projectors on the $\lambda$th row of the irreducible representation $\beta$. Hence the $D_{\lambda}^{n,(\alpha\beta)}$ transform under permutations of the frequencies in the same way as the corresponding $\phi_{\nu,\lambda}^{n,(\alpha\beta)}$ under permutations of the polarizations.

# Appendix B

# Polarization dependence of three-photon transitions

In this appendix we give the polarization dependence of three-photon transitions for the point groups $O_h$, $T_d$ and $C_{6v}$ explicitly. We give the $\phi^{n,(\alpha\beta)}_{\nu,\lambda}$ of Eq. 3.6. The $\phi$'s transform as rows of the irreducible representations of $S_3$ which are given in Fig. 3.2. We note that the geometrical factors of a given symmetry of the point group which transform as $\tilde{\Gamma}_2$ appear always in pairs, as they correspond to the two rows of the $\tilde{\Gamma}_2$ representation.

For the $O_h$ point group we use the shorthand notation $(ijk)$ for $\epsilon_{1i}\epsilon_{2j}\epsilon_{3k}$ and $\phi^{(n)}_{\alpha\nu}$ for the geometrical factors, dropping the indices which refer to the permutation symmetry. The basis for the polarization vectors has been chosen along the cubic axes. The geometrical factors which transform as the symmetric representation $\tilde{\Gamma}^+_1$ are given by [42]:

$$\begin{aligned}\phi_2 &= \frac{1}{\sqrt{6}}[(xyz)+(zxy)+(yzx) \\ &\quad +(zyx)+(yxz)+(xzy)],\end{aligned} \tag{B.1}$$

$$\begin{aligned}
\phi_{4x}^{(1)} &= (xxx), \\
\phi_{4y}^{(1)} &= (yyy), \\
\phi_{4z}^{(1)} &= (zzz),
\end{aligned} \tag{B.2}$$

$$\begin{aligned}
\phi_{4x}^{(2)} &= \frac{1}{\sqrt{6}}[(xyy)+(yxy)+(yyx) \\
&\quad +(xzz)+(zxz)+(zzx)], \\
\phi_{4y}^{(2)} &= \frac{1}{\sqrt{6}}[(yzz)+(zyz)+(zzy) \\
&\quad +(yxx)+(xyx)+(xxy)], \\
\phi_{4z}^{(2)} &= \frac{1}{\sqrt{6}}[(zxx)+(xzx)+(xxz) \\
&\quad +(zyy)+(yzy)+(yyz)],
\end{aligned} \tag{B.3}$$

$$\begin{aligned}
\phi_{5yz}^{(1)} &= \frac{1}{\sqrt{6}}[(xyy)+(yxy)+(yyx) \\
&\quad -(xzz)-(zxz)-(zzx)], \\
\phi_{5zx}^{(1)} &= \frac{1}{\sqrt{6}}[(yzz)+(zyz)+(zzy) \\
&\quad -(yxx)-(xyx)-(xxy)], \\
\phi_{5xy}^{(1)} &= \frac{1}{\sqrt{6}}[(zxx)+(xzx)+(xxz) \\
&\quad -(zyy)-(yzy)-(yyz)].
\end{aligned} \tag{B.4}$$

The geometrical factors which transform as the twodimensional representation $\tilde{\Gamma}_2$ are:

$$\begin{aligned}
\phi_{31}^{(1)} &= \frac{1}{2\sqrt{3}}[(zxy)+(xyz)-(yxz)-(zyx)] \\
&\quad +\frac{1}{\sqrt{3}}[(xzy)-(yzx)], \\
\phi_{32}^{(1)} &= \frac{1}{2}[(yxz)-(zxy)-(zyx)+(xyz)],
\end{aligned} \tag{B.5}$$

$$\begin{aligned}
\phi_{31}^{(2)} &= \frac{1}{2\sqrt{3}}[(zyx)+(xzy)-(yzx)-(zxy)] \\
&\quad +\frac{1}{\sqrt{3}}[(xyz)-(yxz)], \\
\phi_{32}^{(2)} &= \frac{1}{2}[(yzx)-(zyx)-(zxy)+(xzy)], \qquad \text{(B.6)}
\end{aligned}$$

$$\begin{aligned}
\phi_{4x}^{(3)} &= \frac{1}{2}[(xyy)-(yyx)-(zzx)+(xzz)], \\
\phi_{4y}^{(3)} &= \frac{1}{2}[(yzz)-(zzy)-(xxy)+(yxx)], \qquad \text{(B.7)} \\
\phi_{4z}^{(3)} &= \frac{1}{2}[(zxx)-(xxz)-(yyz)+(zyy)],
\end{aligned}$$

$$\begin{aligned}
\phi_{4x}^{(4)} &= \frac{1}{2}[(xyy)-(yxy)-(zxz)+(xzz)], \\
\phi_{4y}^{(4)} &= \frac{1}{2}[(yzz)-(zyz)-(xyx)+(yxx)], \qquad \text{(B.8)} \\
\phi_{4z}^{(4)} &= \frac{1}{2}[(zxx)-(xzx)-(yzy)+(zyy)],
\end{aligned}$$

$$\begin{aligned}
\phi_{5yz}^{(2)} &= \frac{1}{2}[(xyy)-(yyx)+(zzx)-(xzz)], \\
\phi_{5zx}^{(2)} &= \frac{1}{2}[(yzz)-(zzy)+(xxy)-(yxx)], \qquad \text{(B.9)} \\
\phi_{5xy}^{(2)} &= \frac{1}{2}[(zxx)-(xxz)+(yyz)-(zyy)],
\end{aligned}$$

$$\begin{aligned}
\phi_{5yz}^{(3)} &= \frac{1}{2}[(xyy)-(yxy)+(zxz)-(xzz)], \\
\phi_{5zx}^{(3)} &= \frac{1}{2}[(yzz)-(zyz)+(xyx)-(yxx)], \qquad \text{(B.10)} \\
\phi_{5xy}^{(3)} &= \frac{1}{2}[(zxx)-(xzx)+(yzy)-(zyy)].
\end{aligned}$$

The only geometrical factor which transforms as the antisymmetric representation $\tilde{\Gamma}_1^-$ is:

$$\begin{aligned}
\phi_1 &= \frac{1}{\sqrt{6}}[(xyz)+(zxy)+(yzx) \\
&\quad -(zyx)-(yxz)-(xzy)]. \qquad \text{(B.11)}
\end{aligned}$$

In the case of the $T_d$ point group the polarization dependence is the same as for the $O_h$ group, only the nomenclature is different: the $\Gamma_1^-$, $\Gamma_2^-$, $\Gamma_3^-$, $\Gamma_4^-$, and $\Gamma_5^-$ of $O_h$ correspond to the $\Gamma_2$, $\Gamma_1$, $\Gamma_3$, $\Gamma_5$, and $\Gamma_4$ of $T_d$, respectively.

For the point group $C_{6v}$, we use the shorthand notation, for example, $(0+-)$ for $\epsilon_z\sigma_+\sigma_-$, where $\sigma_\pm$ correspond to the circular polarizations $\mp(1/\sqrt{2})(\epsilon_x \pm i\epsilon_y)$. The components of the polarization vectors are taken as in Ref. [45]. The symmetric geometrical factors are given by:

$$\phi_1^{(1)} = (000), \tag{B.12}$$

$$\phi_1^{(2)} = \frac{1}{\sqrt{6}}[(0+-)+(+0-)+(+-0) +(0-+)+(-0+)+(-+0)], \tag{B.13}$$

$$\phi_3 = \frac{1}{\sqrt{2}}[(---)+(+++)], \tag{B.14}$$

$$\phi_4 = \frac{1}{\sqrt{2}}[(---)-(+++)], \tag{B.15}$$

$$\phi_{5-}^{(1)} = \frac{1}{\sqrt{3}}[(+--)+(-+-)+(--+)],$$

$$\phi_{5+}^{(1)} = \frac{1}{\sqrt{3}}[(-++)+(+-+)+(++-)], \tag{B.16}$$

$$\phi_{5-}^{(2)} = \frac{1}{\sqrt{3}}[(-00)+(0-0)+(00-)],$$

$$\phi_{5+}^{(2)} = \frac{1}{\sqrt{3}}[(+00)+(0+0)+(00+)], \tag{B.17}$$

$$\phi_{6-}^{(2)} = \frac{1}{\sqrt{3}}[(0++)+(+0+)+(++0)],$$

$$\phi_{6+}^{(2)} = \frac{1}{\sqrt{3}}[(0--)+(-0-)+(--0)]. \tag{B.18}$$

The geometrical factors which transform as the $\tilde{\Gamma}_2$ representation are

$$\phi_1^{(3)} = \frac{1}{2}[(+-0)-(0-+)+(-+0)-(0+-)], \tag{B.19}$$

$$\phi_1^{(4)} = \frac{1}{2}[(+0-)-(0+-)+(-0+)-(0-+)], \tag{B.20}$$

$$\phi_2^{(1)} = \frac{1}{2}[(+-0)-(0-+)-(-+0)+(0+-)], \tag{B.21}$$

$$\phi_2^{(2)} = \frac{1}{2}[(+0-)-(0+-)-(-0+)+(0-+)], \tag{B.22}$$

$$\begin{aligned} \phi_{5-}^{(3)} &= \frac{1}{\sqrt{2}}[(-00)-(00-)], \\ \phi_{5+}^{(3)} &= \frac{1}{\sqrt{2}}[(+00)-(00+)], \end{aligned} \tag{B.23}$$

$$\begin{aligned} \phi_{5-}^{(4)} &= \frac{1}{\sqrt{2}}[(-00)-(0-0)], \\ \phi_{5+}^{(4)} &= \frac{1}{\sqrt{2}}[(+00)-(0+0)], \end{aligned} \tag{B.24}$$

$$\begin{aligned} \phi_{5-}^{(5)} &= \frac{1}{\sqrt{2}}[(--+)-(+--)], \\ \phi_{5+}^{(5)} &= \frac{1}{\sqrt{2}}[(-++)-(++-)], \end{aligned} \tag{B.25}$$

$$\begin{aligned} \phi_{5-}^{(6)} &= \frac{1}{\sqrt{2}}[(-+-)-(+--)], \\ \phi_{5+}^{(6)} &= \frac{1}{\sqrt{2}}[(-++)-(+-+)], \end{aligned} \tag{B.26}$$

$$\begin{aligned} \phi_{6-}^{(2)} &= \frac{1}{\sqrt{2}}[(++0)-(0++)], \\ \phi_{6+}^{(2)} &= \frac{1}{\sqrt{2}}[(--0)-(0--)], \end{aligned} \tag{B.27}$$

$$\begin{aligned} \phi_{6-}^{(3)} &= \frac{1}{\sqrt{2}}[(+0+)-(0++)], \\ \phi_{6+}^{(3)} &= \frac{1}{\sqrt{2}}[(-0-)-(0--)]. \end{aligned} \tag{B.28}$$

The only antisymmetric geometrical factor is given by

$$\begin{aligned}\phi_2^{(3)} &= \frac{1}{\sqrt{6}}[(0+-)-(+0-)+(+-0) \\ &\quad -(0-+)+(-0+)-(-+0)]. \end{aligned} \tag{B.29}$$

# Appendix C

# Matrix elements between continuum states

In this appendix we give explicit results for the matrix elements between continuum states (4.17) and (4.18), which have been used in Section 2.2 in the calculation of the two-photon transition rate (4.8) for $z$-polarization. The matrix elements between discrete states or between a continuum and a discrete state can be obtained by a straightforward calculation and yield always finite results, for which no distribution formalism is needed. The interband as well as the intraband matrix elements of $p_z$ between continuum states are obtained making use of

$$\int_0^\infty dx\, e^{ikx} = \mathcal{P}\frac{i}{k} + \pi\,\delta(k), \tag{C.1}$$

where $\mathcal{P}$ indicates the principal-part distribution. The principal-part as well as the delta distribution can be used because of the integral over the intermediate states, which appears in (4.8). For the interband matrix elements (4.22) between

continuum valence and conduction states, we have used

$$\langle f^c_{E\pm}|f^v_{E'\pm}\rangle = AA'\left[\frac{\sin[(k-k')d/2]}{(k-k')d} \pm \frac{\sin[(k+k')d/2]}{(k+k')d}\right]$$

$$-GG'\left[\frac{\sin[(g-g')d/2+\delta-\delta'] - \sin(\delta-\delta')}{(g-g')d} + \frac{\sin[(g+g')d/2+\delta+\delta']}{(g+g')d}\right]$$

$$+GG'\left[\pi\delta(gd-g'd)\cos(\delta-\delta') - \mathcal{P}\frac{\sin(\delta-\delta')}{(g-g')d}\right], \tag{C.2}$$

and for the intraband matrix elements (4.13) of $p_z$ between conduction continuum states,

$$\langle f^c_{E\pm}|p_z|f^c_{E'\mp}\rangle = \mp i\hbar k' AA'\left[\frac{\sin[(k-k')d/2]}{(k-k')d} \pm \frac{\sin[(k+k')d/2]}{(k+k')d}\right]$$

$$-i\hbar g' GG'\left[\frac{\cos[(g-g')d/2+\delta-\delta'] - \cos(\delta-\delta')}{(g-g')d} - \frac{\cos[(g+g')d/2+\delta+\delta']}{(g+g')d}\right]$$

$$-i\hbar g' GG'[\pi\delta(gd-g'd)\sin(\delta-\delta') + \mathcal{P}\frac{\cos(\delta-\delta')}{(g-g')d}]. \tag{C.3}$$

The intraband matrix elements of $z$ between continuum states are more complicated. They can either be obtained by a straightforward calculation or from the matrix elements of $p_z$ using the relation $p_z/m_c = [z, H^c]/(i\hbar)$, where $H^c$ is the effective-mass Hamiltonian for the conduction band as defined by Eq. (4.15). In the latter case, the matrix elements of $z$ between states of different energy are obtained, apart from some constants, by dividing the matrix elements of $p_z$ by the energy difference. However, also the case of vanishing energy difference must be accounted for. This division problem for distributions has carefully been studied [85]. The correct distribution for the matrix elements of $z$ is obtained making use of the theorem of Ref. [85]. The solution is now completely

determined apart from one term, an unknown constant times the solution of the homogeneous equation. This constant can be obtained from the straightforward calculation. Apart from this constant, it can be checked that the results provided by the two methods are the same. We obtain for conduction continuum states:

$$\langle f^c_{E\pm}|z|f^c_{E'\mp}\rangle = \mathcal{P}\frac{i\hbar}{(E'-E)m_c}\Bigg\{\mp i\hbar k' AA' \left[\frac{\sin[(k-k')d/2]}{(k-k')d} \pm \frac{\sin[(k+k')d/2]}{(k+k')d}\right]$$

$$-i\hbar g' GG' \left[\frac{\cos[(g-g')d/2+\delta-\delta'] - \cos(\delta-\delta')}{(g-g')d} - \frac{\cos[(g+g')d/2+\delta+\delta']}{(g+g')d}\right]\Bigg\}$$

$$-GG'\pi\sin(\delta-\delta')\frac{\partial}{\partial g'}\delta(gd-g'd) + \mathcal{D}_E\left[\frac{i\hbar}{(E'-E)m_c}\frac{\cos(\delta-\delta')}{(g-g')d}\right], \tag{C.4}$$

where $\mathcal{D}$ indicates a distribution which acts as follows on a test function $h$:

$$\int dx\, \mathcal{D}_{x_0}\left[\frac{f(x)}{(x-x_0)^2}\right] h(x) = \lim_{\epsilon\to 0}\left\{\left[\int^{x_0-\epsilon} + \int_{x_0+\epsilon} dx \frac{f(x)h(x)}{(x-x_0)^2}\right] + \frac{2f(x_0)h(x_0)}{\epsilon}\right\}. \tag{C.5}$$

In Eq. (C.4) the function which plays the role of $f$ in (C.5) can be obtained using the definition (4.19) for $g$ and $g'$ and is given by

$$f(E') = -\frac{i\hbar^3 cos(\delta-\delta')(g+g')}{2m_c^2 d}. \tag{C.6}$$

The intraband matrix elements between continuum valence states are analogous.

# Bibliography


[1] M. Göppert-Mayer, Ann. Phys. (Leipzig) **9**, 273 (1931).

[2] W. Kaiser and C. G. B. Garett, Phys. Rev. Lett. **7**, 229 (1961).

[3] F. Beerwerth and D. Fröhlich, Phys. Rev. Lett. **55**, 2603 (1985).

[4] E. Doni, R. Girlanda, and G. Pastori Parravicini, Solid State Commun. **17**, 189 (1975).

[5] D. Fröhlich and B. Staginnus, Phys. Rev. Lett. **19**, 496 (1967).

[6] D. Fröhlich, B. Staginnus, and S. Thurm, Phys. Status Solidi **40**, 287 (1970).

[7] D. Fröhlich and H. Volkenandt, Solid State Commun. **43** 189 (1982).

[8] D. Fröhlich, E. Mohler, and P. Wiesner, Phys. Rev. Lett. **26**, 554 (1971).

[9] D. Fröhlich, St. Kirchhoff, P. Köhler, and W. Nieswand, Phys. Rev. B **40**, 1976 (1989); Phys. Status Solidi (b) **158**, 267 (1990).

[10] J. E. Bjorkholm and P. F. Liao, Phys. Rev. Lett. **33**, 128 (1974).

[11] E. Doni, R. Girlanda, and G. Pastori Parravicini, Phys. Status Solidi (b) **65**, 203 (1974).

[12] D. Fröhlich, Com. Sol. State Phys. **4**,179 (1972).

[13] K. Tai, A. Mysyrowicz, R. J. Fisher, R. E. Slusher, and A. Y. Cho, Phys. Rev. Lett. **62** 1784 (1989).

[14] I. M. Catalano, A. Cingolani, R. Cingolani, M. Lepore, and K. Ploog, Phys. Rev. B **40**, 1312 (1989); I. M. Catalano, A. Cingolani, M. Lepore, R. Cingolani, and K. Ploog, Solid State Commun. **72**, 217 (1989).

[15] A. Quattropani and N. Binggeli, in the *The Hydrogen Atom*, edited by G. F. Bassani, M. Inguscio, and T. W. Hänsch (Springer, Berlin, 1989).

[16] F. Beerwerth and D. Fröhlich, Phys. Rev. Lett. **57**, 1344 (1986).

[17] F. Beerwerth and D. Fröhlich, Phys. Rev. B **36**, 6239 (1987).

[18] F. Beerwerth, D. Fröhlich, P. Köhler, V. Leinweber, and A. Voss, Phys. Rev. B **38**, 4250 (1988).

[19] D. A. Kleinman, Phys. Rev. **125**, 87 (1962).

[20] R. Braunstein, Phys. Rev. **125**, 475 (1962).

[21] R. Loudon, Proc. Roy. Soc. (London) **80**, 952 (1962).

[22] G. D. Mahan, Phys. Rev. Lett. **20**, 332 (1968); Phys. Rev. **170**, 825 (1968).

[23] W. L. Peticolas, R. Norris and K. E. Rieckhoff, J. Chem. Phys. **42**, 4164 (1968).

[24] J. J. Forney, A. Quattropani, and F. Bassani, Nuovo CimentoB **37**, 78 (1977).

[25] Y. Aharonov and C. K. Au, Phys. Rev. A **20**, 1553 (1979); Phys. Lett. A **86**, 269 (1981).

[26] F. Bassani, J. J. Forney, and A. Quattropani, Phys. Rev. Lett. **39**, 1070 (1977).

[27] G. W. Robinson, Phys. Rev. B **26**, 1482 (1982).

[28] A. F. Starace, Phys. Rev. A **3**, 1242 (1971).

[29] R. Girlanda, A. Quattropani, and P. Schwendimann, Phys. Rev. B **24**, 2009 (1981); A. Quattropani and R. Girlanda, Riv. Nuovo Cimento **6**, 1 (1983).

[30] E. De Salvo, R. Girlanda, and A. Quattropani, Nuovo Cimento **5D**, 63 (1985).

[31] S. Baroni and A. Quattropani, Nuovo Cimento D **5**, 89 (1985).

[32] C. Schwartz and J. J Tiemann, Ann. Phys. (New York) **2**, 178 (1959).

[33] Y. Gontier, N. K. Rahman, and M. Trahin, Nuovo Cimento D **4**, 1 (1984).

[34] L. C. Andreani, N. Binggeli, A. Pasquarello, and A. Quattropani, (unpublished).

[35] A. Dalgarno and J. T. Lewis, Proc. Roy. Soc. (london) **A233**, 70 (1955).

[36] see for instance, H. A. Bethe and E. E. Salpeter, *Quantum Mechanics of One and Two-Electron Atoms*, (Springer, Berlin, 1957).

[37] M. Inoue and Y. Toyozawa, J. Phys. Soc. Jpn. **20**, 363 (1965).

[38] A. I. Bobrysheva and S. A. Moskalenko, Sov. Phys.-Solid. State **8**, 2177 (1968) [Fizika Tverdogo Tela, **8**, 2730 (1966)].

[39] T. R. Bader and A. Gold, Phys. Rev. **171**, 997 (1968).

[40] see for example A. Messiah, *Mécanique Quantique*, (Dunod, Paris, 1964), Tome II, and references therein.

[41] A. Pasquarello and A. Quattropani, Phys. Rev. B **43**, 3837 (1991).

[42] A. Pasquarello and L. C. Andreani, Phys. Rev. B **41**, 12230 (1990).

[43] N. Bloembergen, in *Nonlinear Spectroscopy*, edited by N. Bloembergen (Amsterdam, North-Holland, 1977), p. 1.

[44] M. M. Denisov and V. P. Makarov, J. Phys. C **5**, 2651 (1972).

[45] G. F. Koster, J. O. Dimmock, R. G. Wheeler, and H. Statz, *Properties of the Thirty-Two Point Groups* (MIT, Cambridge, 1963).

[46] A. R. Hassan and R. Raouf, Phys. Status Solidi (b) **104**, 703 (1981).

[47] D. Fröhlich, B. Staginnus, and Y. Onodera, Phys. Status Solidi **40**, 547 (1970).

[48] D. L. Andrews and W. A. Ghoul, J. Chem. Phys. **75**, 530 (1981).

[49] D. L. Andrews and P. J. Wilkes, J. Chem. Phys. **83**, 2009 (1985).

[50] J. R. Cable and A. C. Albrecht, J. Chem. Phys. **85**, 3145 (1986).

[51] See for example B. A. Joyce, Rep. Prog. Phys. **48**, 1637 (1985).

[52] R. Dingle, A. C. Gossard, and W. Wiegmann, Phys. Rev. Lett. **34**, 1327 (1975); R. C. Miller and D. A. Kleinman, J. Luminescence **30**, 520 (1985).

[53] G. Bastard, Phys. Rev. B **24**, 5693 (1981); **25** 7484 (1982).

[54] M. Altarelli, U. Ekenberg, and A. Fasolino, Phys. Rev. **32**, 5138 (1985).

[55] L. C. Andreani, A. Pasquarello, and F. Bassani, Phys. Rev. **36**, 5887 (1987).

[56] K. S. Chan, J. Phys. C **19**, L125 (1986); U. Ekenberg and M. Altarelli, Phys. Rev. B **35**, 7585 (1987); Bangfen Zhu and Kun Huang, Phys. Rev. B **36**, 8102 (1987); Bangfen Zhu, Phys. Rev. B **37**, 4689 (1988); L. C. Andreani and A. Pasquarello, Europhysics Lett. **6**, 259 (1988); G. E. W. Bauer and T. Ando, Phys. Rev. **38**, 6015 (1988); L. C. Andreani and A. Pasquarello, Phys. Rev. B **42**, 8928 (1990).

[57] G. Bastard, Phys. Rev. B **24**, 4714 (1981); C. Mailhiot, Yia-Chung Chang, and T. C. McGill, Phys. Rev. B **26**, 4449 (1982); R. L. Greene and K. K. Bajaj, Solid State Commun. **45**, 825 (1983); S. Fraizzoli, F. Bassani, and R. Buczko, Phys. Rev. B **41**, 5096 (1990);

[58] W. T. Masselink, Y.-C. Chang, and H. Morkoç, Phys. Rev. B **28**, 7373 (1983); **32**, 5190 (1985); A. Pasquarello, L. C. Andreani, and R. Buczko, Phys. Rev. B **40**, 5602 (1989); S. Fraizzoli and A. Pasquarello, Phys. Rev. B **42**, 5349 (1990).

[59] D. Fröhlich, R. Wille, W. Schlapp, and G. Weinmann, Phys. Rev. Lett. **61**, 1878 (1988).

[60] M. Nithisootorn, K. Unterrainer, S. Michaelis, and N. Sawaki, Phys. Rev. Lett. **62**, 3078 (1989).

[61] H. N. Spector, Phys. Rev. B **35**, 5876 (1987).

[62] A. Pasquarello and A. Quattropani, Phys. Rev. B **38**, 6206 (1988).

[63] A. Shimizu, Phys. Rev. B **40**, 1403 (1989).

[64] L. C. Andreani, F. Bassani, and A. Pasquarello, in *Symmetry in Nature*, Quaderni of the Scuola Normale Superiore, Pisa (1989).

[65] A. Pasquarello and A. Quattropani, Phys. Rev. B **41**, 12728 (1990).

[66] G. Bastard, E. E. Mendez, L. L. Chang, and L. Esaki, Phys. Rev. B **26**, 1974 (1982).

[67] A. Pasquarello and A. Quattropani, Phys. Rev. B **42**, 9073 (1990).

[68] *Landolt-Börnstein, Numerical Data and Functional Relationships in Science and Technology*, edited by O. Madelung (Springer, Berlin, 1982), Gp. III, Vol. 17.

[69] P. Lawaetz, Phys. Rev. B **4**, 3460 (1970).

[70] H. C. Casey and M. B. Panish, *Heterostructures Lasers* (Academic, New York, 1978), part A.

[71] L. C. Andreani and A. Pasquarello, Europhys. Lett. **6**, 259 (1988); Superlattices and Microstructures **5**, 59 (1989); Phys. Rev. B **42**, 8928 (1990).

[72] S. Fraizzoli, F. Bassani, and R. Buczko, Phys. Rev. B **41**, 5096 (1990).

[73] J. M. Luttinger and W. Kohn, Phys. Rev. **97**, 869 (1955).

[74] J. M. Luttinger, Phys. Rev. **102**, 1030 (1956).

[75] M. Shinada and S. Sugano, J. Phys. Soc. Jpn. **21**, 1936 (1966).

[76] S. Baroni and R. Resta, Phys. Rev. B **33**, 7017 (1986).

[77] *Handbook of Mathematical Functions*, edited by M. Abramowitz and I. A. Stegun, (Dover, New York, 1972).

[78] R. Dingle, in *Festkörperprobleme* XV, edited by H. J. Queisser (Vieweg, Braunschweig, 1975).

[79] E. Doni, R. Girlanda, and G. Pastori Parravicini, Phys. Status Solidi (b) **88**, 773 (1978).

[80] B. Kunz, Phys. Rev. **175**, 1147 (1968); J. Phys. Chem. Solids **31**, 265 (1970).

[81] Y. Onodera, J. Phys. Soc. Jpn. **25**, 469 (1968).

[82] K. Teegarden and G. Baldini, Phys. Rev. **155**, 896 (1967).

[83] Y. Onodera and Y. Toyozawa, J. Phys. Soc. Jpn. **22**, 833 (1967).

[84] F. Beerwerth, Ph.D. Thesis, Universität Dortmund, 1987.

[85] L. Hörmander, Arkiv für Matematik **3**, 555 (1958).

# CURRICULUM VITÆ

| | |
|---|---|
| Name | Alfredo Pasquarello. |
| Date of Birth | December 13, 1963. |
| Place of Birth | Karachi (Pakistan). |
| Nationality | Italian. |

## Academic Activities

| | |
|---|---|
| July 1982 | Obtained the European Baccalaureate Certificate at the European School of Varese (Italy). |
| November 1986 | Graduated in Physics at the University of Pisa with the final mark of 110/110 *cum laude*. |
| November 1986 | Obtained the Diploma of the Scuola Normale Superiore. |
| 1987 - 1991 | Assistant at the Ecole Polytechnique Fédérale of Lausanne (Switzerland). |

## LIST OF PUBLICATIONS

*REGULAR ARTICLES:*

*Hole-subbands in strained $GaAs$-$Ga_{1-x}Al_xAs$ quantum wells: Exact solution of the effective mass equation,* L. C. Andreani, A. Pasquarello and F. Bassani, *Physical Review B* **36**, 5887 (Woodbury NY, USA, 1987).

*Electronic structure and optical properties of superlattices,* L. C. Andreani and A. Pasquarello, in *Highlights on Spectroscopies of Semiconductors and Insulators*, ed. by A. Balzarotti, A. Stella, M. Capizzi and G. Guizzetti (World Scientific, Singapore, 1988).

*Effect of subband coupling on exciton binding energies and oscillator strengths in $GaAs$-$Ga_{1-x}Al_xAs$ quantum wells,* L. C. Andreani and A. Pasquarello, *Europhysics Letters* **6**, 259 (Paris, France, 1988).

*Gauge-invariant two-photon transitions in quantum wells,* A. Pasquarello and A. Quattropani, *Physical Review B* **38**, 6206 (Woodbury NY, USA, 1988).

*Theory of excitons in $GaAs$-$Ga_{1-x}Al_xAs$ quantum wells including valence band mixing,* L. C. Andreani and A. Pasquarello, *Superlattices and Microstructures* **5**, 59 (London, Great Brittain, 1989).

*Binding energies of excited shallow acceptor states in $GaAs$-$Ga_{1-x}Al_xAs$ quantum wells,* A. Pasquarello, L. C. Andreani and R. Buczko, *Physical Review B* **40**, 5602 (Woodbury NY, USA, 1989).

*One-dimensional random potentials allowing for extended states,* A. Crisanti, C. Flesia, A. Pasquarello and A. Vulpiani, *Journal of Physics: Condensed Matter* **1**, 9509 (Bristol, Great Brittain, 1989).

*Symmetry properties and selection rules of excitons in quantum wells,* L. C.

Andreani, F. Bassani and A. Pasquarello, in *Symmetry in Nature*, Quaderni della Scuola Normale Superiore, Pisa (1989).

*Effect of continuum states on two-photon transitions in quantum wells,* A. Pasquarello and A. Quattropani, *Physical Review B* **41**, 12728 (Woodbury NY, USA, 1990).

*Two-photon transitions with time-delayed radiation pulses,* A. Pasquarello and A. Quattropani, in *Applied Laser Spectroscopy*, ed. by M. Inguscio and W. Demtröder (Plenum Publishing, London, Great Brittain, 1990).

*Interpretation of three-photon spectra in alkali halides,* A. Pasquarello and L. C. Andreani, *Physical Review B* **41**, 12230 (Woodbury NY, USA, 1990).

*Binding energies of ground and excited shallow acceptors in $GaAs/Ga_{1-x}Al_xAs$ quantum wells,* S. Fraizzoli and A. Pasquarello, *Physical Review B* **42**, 5349 (Woodbury NY, USA, 1990).

*Polarization dependence of two-photon transitions in quantum wells* A. Pasquarello and A. Quattropani, *Il Nuovo Cimento*, February 1991.

*Comment on "Effect of biaxial strain on acceptor-level energies in $In_yGa_{1-y}As/Al_xGa_{1-x}As$ (on GaAs) quantum wells",* L. C. Andreani, S. Fraizzoli and A. Pasquarello, *Physical Review B* **42**, 7641 (Woodbury NY, USA, 1990).

*Two-photon transitions to excitons in quantum wells,* A. Pasquarello and A. Quattropani, *Physical Review B* **42**, 9073 (Woodbury NY, USA, 1990).

*Accurate calculation of exciton binding energy in $GaAs/Ga_{1-x}Al_xAs$ quantum wells,* L. C. Andreani and A. Pasquarello, *Physical Review B* **42**, 8928 (Woodbury NY, USA, 1990).

*Polarization dependence of multiphoton transitions,* A. Pasquarello and A. Quat-

tropani, *Physical Review B* **43**, 3837 (Woodbury NY, USA, 1991).

*Infrared transitions between shallow acceptor states in $GaAs/Ga_{1-x}Al_xAs$ quantum wells,* S. Fraizzoli and A. Pasquarello, *Physical Review B*, (Woodbury NY, USA) submitted in September 1990.

*CONFERENCE PROCEEDINGS:*

*Binding energies of p-type acceptor states in $GaAs$-$Ga_{1-x}Al_xAs$ quantum wells,* A. Pasquarello, L. C. Andreani and R. Buczko, *Helvetica Physica Acta* **62**, 872 (Basel, Switzerland, 1989).

*Two-photon transitions to excitons in quantum wells,* A. Pasquarello and A. Quattropani, *Proceedings of the 20th International Conference on the Physics of Semiconductors*, Thessaloniki, Greece, 1990.

*Infrared transitions between shallow acceptor states in $GaAs$-$Ga_{1-x}Al_xAs$ quantum wells,* S. Fraizzoli and A. Pasquarello, *Proceedings of the 20th International Conference on the Physics of Semiconductors*, Thessaloniki, Greece, 1990.

*High exciton binding energies in $GaAs/GaAlAs$ quantum wells,* L. C. Andreani and A. Pasquarello, *Superlattices and Microstructures* accepted for publication at *5th International Conference on Superlattices and Microstructures*, Berlin, Germany, 1990.

*Excitonic effects on the two-photon transition rate in quantum wells,* A. Pasquarello and A. Quattropani, *Superlattices and Microstructures* accepted for publication at *5th International Conference on Superlattices and Microstructures*, Berlin, Germany, 1990.